MODELING, SIMULATION AND CONTROL OF STICK-SLIP AND BIT-BOUNCE VIBRATION IN AN OIL WELL DRILLSTRING

MD. MEJBAHUL SARKER

MODELING, SIMULATION AND CONTROL OF STICK-SLIP AND BIT-BOUNCE VIBRATION IN AN OILWELL DRILLSTRING

by

© Md. Mejbahul Sarker

A Thesis submitted to the School of Graduate

Studies in partial fulfillment of the requirements

for the degree of Master of Engineering

Faculty of Engineering and Applied Science

Memorial University of Newfoundland

St. John's, Newfoundland, Canada

July 2012

AUTHOR'S DECLARATION

I hereby declare that I am the sole author of this thesis. This is a true copy of the thesis, including any required final revisions, as accepted by my examiners. I understand that my thesis may be made electronically available to the public.

ABSTRACT

Md. Mejbahul Sarker: Modeling, Similation and Control of Stick-slip and Bit-bounce Vibration in an Oilwell Drillstring. M.Eng. Thesis, Memorial University, July, 2012.

Drillstrings are used in oil and gas production as well as geothermal wells. Drillstrings sometimes vibrate severely and can twist off in hard rock drilling. Stick-slip and bit-bounce are predominant to oilwell drilling operations. Stick-slip vibration particularly has received considerable attention in recent years with increasing use of polycrystalline diamond compact (PDC) bits in harder formations, and has motivated extensive research on this type of drillstring vibration. Stick-slip vibration may also excite severe axial and lateral vibrations in the bottom hole assembly (BHA), causing damage to the drillstrings and downhole equipment. Failure of oilwell drillstrings is very costly in terms of money and time. Controlling these vibrations is essential to improving the efficiency and minimizing the cost of drilling.

A bond graph model of a drillstring has been developed that predicts axial vibration, torsional vibration, and coupling between axial and torsional vibration due to bit-rock interaction. Axial and torsional submodels use a lumped-segment approach, with each submodel having a total of 21 segments to capture vibration of the kelly, drillpipes, and drillcollars. In addition, the model incorporates viscous damping, hydrodynamic damping, and hydraulic forces due to drilling mud and an empirical treatment of rock-bit interaction and top drive motor.

The model predicts the expected coupling between weight on bit (WOB), bit speed, and rock-bit interface condition, and their effect on stick-slip and bit-bounce. Low bit speed and high WOB cause stick-slip, and avoiding critical bit speed and low WOB cause bit-bounce. Mitigating measures used in the drilling industry (changing rotary speed, and adjusting WOB through changing derrick cable tension) were applied to the model, and successfully eliminated stick-slip or bit-bounce.

A linear quadratic regulator (LQR) controller was then implemented which controlled stick-slip and eliminated bit-bounce. Finally, the advantages of an LQR controller, compared to a spring-damper isolator currently applied in oilwell drilling, for stick-slip and bit-bounce mitigation in an oilwell drillstring are studied.

The simulation time is very fast compared to high order finite- and discrete-element models, making the model suitable as a tool for design and sensitivity analysis.

Indexing terms: Oilwell drilling, lumped-segment model, stick-slip, bit-bounce, bit-rock interaction, linear quadratic regulator, torsion spring-damper.

ACKNOWLEDGEMENTS

All praise is due to Allah, and may his peace and blessings be upon the Prophet (peace be upon him) who said: "Should not I be a grateful servant." [*Sahîh al-Bukhârî* and *Sahîh Muslim*]

I would like to express my gratitude to my supervisor, Dr. Geoff Rideout, for his professional supervision, critical discussions and immeasurable contributions. Without his encouragement and ideas this work would have never been completed. I would like also to thank Dr. Stephen Butt for his continuous support, encouragement and guidance throughout my studies. To him also belongs the credit for proposing the research project and attracting several sources of funding.

I am also indebted to Farid Arvani, Project Manager of the Advance Exploration Drilling Technology (ADG) laboratory at Memorial University whose suggestions, encouragement and kindness helped me to pursue my research under severe critical situations and knowledge limitations.

I would like to thank my colleagues in the Advance Exploration Drilling Technology laboratory for their continuous help with matters of drilling.

I would also like to thank the Atlantic Canada Opportunity Agency (AIF Contract no. 781-2636-1920044), Husky Energy, and Suncor Energy for funding this research. Finally, I wish to thank the Faculty of Engineering and Applied Science at Memorial University for financial support.

Dedicated to my parents

NOTE ON THE UNITS OF MEASUREMENTS

Throughout this thesis, S.I. and imperial units of measurements are used. Where appropriate and possible however, the S.I. metric equivalent of imperial units have been provided. The reason for adopting imperial units is justified by the following:

1. This work is oriented towards technical advances in the drilling industry. However, the drilling industry worldwide commonly in the United States where imperial units uses.
2. Most drilling equipment conforms to API standards which recently are generally in non-S.I. units. Issues like thread size, pipe dimensions, pressure gauges etc. will likely continue to be based on traditional units since it is too entrenched in the industry. As well, the traditional units are a mixture of imperial (weight, length) and American (1 usg = 3.785 L and 1 short ton = 2000 lbs).
3. The majority of previous publications relating to the thesis research were in imperial units.

On this basis, it was decided to maintain imperial units for all subsequent data presentation and calculations. The following page provides a Table of Conversion for imperial units to their metric equivalents.

TABLE OF CONVERSION; IMPERIAL TO METRIC

Imperial	Multiplying factor	Metric
feet	0.3048	m
in	25.4	mm
ft/hr	0.3048	m/hr
psi	0.0069	MPa
lb mass	0.4536	kg
rev/min (rpm)	0.1047	rad/s
ft-lb	1.36	N.m

Table of Contents

List of Tables

List of Figures

List of Symbols

C_{rt} = Equivalent viscous damping coefficient, N-m-sec/rad

I = Current, A

J = Drillstring mass moment of inertia, kg-m^2

J_k = Inertia of kelly, kg-m^2

J_m = Inertia of motor, kg-m^2

J_{rt} = Inertia of rotary table, kg-m^2

K_m = Motor constant, V-s

K_t = Torsional stiffness, N-m/rad

L = Motor inductance, H

n = Gear ratio

R_m = Armature resistance, Ω

C_v = Viscous damping coefficient, N-m-sec/rad

$\dot{\emptyset}_{rt}$ = Rotary table speed, rad/sec

$\emptyset_{rt}$ = Rotary table angular displacement, rad

r_w = Wellbore radius, m

r_0 = Drill pipe/collar outer radius, m

r_i = Drill pipe /collar inner radius, m

ω_n = rotary speed of n^{th} cell, rad/sec

ρ = Drillstring material density, kg/m^3

L_k = Kelly total length, m

r_{ok} = Kelly outer radius, m

r_{ik} = Kelly inner radius, m

J_p = Drill pipe inertia, kg-m^2

J_c = Drill collar inertia, kg-m^2

L_p = Drill pipe total length, m

r_{op} = Drill pipe outer radius, m

r_{ip} = Drill pipe inner radius, m

L_c = Drill collar total length, m

r_{oc} = Drill collar outer radius, m

r_{ic} = Drill collar inner radius, m

G = Drillstring modulus of rigidity, N/m^2

μ_e = Equivalent fluid viscosity for fluid resistance to rotation, N-sec/m^2

d_h = wellbore diameter, m

S_0 = Surface elevation amplitude, m

b = Bit factor

W_{fs} = Threshold force, N

Q = Mud flow rate, m^3/sec

Q_m = Mean mud flow rate, m^3/sec

Q_a = Mud flow pulsation amplitude, m^3/sec

q = Freq. of variation in mud flow rate, rad/sec

α_a = Weisbach friction factor outside drill pipe or collar

α_p = Weisbach friction factor inside drill pipe or collar

CHAPTER 1

INTRODUCTION

Oil and natural gas are non-renewable natural resources vital to the maintenance of our day-to-day life, as well as being essential to industry. The production of these hydrocarbons depends mainly on the drilling process. Efficient, reliable rotary drilling has acquired greater economic significance to the drilling industry in the development of oil and gas resources due to increased exploration in less familiar territories and to greater depth. Drilling operation costs represent approximately 40% of all exploration and production costs; therefore, it is a challenge for oil companies to minimize the costs of drilling process [1]. Field observations have revealed that severe vibration occurs during drilling operations which severely affects the overall drilling performance. Oilwell drillstrings play an integral role in drilling operations. Failure in drillstrings can significantly add to the total cost of the extraction process. Vibrations in oilwell drillstrings may minimize the life of the pipe by accelerating the process of fatigue. Also excessive vibrations can cause downhole equipment failure, wash-outs and decrease in the penetration rate. In 2003, when a company was drilling in Longhupao of Daqing, the drilling system reached to a depth of 2390-3042m, and the drillstring was broken 7 times. The cost was so high that some wells could not be drilled continually. The treatment of these accidents had consumed great manpower and material resources. At the same time it

affected drilling speed badly. Excessive vibration was the main reason for fatigue failure of the drill tool [2].

Stick-slip vibration has received considerable attention in recent years, with increasing use of polycrystalline diamond compact (PDC) bits in harder formations, and has motivated extensive research on this type of drillstring vibration. Stick-slip vibration may also excite severe axial and lateral vibrations in the bottom hole assembly (BHA), causing damage to the drillstrings and downhole equipment. Controlling these vibrations is essential to improving the efficiency and minimizing the cost of drilling. In this thesis, the focus is on stick-slip vibration, and the coupling between stick-slip and bit-bounce vibrations of an oilwell drillstring.

Usually, the more that is known about a system, the better it can be controlled and optimized. Such knowledge can come from direct state measurement or from estimates of state, using some facsimile of the assemblage, or both. For a complicated system such as rotary rock drilling in which measurements are limited, a model is required not only to supplement the available measurements but to provide a basis for useful interpretation of the data. Such a model must meet certain criteria including adequate description of the system under most operating conditions. Where these conditions are highly variable or little known, the model should be of such a nature that it can be used adaptively. The model must be such that it can be utilized simply and quickly to achieve desired objectives [3]. This present work represents a bond graph dynamic model of a whole drillstring including both drill pipes and drill collars. In addition to the axial vibration, torsional vibration, and axial-torsional coupling due to bit-rock interaction, the developed

model accounts for the self weight effect, the associated tension and compression fields, viscous damping, hydrodynamic damping, and hydraulic forces due to drilling mud within the drillstring and it incorporates an empirical treatment of rock-bit interaction, and top drive motor dynamics. The main contribution of this work is a model suitable for parametric study of the effect of table rotary speed, mud parameters, drillstring length and pipe weight, and weight on bit on stick-slip vibration and the coupling between stick-slip and bit-bounce vibrations.

1.1 Overview of an Oilwell Drilling System

An oil well is a general term for any boring through the surface of the Earth that is designed to find and acquire petroleum. Usually, some natural gas is produced along with the oil. A well that is designed to produce mainly or only gas may be termed a gas well.

The earliest oil wells in modern times were drilled percussively, by hammering a cable tool into the earth. Soon after, cable tools were replaced with rotary drilling, which could drill boreholes to much greater depths and in less time. The record-depth Kola Borehole used non-rotary mud motor drilling to achieve a depth of over 12,000 m (39,000 ft) [4]. Until the 1970s, most oil wells were vertical, although lithological and mechanical imperfection cause most wells to deviate at least slightly from true vertical. However, modern directional drilling technologies allow for strongly deviated wells which can, given sufficient depth and with the proper tools, actually become horizontal [4].

A rotary drilling system creates a borehole by means of a rock-cutting tool (drill bit). The torque driving the bit is generated at the surface by a motor, through a mechanical transmission box, to the rotary table via the kelly (a square, hexagonal or

octagonal shaped tubing that is inserted through and is an integral part of the rotary table that moves vertically while the rotary table turns it). The medium to transport the energy from the surface to the bit is a drill-string, mainly consisting of drill pipes. The drillstring can be up to 8 km long. The lowest part of the drillstring is the BHA consisting of drill collars and bit. The BHA can be several hundred meters long. A sketch illustrating the oilwell drilling system is depicted in Figure 1.1.

The rotary drilling process consists of two major steps: (a) penetrating into the rocks; and (b) removing the rock chips. The first step generally involves crushing or shearing actions, which produce rock chips. The crushing and shearing is performed by means of special cutters installed on the drill bit which are pushed downward while drilling. To proceed in the drilling process, the generated rock chips must be extracted to the surface.

The drill rig is a machine used to drill boreholes in the ground. This machine accommodates the vertical and rotational motion of the drillstring and circulates the drilling fluid. The main parts of the drill rig are the derrick, rotary table, drillstring, and drill bit. The derrick is a structure which is used to support the drillstring. The rotary table provides the required torque to turn the drillstring. The drill bit and the drillstring are the main tools which perform the drilling and penetrating steps. The oilwell drilling rigs can be classified broadly as onshore and offshore rigs. The photos in Figures 1.2 and 1.3 show onshore and offshore drilling rigs, respectively.

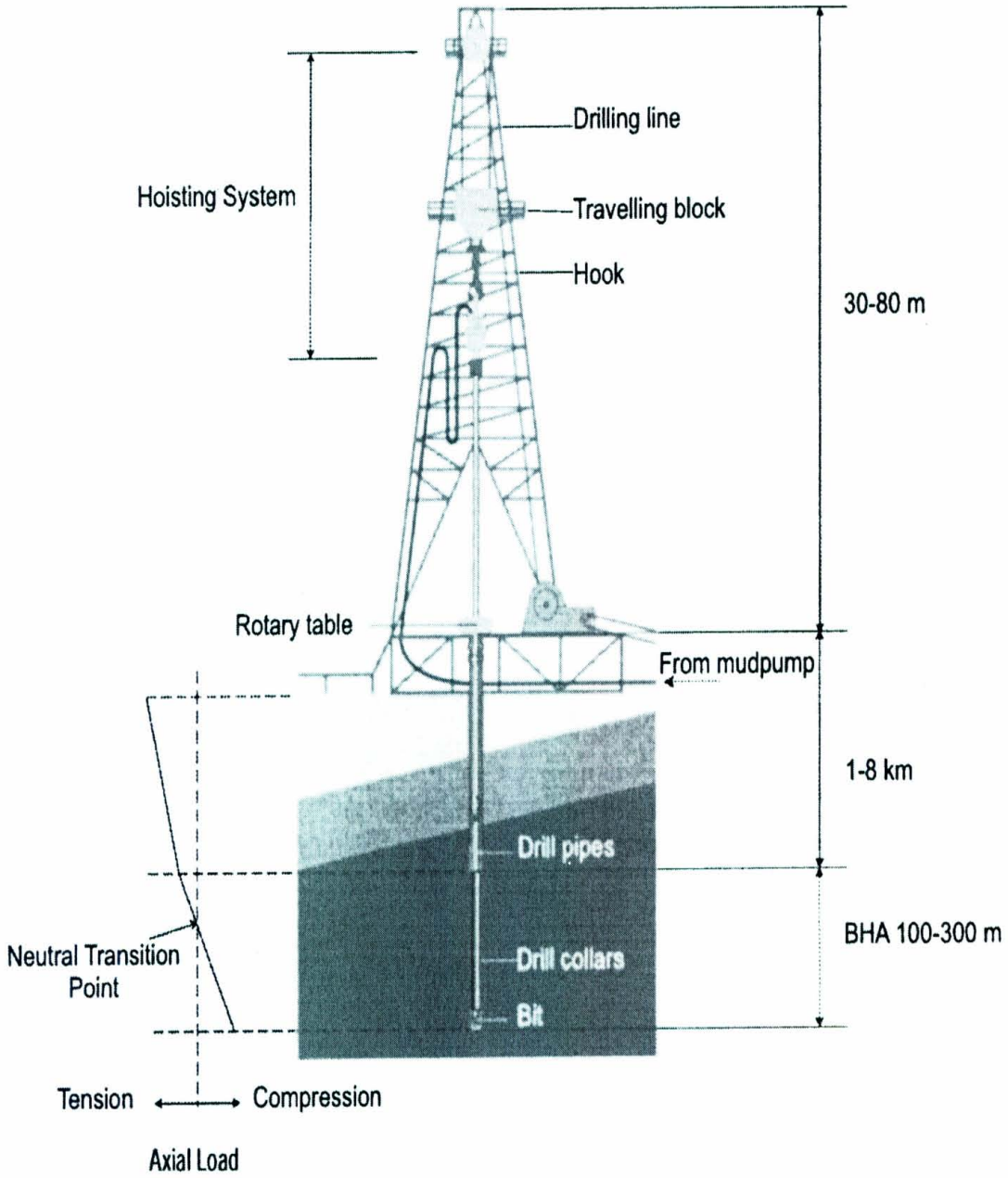

Figure 1.1: Oilwell drilling system (adopted from [6])

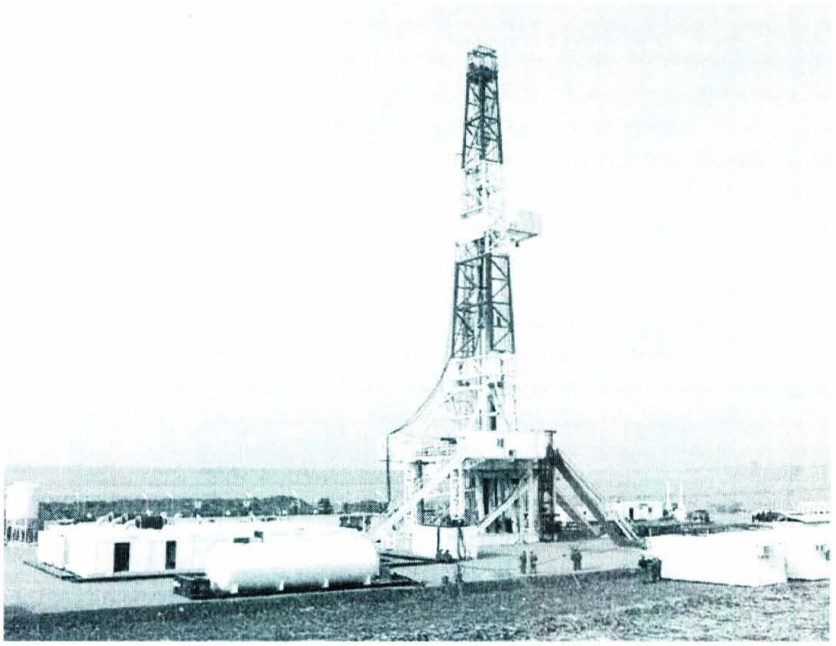

Figure 1.2: Onshore drilling rig

Figure 1.3: Offshore drilling rig

Offshore oil and gas production is more challenging than land-based installations due to the remote and harsher environment. Much of the innovation in the offshore petroleum sector concerns overcoming these challenges, including the need to provide very large production facilities. Notable offshore fields today are found in the North Sea, the Gulf of Mexico (mostly offshore Texas and Louisiana, but also Mississippi and Alabama), California (in the Santa Barbara basin), the Caspian Sea (notably some major fields offshore Azerbaijan) the Campos and Santos Basins off the coasts of Brazil, Newfoundland and Nova Scotia (Atlantic Canada), several fields off West Africa most notably west of Nigeria and Angola, as well as offshore fields in South East Asia and Sakhalin, Russia. Also major offshore oil fields are located in the Persian Gulf such as Safaniya, Manifa, and Marjan which belong to Saudi Arabia and are developed by Saudi Aramco [5].

The drill bit, which crushes the rock and penetrates into the formation, is mostly comprised of drilling cutters installed on a rotating element that are capable of crushing or shearing rock. The drill bit is attached to the bottom end of the drillstring and receives the rotary motion and downward force transmitted by the drillstring. A drilling fluid consisting of special liquids is ejected from nozzles in the bit to the borehole to extract the cutting chips to the surface through the annulus between the borehole wall and the drillstring. The two main types of drill bits used are the rotary cone (RC) bits and the PDC bits.

An RC bit consists of three cones which are mounted on assigned arms. The arms are welded together forming the body of the bit. The outside area of the cones is covered

by different rows of hard-material inserts, which are used for crushing the rocks. A sketch illustrating the RC bit is depicted in Figure 1.4.

PDC bits, as shown in Figure 1.5, use a dragging or shearing action and do not have any rotating elements. The cutters are installed on the body of the bit and shear the rock and generate rock chips. This type of bit is generally used in soft and medium-hard formations; the rotary cone bits are more desirable for hard formations.

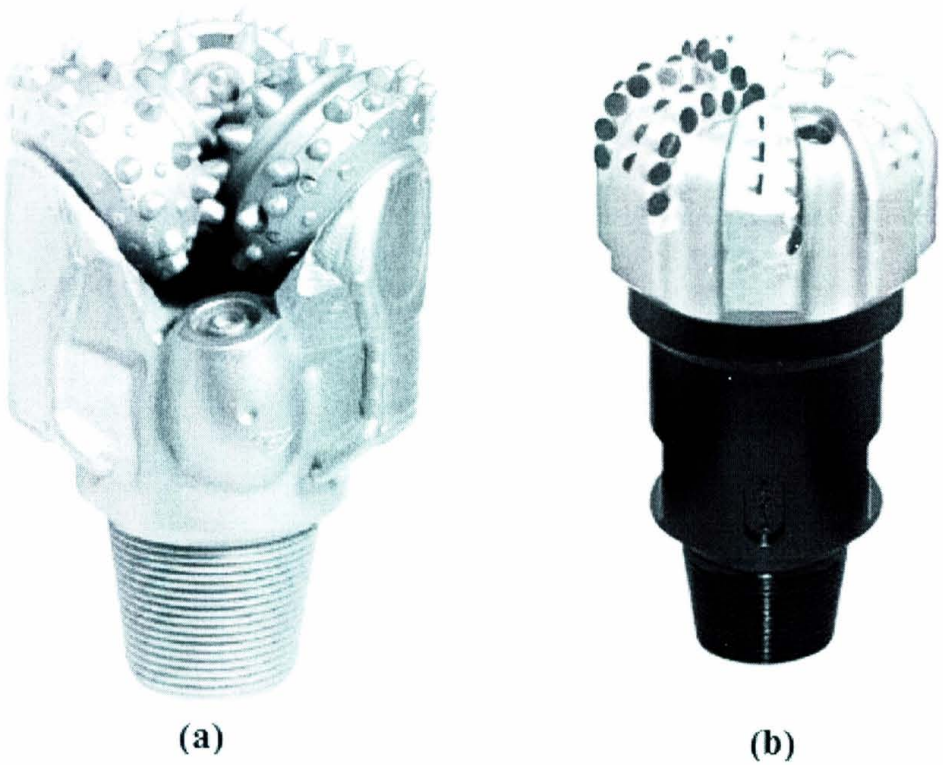

Figure 1.4: (a) RC bit (Baker Hughes), (b) PDC bit (Baker Hughes) [66]

1.1.1. Surface Rotary System

There are two types of surface rotary systems in use: (i) rotary table, and (ii) top drives. Almost all rigs today have a rotary table, either as primary or backup system for rotating the drillstring. Top drive technology, which allows continuous rotation of the drillstring, has replaced the rotary table in certain operations. A few rigs are being built today with top drive systems only, and lack the traditional kelly system [51].

A rotary table is the revolving or spinning section of the drill floor that provides power to turn the drillstring in a clockwise direction (as viewed from above). The rotary motion and power are transmitted through the kelly bushing and the kelly to the drillstring. When the drillstring is rotating, the drilling crew commonly describes the operation as simply, "rotating to the right", "turning to the right", or, "rotating on the bottom"[51]. Figure 1.5 shows the photos of rotary tables.

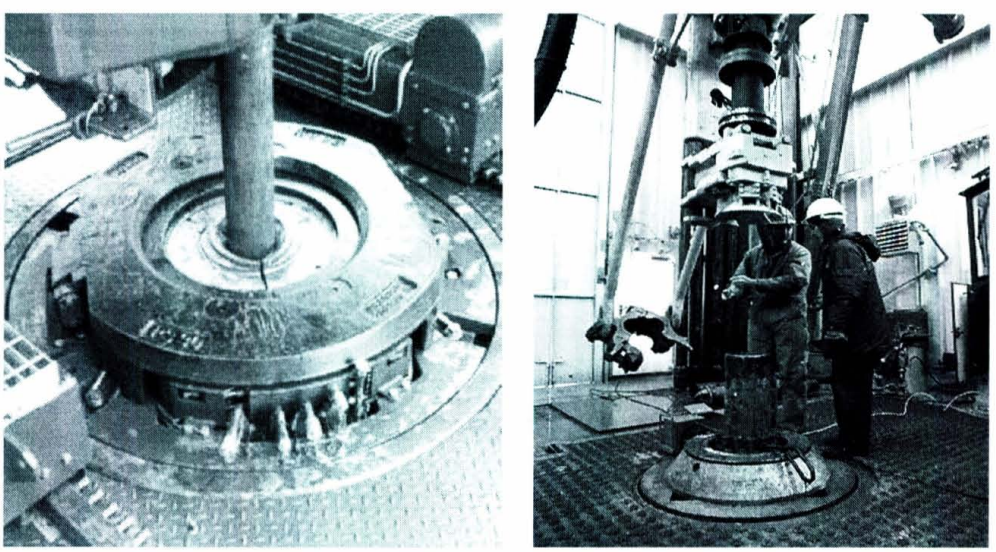

Figure 1.5: Rotary tables (adopted from [52] & [53])

The top drive is a device that turns the drillstring. It is an alternative to the rotary table. It consists of one or more motors (electric or hydraulic) connected with appropriate gearing to a short section of pipe called a quill, which in turn may be screwed into a saver sub or the drillstring itself. The top drive is suspended from the hook, so the rotary mechanism is free to travel up and down the derrick. This is radically different from the more conventional rotary table and kelly method of turning the drillstring because it enables drilling to be done with three joint stands instead of single joints of pipe. It also enables the driller to quickly engage the pumps or the rotary while tripping pipe, which cannot be done easily with the kelly system. Figure 1.6 shows the photos of top drive system.

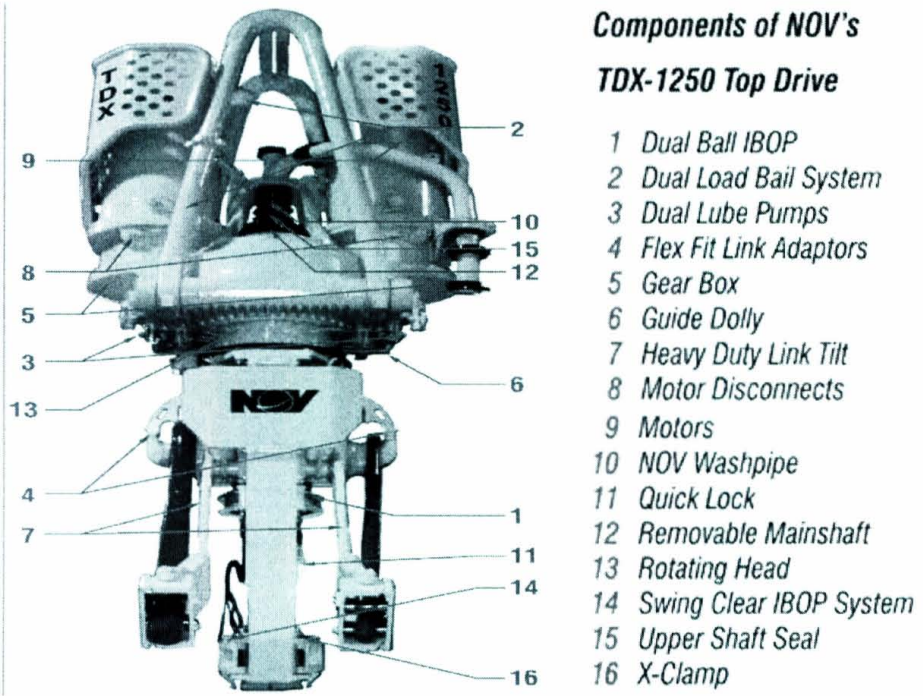

Figure 1.6: Top drive system (adopted from [55])

While not a panacea, modern top drives are a major improvement to drilling rig technology and are a large contributor to the ability to drill more difficult extended-reach wellbores. In addition, the top drive enables drillers to minimize both frequency and cost per incident of stuck pipe.

1.1.2. Mud Motor

There are two major types of downhole motors powered by mud flow: (a) the turbine, which is basically a centrifugal or axial pump, and (b) the positive displacement mud motor (PDM). The principles of operation are shown in Figure 1.7 and the designs of the tool are totally different. Turbines were in wide use a number of years ago and are seeing some increased use lately but the PDM is the main workhorse for directional drilling [57].

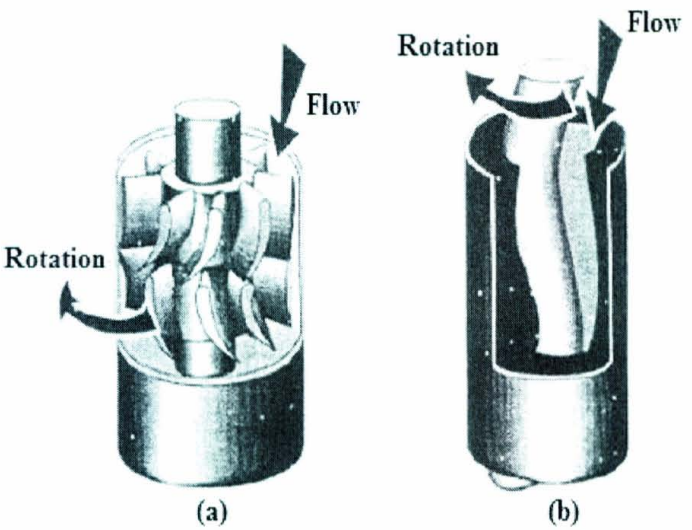

Figure 1.7: (a) Turbine motor and (b) Positive displacement motor [57]

The Mud Motor uses different rotor and stator configurations to provide optimum performance for the desired drilling operation, typically increasing the number of lobes and length of power assembly for greater horsepower. In certain applications, compressed air, or other gas, can be used for Mud Motor input power. Normal rotation of the bit while using a Mud Motor can be from 60 rpm, to over 100 rpm [56].

This motor can be used in directional and horizontal wells, hard formation drilling, and PDC bit drilling operations [57]. Figure 1.8 shows a sketch of the motor section in a BHA.

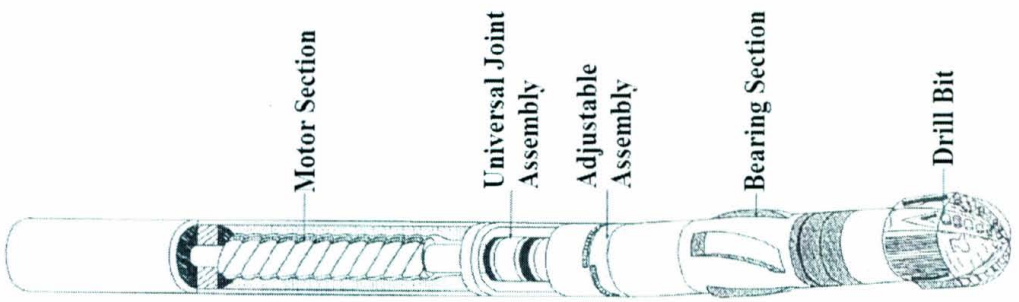

Figure 1.8: Sketch of motor section in BHA [57]

1.1.3 Shock-sub

The shock-sub impact and vibration reduction sub is a drillstring component that absorbs and dampens the variable axial dynamic loads produced by the drill bit during routine drilling and milling operations. The tool is most beneficial when drilling in hard rock, broken formations, and intermittent hard and soft streaks. Reducing the impact loads helps to increase ROP; improve borehole quality; and extend the life of the cutting

structure, bearings, connections, and surface equipment – all translating to a lower cost of drilling per foot [58].

A shock-sub will be positioned close behind the bit where hard formations cause the bit to bounce on the bottom of the hole. They are designed to absorb the impact from this bouncing in order to prevent damaging the remaining part of the drillstring. This may be done by way of springs or rubber packing [21]. Figure 1.9 shows the photos of ST5 shock tool at just behind the bit.

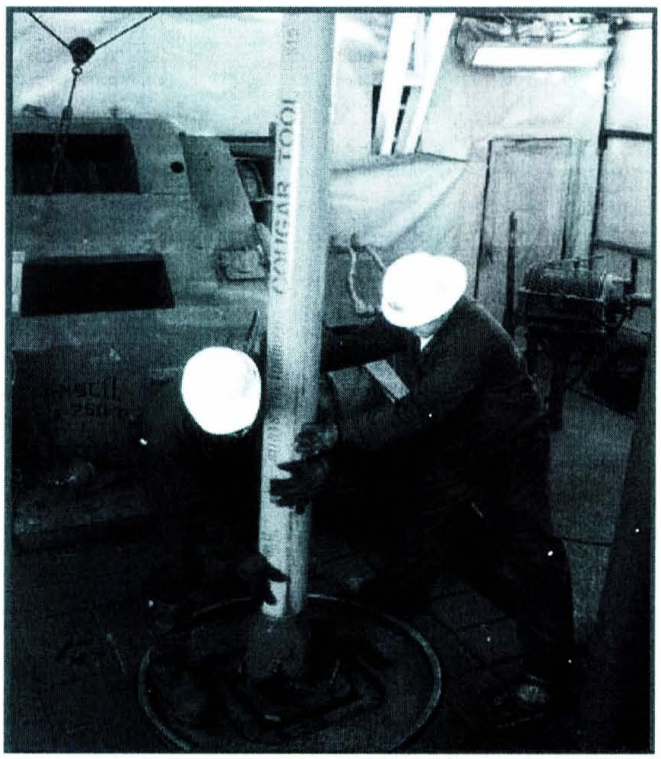

Figure 1.9: Cougar ST5 steel spring shock tool [59]

1.1.4 Packed Assembly or Holding Assembly

A BHA consisting of stabilizers and large-diameter drill collars arranged in a particular configuration to maintain drift angle and direction of a hole is called a packed assembly.

The holding or packed assembly uses packed hole stabilization principles to maintain the inclination and direction. Once the inclination has been built to the required angle, the tangential section of the well is drilled using a holding assembly or packed assembly. The object here is to reduce the tendency of the BHA to build or drop angle [60].

1.2 Thesis Background

This work will focus on the computer simulation of drillstring vibrations. Since stick-slip vibration is the prominent mode of vibration when drilling with drag bits (especially with PDC bits) and may excite severe axial and lateral vibrations in the BHA, it is, therefore the, main concentration of this work. Due to time constraints, this thesis will consider only the coupling between axial and torsional vibrations due to bit-rock interaction. In practice, the only means of controlling vibration with current monitoring technology is to change either the rotary speed or the weight on bit, which is why the emphasis is on investigating an active controller for mitigating stick-slip and bit-bounce vibrations without affecting drilling performance or worsening other modes of vibration.

As stated earlier, this thesis concentrates on stick-slip vibration and coupling between axial and torsional vibrations due to bit-rock interaction without paying attention

to the effects of lateral vibration. At the end of this work, a linear quadratic regulator (LQR) controller will be discussed together with its advantages, compared to a spring-damper isolator, for stick-slip and bit-bounce mitigation in an oilwell drillstring.

1.3 Objective

The main objective of this work is to develop a dynamic model of an oilwell drillstring that predicts axial vibration, torsional vibration and coupling between axial and torsional vibration due to bit-rock interaction. The results obtained from the simulation are then analyzed with the qualitative trends from field observations regarding stick-slip oscillations and their relationship to rotary speed, weight on bit, and bit-bounce. Finally a linear quadratic regulator controller is implemented in the model which controls stick-slip and eliminates bit-bounce and the results obtained are compared with a torsion spring-damper isolator near the top drive system.

1.4 Significance

This model gives fast predictions, using a desktop PC, of coupled axial and torsional vibrations in multiple modes, instead of the just the first mode. The current model can be parameterized to match field drillstrings for studying field vibration data. Finally, the feedback controller (LQR) that is discussed earlier can be applied to petroleum engineering particularly in drilling operations to increase the range of speeds for which stick-slip will not occur.

1.5 Scope

The study is limited to axial vibration, torsional vibration, and coupling between axial and torsional vibration due to bit-rock interaction. The LQR controller can suppress stick-slip and bit-bounce vibration but its effects on lateral vibration are beyond the scope of this thesis. Finally, the study is limited to vertical drilling systems.

1.6 Methodology

Bond graph method using 20-sim (software for modeling dynamic systems) is applied throughout the modeling and simulation. The simulation time is very fast compared to high order finite-and discrete-element models, making the model suitable as a tool for design and sensitivity analysis. Mathematical methods for the derivation of viscous damping, hydrodynamic damping and linear quadratic regulator controller etc. are also applied in this thesis.

This chapter has provided a brief introductory description of this thesis work and overview of rotary drilling process in oil and gas well drilling operation. It has also provided an overview and background of this research work as well as its objective, scope, significance and methodology. In the next chapter, general vibration will be discussed including the various modes of vibration and their specific subsets or consequences.

CHAPTER 2

DRILLSTRING VIBRATION REVIEW

Field experience manifests that drillstring vibration is one of the major causes of deteriorated drilling performance. Vibration detection has revealed that vibrations are always present to some degree, but can be especially bad in difficult drilling environments (e.g. hard formations, steep angle wells). Vibration can affect WOB, rate of penetration (ROP), and drilling direction and can also cause severe damage to drilling tools, such as BHA, measuring while drilling (MWD) tools, cutters, and bearings [7-16]. Initially, Finnie & Bailey conducted the first analytical and experimental study of drillstring vibration in the 1960's [17-18], and showed that the various modes of vibrations produce rather similar effects, which are namely decreasing ROP and premature failure of downhole equipment. Whether observable or not, these unwanted vibrations significantly increase the cost of drilling an oilwell. Although the exact figure is still being assessed, large costs—an estimated 2% to 10% of well costs—can arise from vibration-related problems, such as lost time while pulling out of hole and fishing, reduced ROP, poor quality wellbore and increased service cost because of the need for ruggedized equipment [19].

The downhole dynamics of drilling tools are complex. It involves a combination of simultaneous vibrational phenomena which render the analysis of drillstring vibrations

extremely challenging. Drillstring vibrations can be divided into three types, or modes: axial, torsional, and lateral (Figure 2.1).

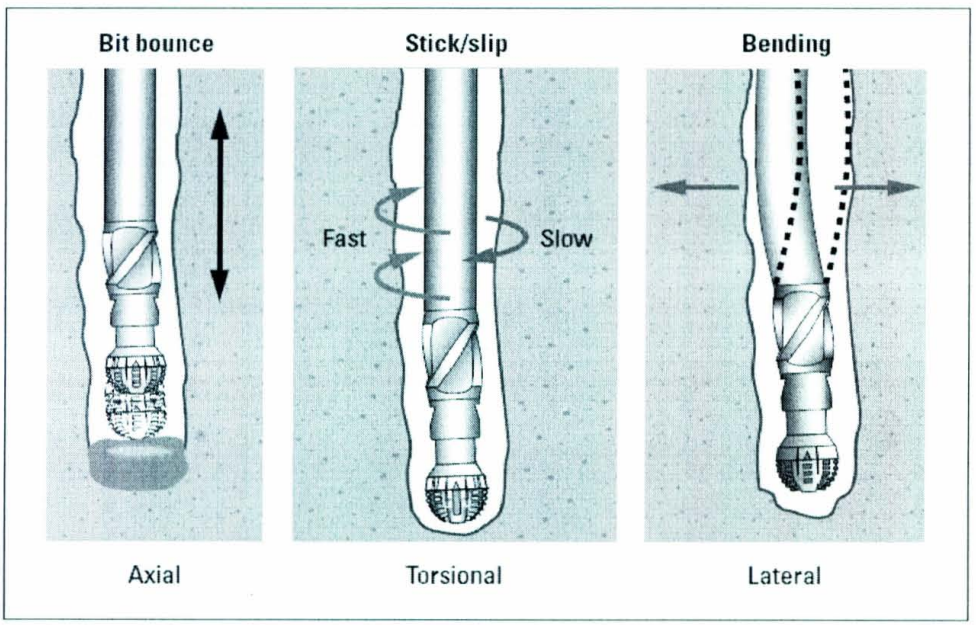

Figure 2.1: Modes of vibration in drillstring (adopted from [20])

2.1 Axial Vibration

Axial vibrations of a drillstring involve motions of its components along its longitudinal axis (Figure 2.1). Axial vibration appears during the drilling operation in two forms: (a) vertical vibration while the bit is still in contact with the formation; and (b) bit bounce when contact is repeatedly lost as the bit bounces on and off the bottom.

Axial vibrations are present during all phases of the drilling operation. The axial vibration phase in the drillstring is produced by the initial impact of the bit with the formation on bottom. This vibration is more common when drilling with RC bits. The

multi-lobes pattern (Figure 2.2) generated specifically by tricone bits (3 roller RC bits) at the bottom of the well is a major source of axial excitations of vertical or near vertical wells, limiting drillstring-borehole interactions and reducing effective damping. In the case of shallow vertical wells the vibration can be noticed at the surface with variations in the hook load and bouncing of the kelly or top drive. At greater depths and/or directional wells the vibration may be damped and a vibration detection system is needed to identify the problem at the surface, although the damage in the bit and BHA will still be the same [16, 20].

Figure 2.2: Multi-lobed surface of a formation [69]

2.1.1 Bit-bounce

The bit-bounce pattern is likely to develop when drilling with RC bits. As the multi-lobes pattern (Figure 2.2) develops at the bottom of the well, it results in erratic interaction of the bit with the bottom of the well, which makes the bit lose contact with the rock formation. Consequently, the severe axial stress wave induced by lift-off of the bit constitutes a primary source of excitation to the entire drilling assembly. The surface

indicators may be top drive or kelly shaking axially and fluctuating WOB on the weight indicator. This mechanism can result in premature bit and BHA component failure and reduced ROP. Potential cures include reducing WOB and increasing RPM.

2.1.2 Problems

The main problems include: (a) broken or rapidly worn bits, BHA failures (breaking cutters and bearings and leading to fatigue failure); (b) reduced ROP; and (c) impact inducing other vibration modes [20-21].

2.1.3 Sources

Axial vibrations are most common in hard drilling regions, in vertical wells (where the propagation of energy, along the string, is easier and in deviated holes axial vibration is dampened through contact with the string), and when drilling with tri cone bits (RC bits induce axial vibration by their mode of action and penetration) [21, 68].

2.1.4 Remedial Action

Once axial vibration has been identified, the potential cures are to change WOB (increase for bit-bounce vibration) and adjust RPM. Other solutions for mitigating axial vibration are to use PDC bit and shock-sub [21, 68].

In a soft formation such as sandstone, increasing the WOB even slightly will increase the amplitude and frequency of axial vibration. Increasing RPM will have the effect of reducing the severity of any torsional vibration, which may be present

concurrently with the axial. This would be effective as it is often torsional behavior that induces axial vibration in the first place, notably in harder lithologies [21].

The use of PDC bits reduces axial excitement when compared with tri-cone bits, but is not as effective as the use of a shock sub which should be installed just behind the bit (and motor if present) [21].

2.2 Torsional Vibration

Torsional vibration occurs when the rotation of the drill string is slowed down (or stopped) at the bottom and released when the torque overcomes the static friction resisting string rotation. This vibration of the drillstring is not seen uphole due to the fact that the rotary system in the surface acts as a clamp and attenuates most of the vibrations (Figure 2.1). Measurement While Drilling (MWD) devices have assisted researchers in obtaining a better understanding of this type of drillstring vibrations and its effect on downhole tools and drilling performance. Downhole measurements show that applying a constant rotary speed at the surface does not necessarily translate into a steady rotational motion of the bit. In fact, the downhole torsional speed typically exhibits large amplitude fluctuations during a significant fraction of the drilling time. This non-uniform rotational speed of the bit is due primarily to the large torsional flexibility of the drilling assembly [16, 20].

Some degree of torsional vibration is unavoidable as it begins as soon as the string begins to rotate. During lowering of the assembly to bottom, the rotary system generates a torsional wave that propagates to the bit. Depending on the time for the bit to impact on bottom, the torsional disturbance reflects (often more than once) from the bit, which is

undergoing a steady acceleration. These reflections cause propagation torque pulses along the string. Once bit contact is made with bottom, the bit RPM decelerates and a much more severe torque pulse travels to the top, where an RPM decrease can be observed [21].

2.2.1 Stick-slip

The most common torsional vibration is called stick-slip. Stick-slip can result in harmful rotational vibrations in the drill-string. Although the drill-string is continuously rotating at surface during the drilling operation, friction on the bit, BHA and/or drill-string itself can cause it to "stick" down-hole. As rotation at the surface continues and torque in the drill-string builds up, this 'stick' friction is suddenly overcome causing a sudden increase in speed ("slip") as the drill-string 'unwinds' itself. When fully developed, stick-slip can cause the bit and BHA rotation to completely stop and accelerate up to 5-6 times the surface rpm [22].

The use of a mud motor may help to address sick-slip if the main source of excitation is from the bit, but the presence of a motor does not prevent stick-slip. The drillstring and BHA above the motor can enter into stick-slip motion even when the motor is turning the bit at a steady rate [20].

There are two clear stick-slip indicators for the driller: (a) large variations in surface torque; and (b) large variations in downhole RPM. The torque variations can be accompanied by "groaning" noise coming from the top drive. Characteristic of the stick-slip behaviour is the saw-tooth behaviour of the torque, which can result in 50% torque variation [22].

Stick-slip vibration decreases the rate of penetration (ROP) by typically 25% due to the nonlinear relationship between the drilling rate and the bit rotational speed [71].

2.2.2 Problems

Torsional vibration creates many problems for drillstring and bits. The main problems include the following [21-22]: (a) damage to, or fatigue failure of bit cutting elements through variable rpm and cutter load; (b) reduced ROP; (c) connection fatigue and premature failure of drillstring, BHA and downhole tools (e.g. rotary steerable system (RSS), MWD devices etc.); (d) washouts, twist-off; (e) fishing trips and replacements; (f) easily generated torsional vibrations with PDC bits; and finally, (g) increased costs.

2.2.3 Sources

Torsional vibrations are often present, to some degree, but are considerably worse in hard drilling regions, hard and abrasive lithologies, high angle and deviated wells (higher hole angle provides more pronounced oscillations), and with PDC bits (it generates high levels of friction to initiate the "stick" phase) [21, 68].

2.2.4 Remedial Action

Once torsional vibration has been identified through high frequency surface torque analysis, or through downhole tools, the potential cures are to increase RPM, either at surface or downhole (motor or turbine), incrementally, until the condition has been eradicated and reduce WOB [21, 68]. Torsional vibrations can also be minimized by

increasing mud lubricity (greater lubricity will reduce friction, reducing the tendency of the drillstring to "stick"), improving hole cleaning and using less-aggressive bit [68].

2.3 Lateral Vibration

Lateral vibration is the most destructive type of vibration and can create large shocks as the BHA impacts the wellbore wall (Figure 2.1). This vibration occurs when the bit or the stabilizer rotates with a center of rotation that is not coincident with the center of the well, which will cause hole enlargement. This rotation may not be noticed at surface and can cause, due to high frequency cyclic tensions in the string, reduction in BHA life [16, 20].

2.3.1 Whirl

The most recognizable manifestation of lateral vibrations is the whirling behavior of the BHA and bit. Depending on the relative position between the bit and the rotary table, lateral vibration can be called forward whirl or backward whirl (Figure 2.3).

Bit whirl is defined as an eccentric rotation of the bit. Instead of rotating around its geometric center, the bit rotates eccentrically as a result of its interaction with the wellbore. Surface detection is nearly impossible but the bit will have noticeable characteristics at the end of a run such as being out of gauge or out of round. Downhole detection is easier due to the presence of high downhole lateral shocks consistent with this mechanism. The high shocks induced by bit whirl can lead to premature BHA component failure, bit failure, and reduced ROP [72].

BHA Whirl is defined as the eccentric rotation of the BHA around the wellbore. This motion can be either in the same direction as the pipe rotation, in reverse, or chaotic (Figure 2.3). The BHA "walks" around the wellbore due to "gearing" of the stabilizers and tool joints when hitting the borehole walls. Surface detection can be indirectly achieved when this mechanism induces bit bouncing or on drill string components after the run. One-sided wear on stabilizers and tool joints are typical signs of BHA whirl. A combination of high downhole lateral and torsional shocks is evident on multi-axis detection devices. These high shocks can easily result in bit and BHA component failure. Drillstring components are flattened on one side and subjected to extreme fatigue. It has been clearly demonstrated in a multitude of tests and publications that BHA resonance in a whirl state is a major contributor to the failure of BHA components. This presentation and its case histories graphically display multiple mechanisms amplified by resonant behavior [72].

Forward BHA whirl (Figure 2.3) describes off-centre BHA rotation, with its centerline rotating in the same direction as the drillstring rotation, i.e. clockwise. Backward BHA whirl (Figure 2.3) occurs where the borehole wall friction causes the centre line rotation to become anti-clockwise, opposite to the rotation of the drillstring. Backward whirl is the most severe form of vibration, creating high-frequency large-magnitude bending moment fluctuations that result in high rates of component and connection fatigue. Imbalance in an assembly will cause centrifugally induced bowing of the drillstring, which may produce forward whirl and result in one-side wear of components [16, 20].

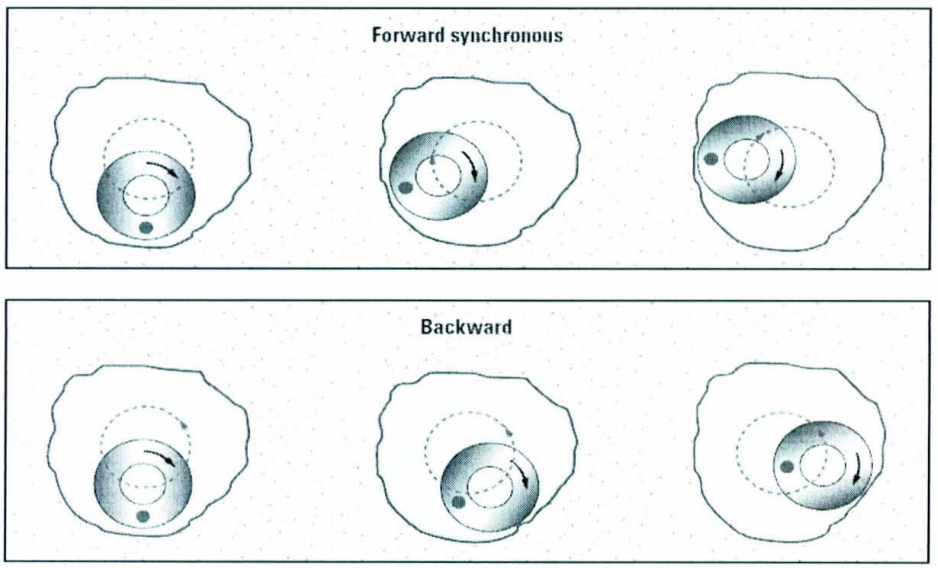

Figure 2.3: BHA whirl phenomena (adopted from [20])

2.3.2 Problems

The main problems include: (a) reduced ROP; (b) premature bit wear; (c) uneven string/stabilizer wear – abrading away the metal of the tools due to impact against the wellbore or casing; (d) BHA washouts and twist offs; (e) Bore hole enlargement, hole instability, casing damage; and (f) lateral impacts inducing other vibrations [20-21].

2.3.3 Sources

Bit whirl generally occurs in near vertical wells, in interbedded soft and hard formations, and with PDC bits with aggressive side cutters (PDC bits will more easily move-off-centre to initiate whirl) [72].

BHA whirl generally occurs in near vertical wells, washed out boreholes, unstabilized BHA sections, pendulum assemblies, and when mud lubricity is not appropriate [72].

2.3.4 Remedial Action

Once bit whirl has been identified the potential cures are to increase WOB and decrease RPM. Other solutions are to use "anti – whirl" bits that have been modified for both enhanced stability and direction, and full-gauge new balance (NB) stabilizer [21, 68].

The potential treatments for BHA whirl are to increase WOB and decrease RPM. Other solutions for eliminating BHA whirl are to use a stiffer BHA, roller reamers and packed assemblies; and increase mud lubricity [68, 72].

2.4 Vibration Coupling

Vibrations of all three types (axial, torsional, and lateral) may occur during rotary drilling and are coupled. Bit whirl can be triggered by high bit speeds generated during stick-slip motion. Stick-slip can generate lateral vibration of the BHA as the bit accelerates during the slip phase. Large lateral vibration of the BHA into the well bore can cause bit-bounce. Induced axial vibrations at the bit can lead to lateral vibrations in the BHA, and axial and torsional vibrations observed at the rig floor may actually be related to severe lateral vibrations down hole near the bit. Bit whirl can induce BHA whirl and vice-versa. Bit torsional vibration can induce BHA torsional vibration and vice-versa [20, 70].

2.5 Shock and Vibration Failures

During rotary drilling, shock (which is an excitation over a relatively short duration) and vibration (which is an excitation over a relatively long duration) failures occur in the drillstring and drillbits. Figures 2.4 and 2.5 show the sketches of obvious and more extreme shock and vibration failures in drilling.

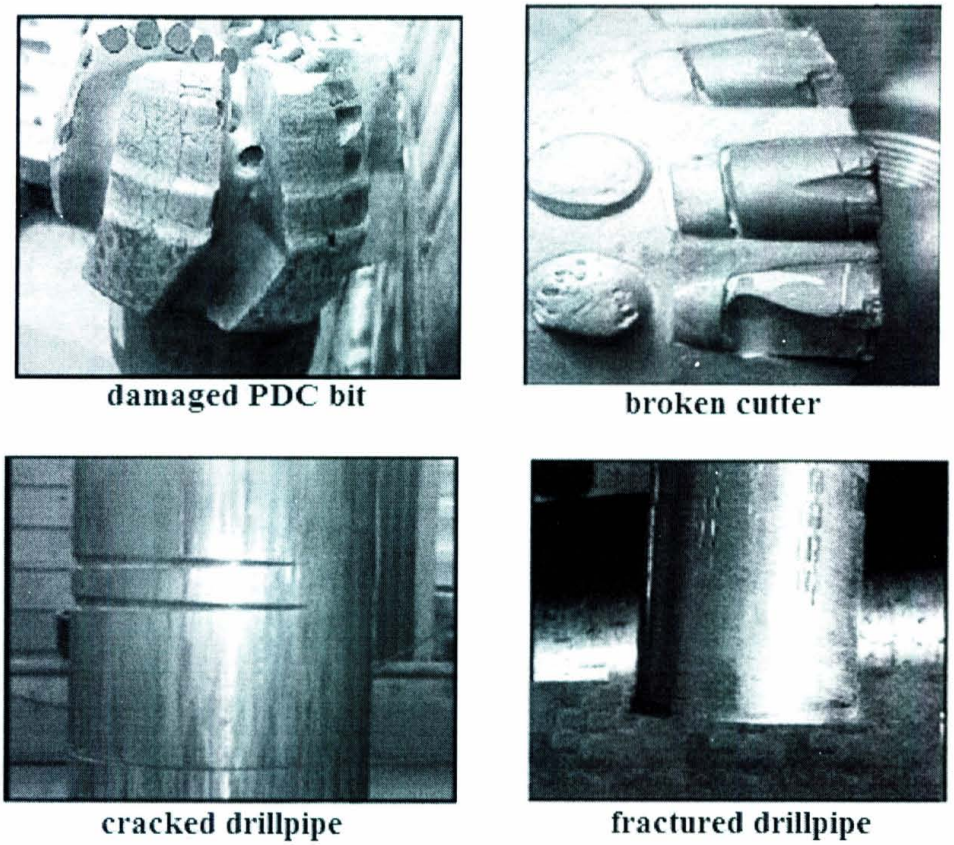

Figure 2.4: Sketches of obvious shock and vibration failures [61]

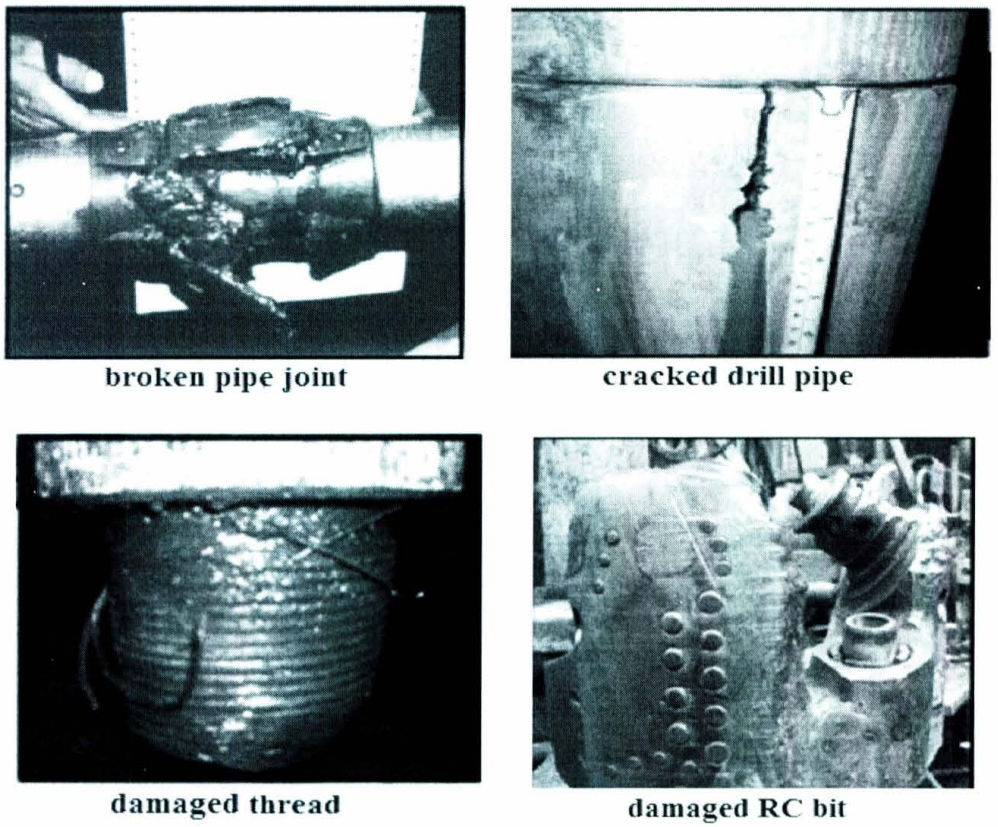

Figure 2.5: Sketches of more extreme shock and vibration damages [61]

This chapter has provided a brief description of drilling vibration together with various modes of vibration and their specific subsets or consequences, and the importance of research on these vibrations. It has also provided brief information about problems, sources and contributing factors, and remedial action of all modes of vibration. In the next chapter, a brief review of drilling model literature will be discussed together with limitation, significance, methodology and results of prior work.

CHAPTER 3

DRILLING MODELS LITERATURE REVIEW

A lot of work has been done in providing descriptions of, and explanations of various aspects of oilwell drilling by a rotary bit. Several dynamic formulations have been reported for investigating specific aspects of drillstring vibrational behavior but few of them have tackled stick-slip. One of the major difficulties in modeling stick-slip stems from the inaccurate description of some parameters and downhole boundary conditions.

Leine *et al.* [6] presented a stick-slip whirl model which consists of a submodel for the whirling motion and a submodel for the stick-slip motion. The stick-slip whirl model was a simplification of drilling confined in a borehole with drilling mud. Their model was a low-dimensional model and it aimed at explaining the basic nonlinear dynamic phenomena observed in downhole experiments. The model system was analyzed with the discontinuous bifurcations method which indicates physical phenomena such as dry friction, impact and backlash in mechanical systems or diode elements in electrical circuits which are often studied by means of mathematical models with some kind of discontinuity. The disappearance of stick-slip vibration when whirl vibration appears was explained by bifurcation theory. Stick slip was prevalent at low angular velocity and backward whirl was prevalent for high angular velocity, consistent with the measurements. They did not consider the effect of axial vibration and rock-bit interaction in the model.

Christoforou and Yigit [24-27] used a simple dynamic model to simulate the effects of varying operating conditions on stick-slip and bit bounce interactions. Figure 3.1 was considered as a necessary geometry for modeling the system. The equations of motion of such a system were developed by using a simplified lumped parameter model with only one compliance. One assumption in their model was that the rotary table is driven by an armature controlled DC motor through a gearbox (Figure 3.1). This model did not account for the effect of higher modes, the flow inside and outside the drillpipe and collars, or complicated cutting and friction conditions at the bit/formation interface.

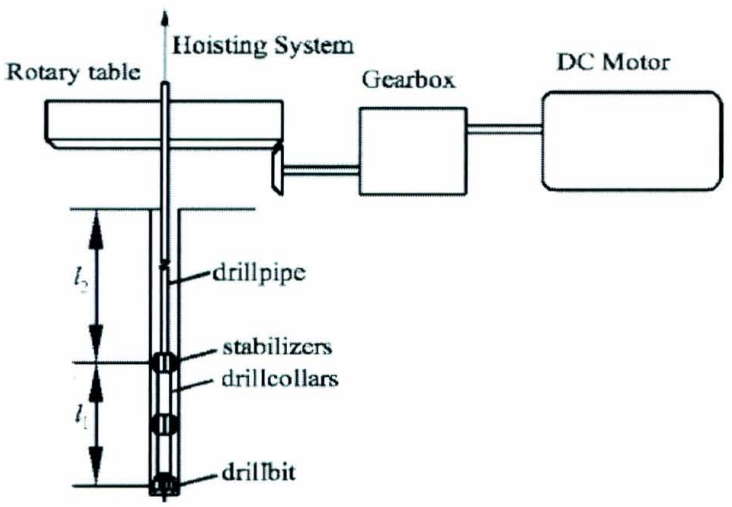

Figure 3.1: Christoforou and Yigit model schematic [24]

Richard *et al.* [28-30] studied the self-excited stick-slip oscillations of a rotary drilling system with a drag bit, using a discrete model which takes into consideration the axial and torsional vibration modes of the bit. Coupling between these two vibration modes took place through a bit-rock interaction law which accounted for both frictional

contact and cutting processes at the bit-rock interface. Figure 3.2 shows their simplified model of a drilling system, where Ω_0, Ω, H, C, M, I, T and W are the steady-state angular velocity, bit angular velocity, hook load, torsional stiffness of the drillpipe, mass of BHA, moment of inertia of BHA, TOB, and WOB. The cutting process introduced a delay in the equations of motion which was ultimately responsible for the existence of self-excited vibrations, exhibiting stick-slip oscillations under certain conditions. One of the limitations of their model is that the simulation stops when the bit lifts off. Furthermore, their model reduced the drillstring to a two degree of freedom system and they were working to capture more modes of vibration.

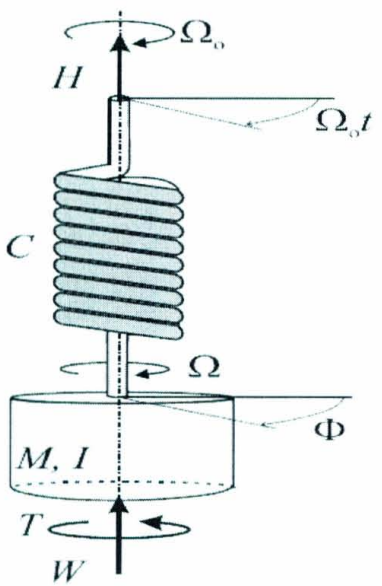

Figure 3.2: Simplified model of a drilling system from Richard *et al.* [30]

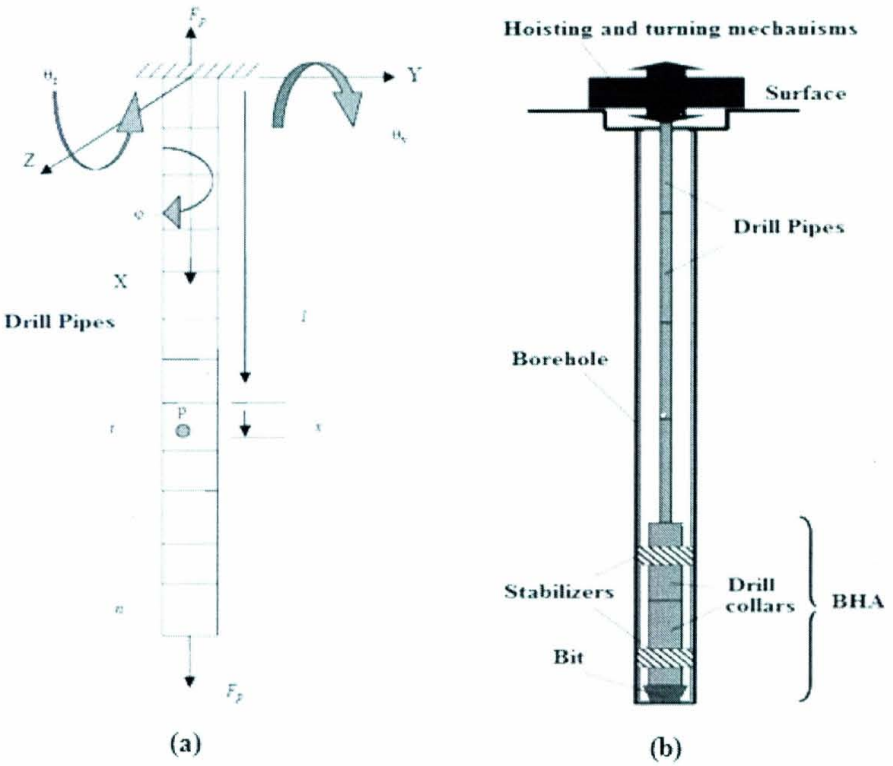

Figure 3.3: Khulief *et al.*: (a) Drillpipe under tension [31]. (b) A typical drillstring configuration [32]

Khulief *et al.* [31-33] formulated a dynamic finite element model of the drillstring including the drill pipes and drill collars. A typical drillstring configuration (Figure 3.3(b)) was used in their model. Drill pipe under tension was applied in their model (Figure 3.3 (a)). The model accounted for the torsional-bending inertia coupling and the axial-bending geometric nonlinear coupling. In addition the model accounted for the gyroscopic effect, the effect of the gravitational force field, and stick-slip interaction forces. Complex modal transformations were applied and reduced-order models were obtained. The finite element formulation was then integrated into a computational scheme [33]

for calculating the natural frequencies of the whole drillstring. The computational scheme was extended further to integrate the equations of motion, either in the full-order or the reduced-order form, to obtain the dynamic response. MATLAB was used as a simulation tool. They did not consider hydrodynamic damping, due to drilling fluid circulation in the drill pipe and the annular space. Stick-slip interaction produced a coupling between axial and torsional vibration, but [27] did not include any discussion of the complex effect of bit rotary speed and threshold force on torque on bit (TOB).

Bailey and Finnie [17] discussed longitudinal and torsional vibrations in a drillstring consisting of drill pipe and collars, and the boundary conditions at the ends of the string. For longitudinal motion, a spring-mass system at the top of the string was taken as a boundary condition (Figure 3.4) and for torsional motion, the top boundary condition was taken as a fixed end. At the bottom of the string, a fixed boundary condition was taken for longitudinal motion and free boundary condition was taken for torsional motion. Only longitudinal and torsional vibrations of the string were considered in their analysis. Lateral motions of the string (due to bending, buckling, whirling, whipping, and so on) were neglected, and it was assumed that the torsional and longitudinal motions considered were independent. In their analysis, they did not discuss a bit-rock model or coupling between axial and torsional vibration modes. Also, the derived differential equations were based on a simplified lumped model, and they ignored hydrodynamic damping due to drilling mud flow into the drillstring and viscous damping in their analysis. Their analysis was limited to finding natural frequencies and the

influence of various parameters on the natural frequencies. They did not discuss stick-slip and bit-bounce vibrations.

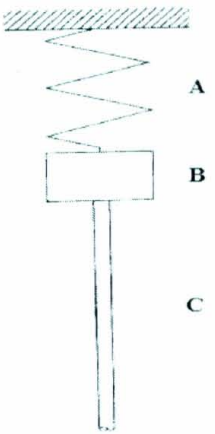

Figure 3.4: Bailey and Finnie: Idealized model of equipment at top end of string: (A) Spring representing derrick and drilling lines; (B) Mass representing traveling block, swivel, and hook; and (C) Rod representing drillstring [17].

Kyllingstad and Halsey [12] presented a mathematical model of stick-slip motion. Their model included parameters describing downhole friction effects and a simplified description of the drillstring. The limitation of their model is that it does not predict whether stick-slip motion will or will not occur under a given set of conditions. Their model does not give any information about a rock-bit interaction model. Also it does not have coupling between axial and torsional vibration, or hydrodynamic damping due to drilling mud flow into the drillstring.

Challamel *et al.* [34] discussed bit stick-slip motion by using rock mechanics considerations coupled with field bottom hole data. They collected data for an instrumented PDC bit. Their analytical equations for TOB (φ) depends on ROP and bit

rotation speed data. They considered the drilling structure as a beam in torsion and represented the BHA as a lumped inertia for simplification. The rotary speed (at the top of the drillstring) was fixed at a constant value. The other extremity (at the bottom of the drillstring), which symbolizes the bit, was subjected to a torque, depending on bit speed (and eventually position). Figure 3.5 shows the torsional model of the drillstring structure that was taken in to consideration for the model in [34], where φ, L, L_0, Ω and t indicate TOB, length of drillpipe, length of BHA, rotary speed and time respectively. Their drillstring model is limited to torsional modes. They included the instantaneous ROP and bit rotation data in their TOB equation, which was the input at the bottom of drillstring for torsional model, but they did not clearly discuss the ROP equation; and the effect of WOB and bit rotation on ROP prediction. Their model does not have the effect of hydrodynamic damping due to drilling mud. Finally, in a real case, WOB fluctuates during drilling. It has an effect on TOB which was not accounted for in [34].

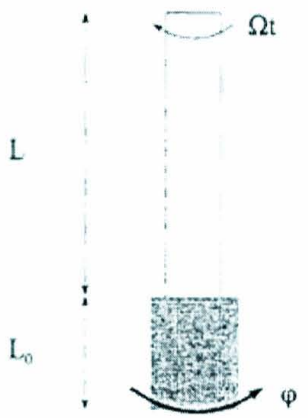

Figure 3.5: Challamel *et al.*: Torsional model of the drillstring structure [34]

Aarrestad and Kyllingstad [35] studied a mechanism that couples longitudinal and torsional drillstring vibrations at the bit (RC bit). They discussed bit-formation interaction, and compared the model results with full scale experimental results. In their results, they did not show the stick-slip and bit-bounce phenomena. Also their mathematical model was simplified. Finally they did not consider hydrodynamic damping due to drilling mud and viscous damping in their model.

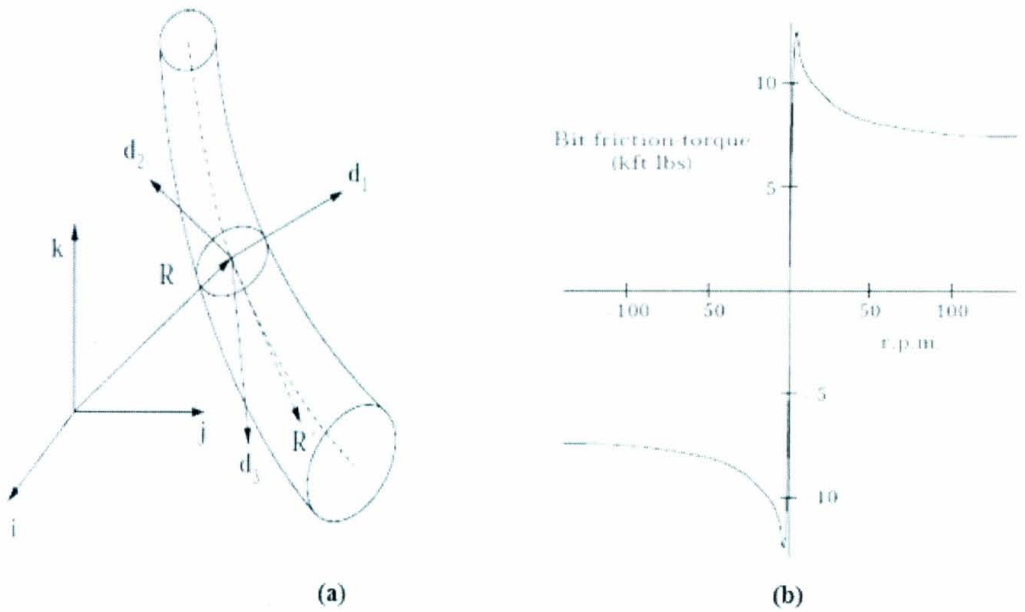

Figure 3.6: Tucker and Wang: (a) Motion of a drill-string segment. (b) Frictional behavior curve in a typical field operation [36]

Tucker and Wang [36] developed an integrated model for drillstring dynamics. Their model had a coupling between axial, torsional and lateral modes. They have considered six continuous independent degrees of freedom in the model (Figure 3.6 (a)).

Three located the position of the centroid of the drillstring in space and three permitted the dynamical state of the drillstring to be expressed in terms of flexural, torsional and shear strain, together with dilation and stretch. Their model provides axial motion along the length of the drillstring, torsional or rotational motion, and transverse or lateral motion. They have discussed appropriate boundary conditions for an active drillstring and BHA stabilizer including an account of frictional simulations at the rock-interface, cutter simulations for different types of drill bit and interactions between the bore cavity and the drillstring. The profile in Figure 3.6, simulating the friction torque experienced in a typical field operation, was applied in their model. They ignored drilling mud circulation effect in their model. Also, in their simulation results, they did not discuss stick-slip and bit-bounce vibration.

Dareing and Livesay [37] developed computer programs based on the theory for analyzing longitudinal and angular drillstring vibration. Forces act at the top of the drillstring and were, therefore, considered part of the drillstring boundary conditions. Cable spring and mass for the kelly, swivel and traveling block were assumed at the top of the drillstring. The source that excites the drillstring was assumed to act at the bit. A three cone RC bit was used in the study. The motion of the bit was assumed to be sinusoidal and the influence of the rock in contact with the bit was ignored. The schematic of the drillstring used in their model is shown in Figure 3.7. For the sake of simplicity, the effect of different types of friction such as fluid, rubbing and material, which act along the string, was approximated by viscous friction. Finally in their simulation results they did not show any stick-slip and bit-bounce vibrations.

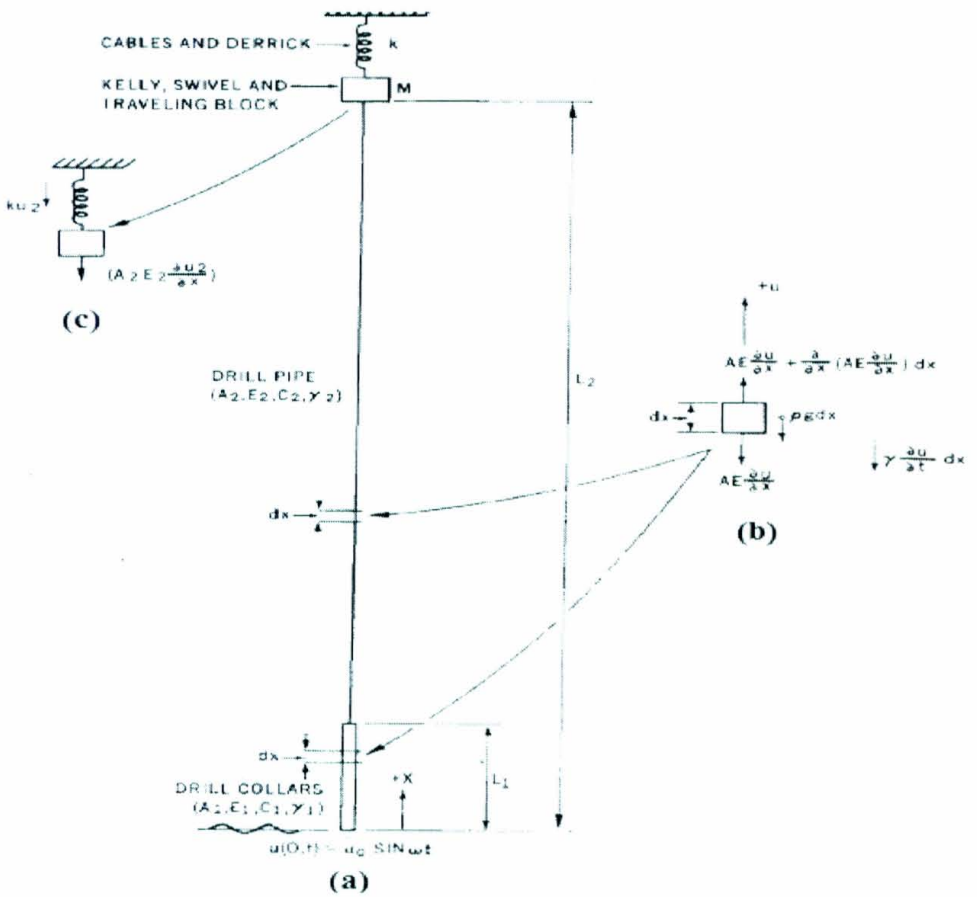

Figure 3.7: Dareing and Livesay schematic of drillstring [37]

Eronini *et al.* [3] developed a rock drilling model as a set of ordinary differential equations describing discrete segments of the drilling rig, including the bit and the rock. The end segment of their model consists of a description of the bit as a nonlinear transformer and a characterization of the rock behavior. Figure 3.8 shows the lumped model of the surface segment. This model includes the effect on rock drilling of bottom hole cleaning, drill string-borehole interaction, and tooth wear. The specialty of their

model was that it predicted the expected relationships between drilling rate and the quantities WOB, differential mud pressure, and rotary speed. Hydrodynamic damping was taken in their longitudinal vibration model instead of taking viscous damping. Pulsation in the mud flow was taken in the model making. Finally, their rock-bit model is applicable only for RC bits. In their results, they did not mention stick-slip and bit-bounce vibrations.

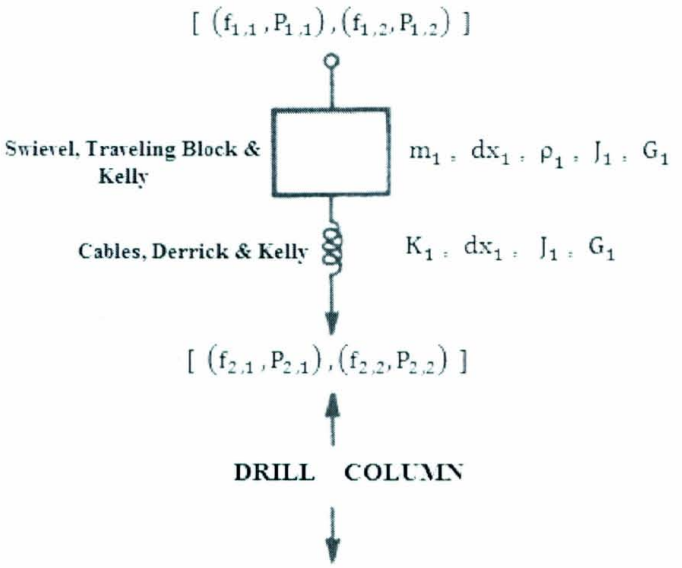

Figure 3.8: Lumped model of surface segment [3]

None of the above models describes a complete stick-slip and bit-bounce phenomenon in their results. From a review of the available literature, it can be assumed that the analysis of the stick-slip phenomenon is numerically challenging, because the static and kinetic friction mechanisms normally result in discontinuities in the dynamic model. Yigit and Christoforou [24-27] discussed a reasonable rock-bit model for a single

cutter PDC bit. A modified form of this rock-bit model will be discussed in the next chapter.

A few models of drillstring stick-slip were based on a single degree of freedom torsional pendulum [24-30], wherein a rigid body with constant mass and moment of inertia was used to model BHA and a linear spring to model the drillstring. Although, the simple models in [24-30] provided some insight into stick-slip and bit-bounce phenomenon, they ignored the continuum nature of the drillstring. Khulief *et al.* [31-33] introduced high order finite element dynamic model and this model does not have any discussion about the complex effect of bit rotary speed and threshold force on TOB. In the next chapter a lumped-segment approach [34-35] will be discussed for making axial and torsional models with multiple modes. Previous works shows the importance of developing a coupling multi-mode model instead of a single mode model. Coupling between axial and torsional vibrations will also be discussed in the next chapter.

CHAPTER 4

OILWELL DRILLSTRING DYNAMIC MODEL

The system being modeled consists of drill pipes, the drill collar assembly (made up of heavier collar pipes), the drill bit at the end of the collar assembly and the rock (formation). Drilling fluid is circulated in the drill pipe and the annular space between the drill pipe and the well bore. The drilling fluid is characterized by the flow rate developed by the mud pumps. The top of the drillstring is subject to a tension force, applied through the surface cables. Rotary motion is applied by an armature-controlled motor, through a gearbox, to the rotary table via the kelly (a square, hexagonal or octagonal shaped tubing that is inserted through and is an integral part of the rotary table that moves freely vertically while the rotary table turns it). In this study, a DC motor with winding inductance and resistance is assumed. The essential components of the oilwell drilling system and the necessary geometry used for the model are shown in Figure 1.1. A lumped-segment approach [39-40] is used in the axial and torsional dynamic models. In the lumped segment approach, the system is divided into a number of elements, interconnected with springs. This method is a more cumbersome bond graph representation and the accuracy of the model depends on the number of elements considered, however, analytic mode shapes and natural frequencies need not be determined. A physical schematic of the lumped-segment models is shown in Figure 4.1.

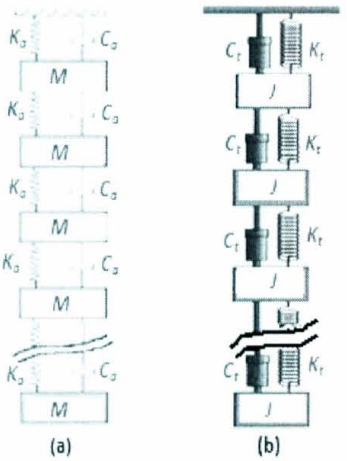

Figure 4.1: Physical schematic of (a) axial segments and (b) torsional segments

4.1 Bond Graph Overview

Bond graphs are an explicit graphical tool for capturing the common energy structure of systems and can increase one's insight into system behavior. In the vector form, they give concise description of complex systems. Moreover, the notation of causality provides a tool not only for formulation of system equations, but also for intuition – based discussion of system behavior, viz. controllability, observability, fault diagnosis, etc. [63]

Bond graphs were introduced by Henry M. Paynter, professor at MIT & UT Austin, who, with introduction of the junctions in April 1959, concluded a period of about a decade in which most of the underlying concepts were formed and put together into a conceptual framework and corresponding notation. In the 1960's the notation, e.g. the half arrow to represent positive orientation and insightful node leveling, was further elaborated by his students, in particular Dean C. Karnopp, later professor at UC Davis,

and Ronald C. Rosenberg, later professor at Michigan State University who also designed the first computer tool (ENPORT) that supported simulation of bond graph models. In the early seventies Jan J. van Dixhoorn, professor at the University of Twente, NL and Jean U. Thoma (1975) professor at the University of Waterloo, Ont. were the first to introduce bond graphs in Europe [62].

These pioneers in the field and their students have been spreading these ideas worldwide. Jan van Dixhoorn realized that an early prototype of the block-diagram-based software TUTSIM could be used to input simple casual bond graphs, which, about a decade later, resulting in a PC-based tool. This laid the basis for the development of the truly port-based computer tool 20-sim at the University of Twente [38]. He also initiated research in modeling more complex physical systems, in particular thermofluid systems.

In the last three decades bond graphs either have been a topic of research or are being used in research at many universities worldwide and are part of (engineering) curricula at a growing number of universities. In the last two decade industrial use has become more and more important [62].

4.1.1 Power Variables of Bond Graphs

The language of bond graphs expresses a general class of physical systems through power interactions. The factors of power i.e., effort and flow, have different interpretations in different physical domains. Yet, power can always be used as a generalized quantity to model coupled systems residing in several energy domains. For example, an electrical motor driving a hydraulic pump, or a thermal engine connected with a muffler; in both systems the form of energy varies within the system. Power

variables of a bond graph may not be always realizable (viz. in bond graphs for economic system); such factual power is encountered mostly in non-physical domains and pseudo bond graphs [63, 39]. In the following table 4.1, effort and flow variables in some physical domains are listed.

Table 4.1: Domains with corresponding flow, effort, generalized displacement and generalized momentum [62]

	f *flow*	E *effort*	$q = \int f\,dt$ *generalized displacement*	$p = \int e\,dt$ *generalized momentum*
Electromagnetic	i current	U voltage	$q = \int i dt$ charge	$\lambda = \int u dt$ magnetic flux linkage
mechanical translation	V velocity	F force	$x = \int v dt$ displacement	$p = \int F dt$ momentum
mechanical rotation	ω angular velocity	T torque	$\theta = \int \omega dt$ angular displacement	$b = \int T dt$ angular momentum
hydraulic/ pneumatic	φ volume flow	P pressure	$V = \int \varphi dt$ volume	$\Gamma = \int p dt$ momentum of a flow tube
Thermal	T temperature	F_S entropy flow	$S = \int f_S dt$ entropy	
Chemical	μ chemical potential	F_N molar flow	$N = \int f_N dt$ number of moles	

4.1.2 Bond Graph Standard Elements

In bond graphs, one needs to recognize only four groups of basic symbols, i.e., three basic one port passive elements, two basic active elements and two basic junctions.

The basic variables are effort (e), flow (f), time integral of effort (P) and the time integral of flow (Q).

4.1.2.1 Basic 1-port elements

A 1-port element is addressed through a single power port, and at the port a single pair of effort and flow variables exists. Ports are classified as passive ports and active ports. The basic ports are idealized elements because they contain no sources of power. The inertia or inductor, compliance or capacitor, and resistor or dashpot are classified as passive elements [39].

R-elements

The 1-port resistor is an element in which the effort and flow variables at the single port are related by a static function. Usually, resistors dissipate energy. This must be true for simple electrical resistors, mechanical dampers or dashpots, porous plugs in fluid lines, and other analogous passive elements. The bond graph symbol for the resistive element is shown in Figure 4.2.

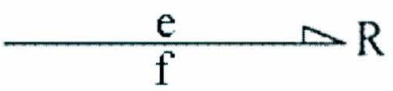

Figure 4.2: Bond graph symbol for resistive element

The half arrow pointing towards *R* means that the power i.e., product of *F* and *V* (or *e* * *f*) is positive and flowing into *R*, where *e*, represents effort or force, and *f*, represents flow or velocity. The constitutive relationship between e, f and *R* is given as:

$$e = R * f \quad (1)$$

Power = $e * f = R * f^2$ (2)

C-elements

Consider a 1-port device in which a static constitutive relation exists between an effort and a displacement. Such a device stores and gives up energy without loss. In bond graph terminology, an element that relates effort to the generalized displacement (or time integral of flow) is called a one port capacitor. In physical terms, a capacitor is an idealization of devices like springs, torsion bars, electrical capacitors, gravity tanks, and accumulators, etc. The bond graphic symbol, defining constitutive for C-element is shown in Figure 4.3.

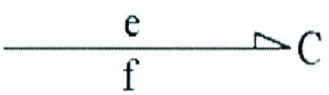

Figure 4.3: Bond graph symbol for capacitive element

In a spring, the deformation (Q) and the effort (e) at any moment is given by,

$Q = \int_{-\infty}^{t} f \, dt,$ (3)

$e = k \int_{-\infty}^{t} f \, dt$ (4)

Here, flow is the cause and deformation (and hence effort) is the consequence.

I-elements

A second energy storing 1-port arises if the momentum, p, is related by a static constitutive law to the flow, f. Such an element is called an inertial element in bond graph terminology. The inertial element is used to model inductance effects in electrical systems

and mass or inertia effects in mechanical or fluid systems. The bond graph symbol for an inertial element is depicted in Figure 4.4.

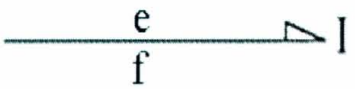

Figure 4.4: Bond graph symbol for inertial element

If the mechanics of a point mass are examined by considering the impulse-momemtum equation, then it can be written as

$$P = \int_{-\infty}^{t} e\, dt, \tag{5}$$

$$f = m^{-1} \int_{-\infty}^{t} e\, dt \tag{6}$$

Here effort is the cause and velocity (and hence momentum) is the consequence.

4.1.2.2 Effort and flow sources

The active ports are those which give reaction to the source. For example, if we step on a rigid body, our feet react with a force or source. For this reason, sources are called active ports. Force is considered as an effort source and the surface of a rigid body gives a velocity source. They are represented as a half arrow pointing away from the source symbol. The effort and flow source can be represented as

Figure 4.5: Bond graph symbol for effort source

Figure 4.6: Bond graph symbol for flow source

4.1.2.3 Basic 2-port elements

There are only two kinds of two port elements, namely "Transformer" and "Gyrator". The bond graph symbols for these elements are TF and GY, respectively. As the name suggests, two bonds are attached to these elements.

The Transformer

The bond graphic transformer can represent an ideal electrical transformer, a mass-less lever, etc. The transformer does not create, store or destroy energy. It conserves power and transmits the factor of power with proper scaling as defined by the transformer modulus. Bond graph representation for a transformer is shown in Figure 4.7.

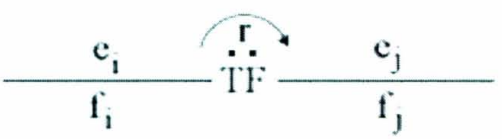

Figure 4.7: Bond graph representation for transformer [63]

The *r* above the transformer denotes the modulus of the transformer, which may be constant or any expression. The small arrow represents the sense in which this modulus is to be used.

$$f_j = r * f_i \text{ , and } e_j = (\frac{1}{r}) * e_i. \tag{7}$$

Thus the following expression establishes the conservation of power,

$$e_j f_j = e_i f_i \tag{8}$$

The Gyrator

A transformer relates flow-to-flow and effort-to-effort. A gyrator establishes relationship between flow-to-effort and effort-to-flow, again maintaining the power on the ports. The simplest gyrator is a mechanical gyroscope. The bond graph representation for a gyrator is shown in Figure 4.8.

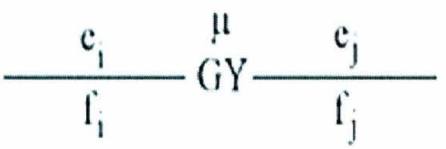

Figure 4.8: Bond graph representation for gyrator [63]

The μ above the gyrator denotes the gyrator modulus. This modulus does not have a direction sense associated with it. This modulus is always defined from flow to effort.

$$e_j = \mu * f_i, \quad e_i = \mu * f_j. \tag{9}$$

Thus the following expression establishes conservation of power,

$$e_i f_i = e_j f_j \tag{10}$$

4.1.2.3 The 3-port junction elements

The name 3-port used for junctions is a misnomer. In fact, junctions can connect two or more bonds. There are only two kinds of junctions, the 1 and the 0 junction. They

conserve power and are reversible. They simply represent system topology and hence the underlying layer of junctions and two-port elements in a complete model (also termed the junction structure) is power conserving.

1-junction

The flows on the bonds attached to a 1-junction (Figure 4.9) are equal and the algebraic sum of the efforts is zero. The signs in the algebraic sum are determined by the half-arrow directions in a bond graph.

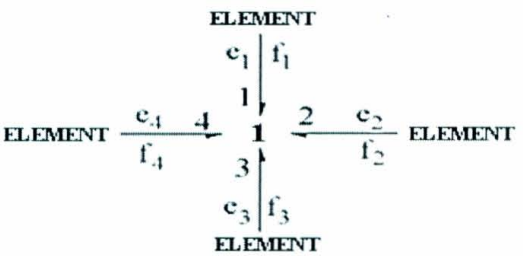

Figure 4.9: Example for 1-junction [63]

According to rules it can be written as:

$$f_1 = f_2 = f_3 = f_4 \text{ and } e_1 + e_2 + e_3 + e_4 = 0 \quad (11)$$

0-junction

The efforts on the bonds attached to a 0-junction (Figure 4.10) are equal and the algebraic sum of the flows is zero. The signs in the algebraic sum are determined by the half-arrow directions in a bond graph.

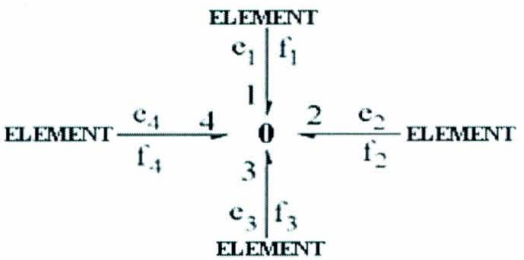

Figure 4.10: Example for 0-junction [63]

According to rules it can be written as:

$$e_1 = e_2 = e_3 = e_4 \text{ and } f_1 + f_2 + f_3 + f_4 = 0 \tag{12}$$

4.1.3 Power Directions on the Bonds

In the analysis of a simple problem of mechanics, for example, a single mass and spring system as shown in the Figure 4.11, one initially fixes a co-ordinate system. A positive displacement, x, may be defined towards right and all its time derivatives are then taken positive towards the right. The force acting on the mass may also be defined positive towards the right. The system, however, in the course of motion may attain such a state that when it is displaced towards the right, the force on the mass happens to be towards the left [63, 39].

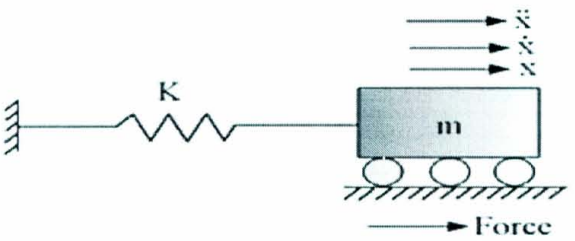

Figure 4.11: Single mass spring system [63]

Bond graphs are drawn for general systems. One has to create a view point which is general and any particular system interpretation should be easily derivable. This is done by assigning the bonds with power directions. For example, a bond graph considers where the power is directed as shown in Figure 4.12; J, E, and half arrow are the junction, element, and direction of power. This assignment means, such variables are chosen for effort and flow, so that whenever the products of these variables is positive, then the power goes from J to E [63, 39].

Figure 4.12: Example of power direction [63]

4.1.4 Causality

The causal stroke, a small stroke normal to one end of a bond, determines the input-output structure of the mathematical equations of the connected elements. A causal stroke adjacent to an element means that the effort variable of the power bond is the input to the constitutive law of that element. The effort input is then manipulated by the element to produce flow as an output. If a causal stroke is not adjacent to an element, then its constitutive law is to be arranged such that flow is an input, and effort is the output. Figure 4.13 shows two generalized elements with constitutive laws expressed in a manner consistent with the causal stroke location.

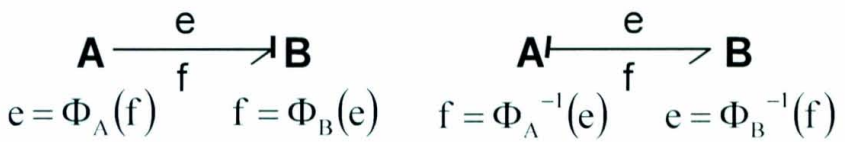

Figure 4.13: Implications of causal stroke for element constitutive laws

Multi-port elements such as TF, GY, and 1- and 0-junctions have causality restrictions. For example, if a transformer law multiplies *port 1* effort by a modulus to create *port 2* effort, then it must also take *port 2* flow and multiply it to create *port 1* flow. Figure 4.14 shows two allowable TF element causalities along with associated constitutive laws.

Figure 4.14: Example of causality restriction for TF element

The 1-junction, since all flows are equal, must have its flow defined by only one connected element. Thus, there can be only one bond at a 1-junction with no adjacent causal stroke. For a 0-junction, only one connected element can define the effort, meaning that only one bond can have a causal stroke adjacent to the junction. Figure 4.15 shows 1- and 0-junctions with constitutive laws consistent with the placement of the causal strokes.

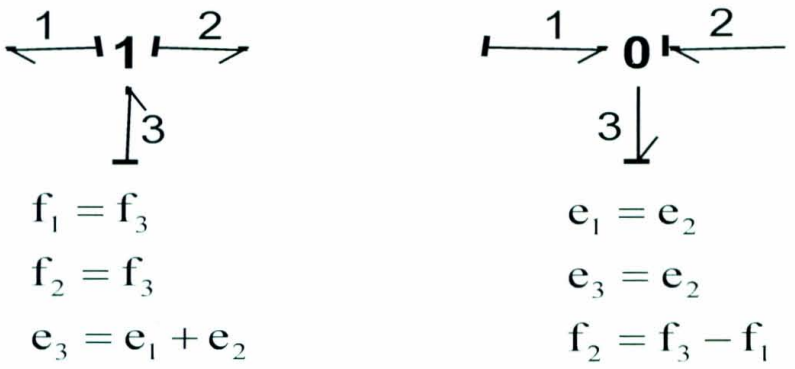

Figure 4.15: Junction constitutive laws consistent with causal strokes

This section has provided a brief history of bond graph method. It has also provided a brief description of bond graph standard elements, power directions on the bonds, and causality. In the next sections, the formulation of a dynamic model of an oilwell drillstring by using the bond graphs method will be discussed.

4.2 Modeling of Axial Dynamics

The main elements in a conventional vertical drillstring that are considered in this model are shown in Figure 4.16. From the figure, five kinds of elements are distinguished: the top rotary system; kelly (Figure 4.17), drill pipes and collars (Figure 4.19) modeled as linear springs of longitudinal stiffness and longitudinal damping; and the bit. Figure 4.16 (a) shows the drilling mud flow in the drilling system; the mud flow inside the drillstring is downward and for the annulus the flow is upward. The terms V_P and V_a in Figure 4.16 (a) indicate drilling mud velocity inside the drill pipe and the annulus, respectively. For the drill collar modeling the values of V_P and V_a will be different, because they depend on the drill pipe/collar and wellbore geometry. The

calculations of these velocities are shown in Appendix E. Figure 4.20 shows the schematic of a drill pipe/collar axial segment model and the FBD of a drill pipe/collar axial segment.

A total of 21 segments are used in the dynamic model to capture the first eight axial natural frequencies of the whole drillstring and the selection of the number of segments will be discussed in a later section. One segment is used for the relatively short kelly, and the kelly model is shown in Figure 4.18. For both drill pipe and collar, 10 segments are used in the model, and a drill pipe/collar bond graph model segment is shown in Figure 4.21. Hydraulic forces are included at the top of the drill collar and bottom of the drillstring to capture the effect of drilling mud density. The calculations of these hydraulic forces are shown in Appendix E. As discussed in the next section, the hydrodynamic damping due to drilling fluid circulation in the drill pipe and the annular space is considered in the drill pipe and collar model instead of viscous damping [3].

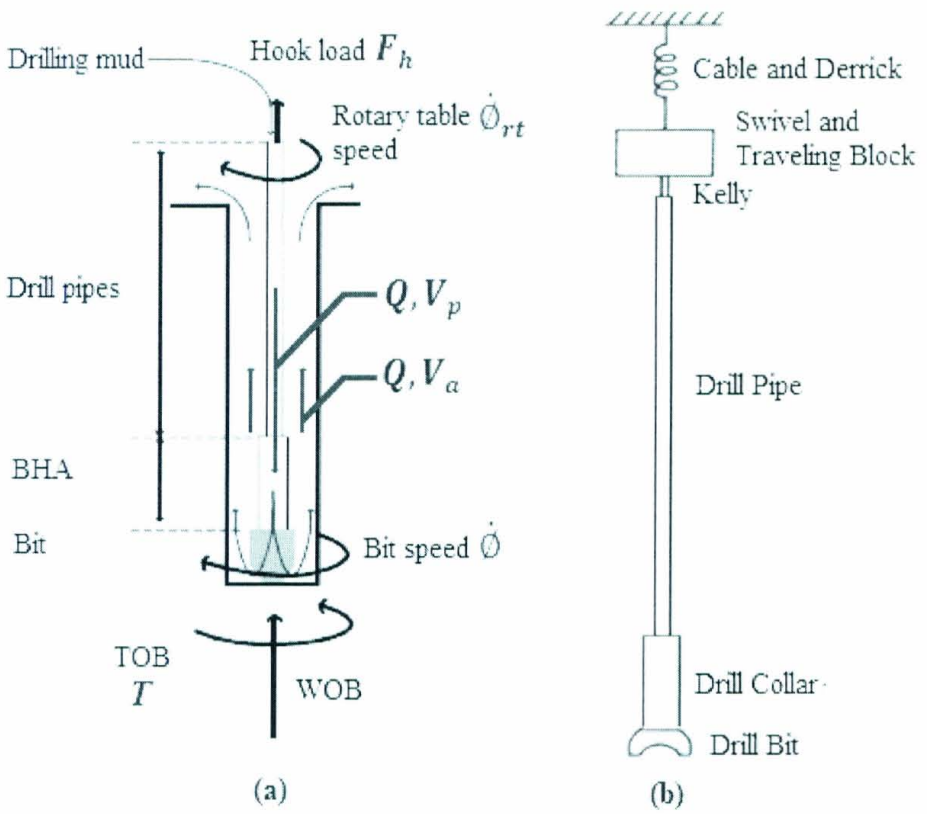

Figure 4.16: (a) A conventional vertical drillstring [1]. (b) Schematic of drillstring used in rotary drilling modeling and simulation.

4.2.1 Fluid Drag Force/Damping for Axial Model

Nonlaminar Newtonian flow formulations are used in calculation of fluid drag force/damping for the axial model. These result in simple expressions which may also approximate laminar flow conditions provided appropriate values of the pertinent variables are used. Figure 4.16 (a) shows the drilling mud flow in a conventional vertical

drillstring. Ignoring any eccentric location of the drill string in the wellbore, the pressure drop in the annulus between the borehole and a stationary drill pipe can be written as [3]

$$\Delta P = \frac{\alpha_a \, \rho_m \, Q^2 \, dx}{4 \, \pi^2 \, (r_w - r_0) \, (r_w^2 - r_0^2)^2} \tag{13}$$

where α_a = Weisbach friction factor; outside drill pipe or collar

ρ_m = drilling mud density

Q = volume rate of flow of drilling mud

dx = drill pipe or collar segment length

r_w = wellbore radius

r_0 = external radius of drillpipe or collar

The resulting longitudinal force, F_A (positive down) exerted on the drillstring segment which is moving with velocity V_n can be written as below [3]

$$F_A = -\left\{\frac{\alpha_a \, \rho_m \, \pi \, (r_w + r_0) \, dx}{4}\right\} \left|\left[\frac{Q}{\pi \, (r_w^2 - r_0^2)}\right] + V_n\right| \left\{\left[\frac{Q}{\pi \, (r_w^2 - r_0^2)}\right] + V_n\right\} \tag{14}$$

And the drag force on the drillstring due to flow in the drillpipe is given by [3]

$$F_p = -\left\{\frac{\alpha_p \, \rho_m \, \pi \, r_i \, dx}{4}\right\} \left|\frac{Q}{\pi \, r_i^2} - V_n\right| \left\{\frac{Q}{\pi \, r_i^2} - V_n\right\} \tag{15}$$

Where, α_p = Weisbach friction factor; inside drill pipe or collar

r_i = internal radius of drillpipe or collar

Equations (14) and (15) are applied to the axial model (Fig. 4.17) for adding the effect of drilling fluid (mud) on drillstring dynamic response. From Figure 4.20, when segment i moves with a velocity V_i downward then the inertia force $M_i \dot{V}_i$ will be upward, the drag

forces F_A and F_P ($V_p > V_i$) will be upward and downward respectively, and the weight M_i g will be always downward.

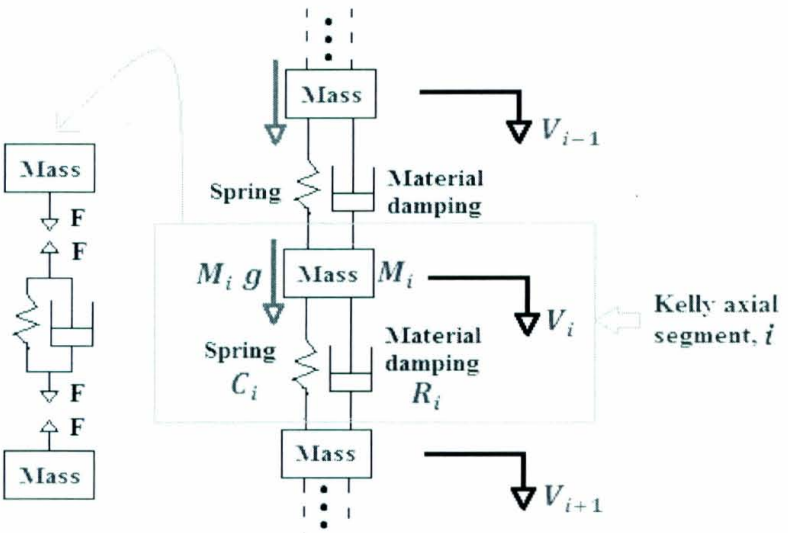

Figure 4.17: Schematic of kelly axial segment

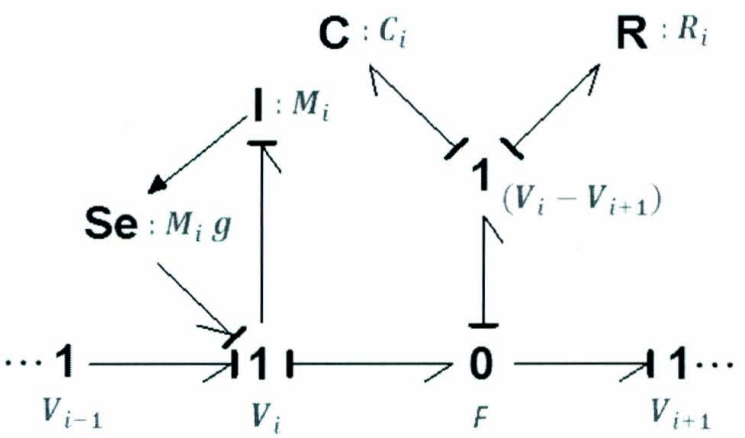

Figure 4.18: Bond graph axial model segment of kelly

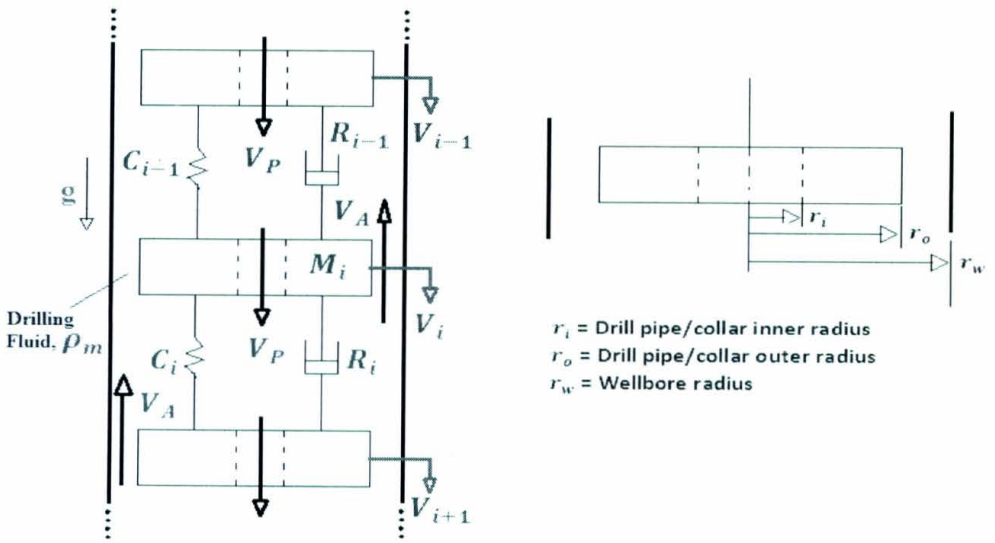

Figure 4.19: Schematic of drill pipe/collar lumped segment model showing drilling fluid (mud) flow.

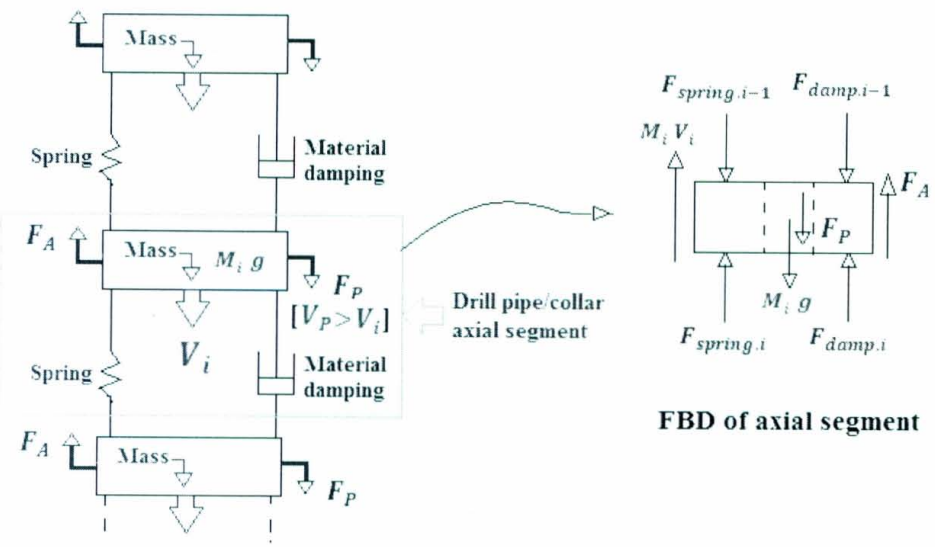

Figure 4.20: Schematic of drill pipe/collar axial segment model.

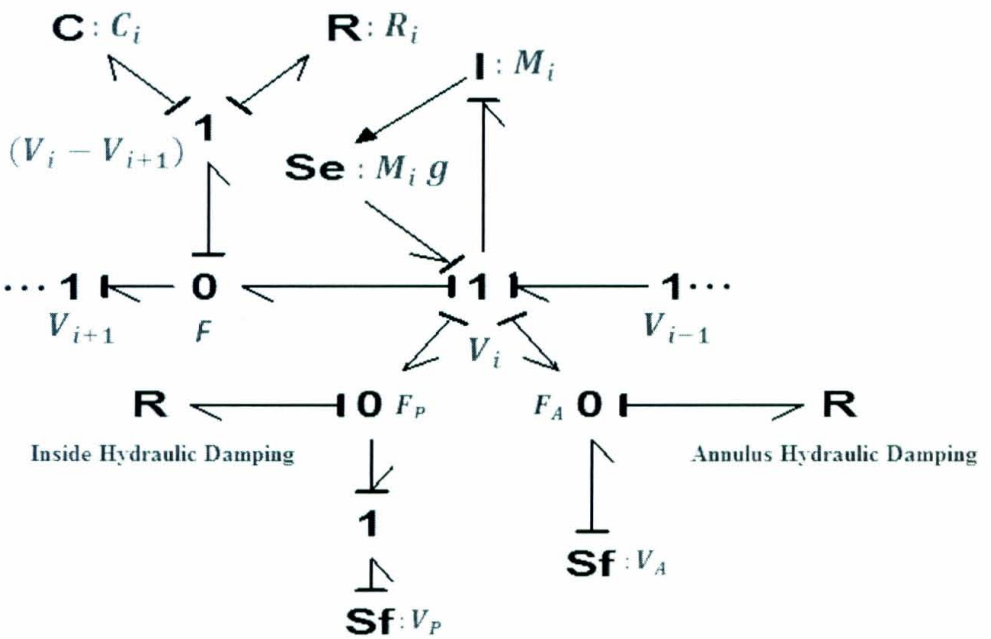

Figure 4.21: Bond graph axial model segment of drill pipe/collar

4.3 Modeling of Torsional Dynamics

Similarly, a total of 21 segments are used in the dynamic model to capture the first eight torsional natural frequencies of the whole drillstring. The number of segments for the kelly, drill pipe and drill collar is the same as in the torsional model. Figures 4.23 and 4.25 depict torsional dynamic submodels for kelly and drill pipe/collar segments. The schematic of kelly and drill pipe/collar torsional segment are shown in Figures 4.22 and 4.24, respectively. The drill pipe and drill collar dynamic models consider viscous damping which results from the contact between drillstring surfaces and drilling fluid [3]. With the exception of the details of fluid friction, the torsional model and bond graphs are rotational analog of the axial models.

4.3.1 Fluid Friction Resistance/Viscous Damping to Rotation

The schematic of rotational fluid friction resistance/viscous damping is shown in Figure 4.24. Again, ignoring any nonconcentric drillpipe location in the borehole, a simple expression for the fluid torque is given by [3, 25-27]

$$T_{R_n} = (R_{Viscous})_n \, dx_n \, \omega_n \tag{16}$$

where, $R_{Viscous}$ indicates viscous damping per unit length of drillpipe/collar and it can be written as [2, 20-22],

$$R_{Viscous} = \frac{2\pi \mu_e r_0^3}{r_w - r_0} \tag{17}$$

where, μ_e = equivalent viscosity for fluid resistance to rotation.

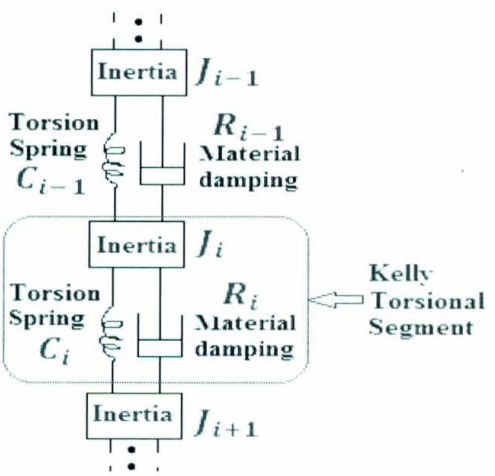

Figure 4.22: Schematic of kelly torsional segment

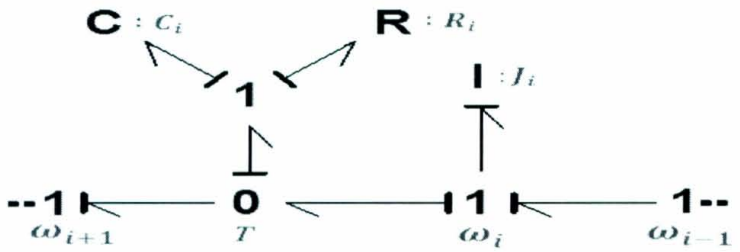

Figure 4.23: Bond graph torsional model segment of kelly

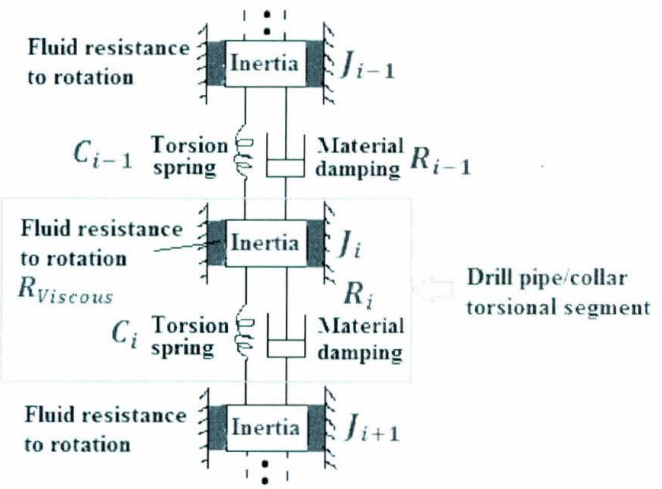

Figure 4.24: Schematic of drill pipe/collar torsional segment

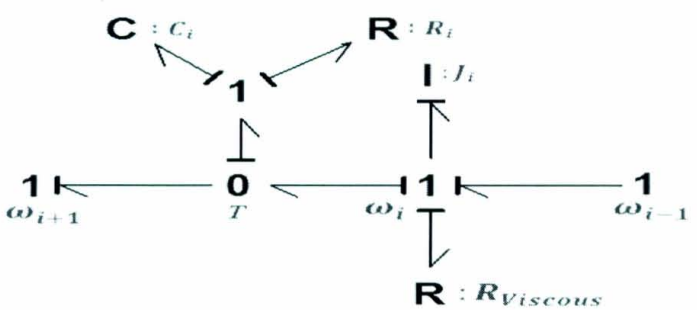

Figure 4.25: Bond graph torsional model segment of drill pipe/collar

4.4 Selection of Number of Segments in Modeling

In this study, a lumped segment approach is used in the axial and dynamic models and the accuracy of the model depends on the number of segments. If a system model is divided in to a large number of elements (segments) then the accuracy of the results will be very high compared to a low number of segments model. However, increasing the number of segment leads to larger simulation times. One must be an optimum number of segments to capture the appropriate system dynamics within suitable simulation times.

Tables 4.2 and 4.3 show the axial and torsional natural frequencies comparison results for different models. From the tables, it is clear that model-1, which has a total of 21 segments, produces comparable results to model-2 (55 segments), and model-3 (105 segments) for the first eight system natural frequencies.

Table 4.2: Natural frequency comparison table for axial model

Natural Frequencies of Axial Model					
Free B.C. at bit (off-bottom)			Fixed B.C. at bit (on-bottom)		
1+10+10 Model-1	5+30+20 Model-2	5+50+50 Model-3	1+10+10 Model-1	5+30+20 Model-2	5+50+50 Model-3
2.3	2.3	2.31	**7.7**	7.765	7.765
8.7	8.69	8.68	**15.1**	15.21	15.23
15.7	15.77	16.79	**20.5**	20.68	20.76
20.9	20.98	21.07	**25.1**	25.33	25.43
25.7	25.86	25.97	**31.8**	32.07	32.22
32.7	33.03	33.2	**37.9**	38.05	38.27
40.0	40.63	40.94	**42.1**	42.57	42.91
47.3	48.25	48.76	**48.0**	49.02	49.57
48.22	55.77	56.56	50.47	56.28	57.12
51.29	63.13	64.27	53.38	63.59	64.82
54.17	70.25	71.78	58.19	70.81	72.53
1+10+10 = **1** means number of kelly segment, **10** means number of drill pipe segment, **10** means number of drill collar segment.					

Table 4.3: Natural frequency comparison table for torsional model

Natural frequencies of Torsional Model		
Free B.C. at bit		
1+10+10 Model-1	5+30+20 Model-2	5+50+50 Model-3
1.2	1.154	1.152
5.3	5.301	5.302
10.1	10.14	10.15
14.9	15.04	15.08
19.8	19.93	20.02
24.4	24.77	24.95
28.9	29.55	29.86
33.3	34.24	34.73
36.34	38.83	39.54
40. 1	43.27	44.25
44.69	47.41	48.39

Up to eight correct natural frequencies are sufficient in this study, so model-1 is used. This model provides results that are comparable with field results, and also the simulation time is very fast compared with model-2 and model-3. Table 4.4 shows the simulation time comparison results for the models for a 50 seconds event.

Table 4.4: Simulation time comparison results for models

Models	Simulation time
Model-1	72 Sec
Model-2	204 Sec
Model-3	509 Sec

4.5 Coupling Between Axial and Torsional Dynamics

The bit-rock interaction provides coupling between axial and torsional drillstring dynamics. In this present work a quasi-static rock-bit model is used instead of a computationally intensive and difficult-to-parameterize complete dynamic representation. Yigit and Christoforou [25, 26] have shown a static rock-bit interaction model in a drillstring represented using only two inertias and one compliance for both axial and torsional vibration. Their model is modified as described below. The original model in [25] assumed both friction and cutting torque regardless of whether or not the dynamic weight on the bit was sufficient to create penetration and cuttings. Depth of cut was a function of average rather than instantaneous rotation speed, along with rate of penetration. Rate of penetration was a function of average rotation speed and a constant applied weight on bit (WOB), rather than dynamic weight on bit. The current model incorporates threshold force and the effect of instantaneous WOB and bit rotation speed on cutting torque on bit (TOB). Below a threshold force W_{fs}, the drill tool does not penetrate into the rock, leaving only friction as a source of TOB. The model equations are presented in two parts. First, the dynamic WOB, which is the axial force applied at the bit under dynamic conditions is given as [25]

$$\mathrm{WOB} = \begin{cases} \mathrm{k_c}(\mathrm{x} - \mathrm{s}) & \text{if } x \geq \mathrm{s} \\ 0 & \text{if } x < s \end{cases} \tag{18}$$

where k_c and s indicate formation contact stiffness and bottom-hole surface profile. Surface profile is given as [25]

$$\mathrm{s} = \mathrm{s_0}\, f(\emptyset) \tag{19}$$

The formation elevation function $f(\emptyset)$ is chosen to be sinusoidal as in [25], $f(\emptyset) = \sin(b\emptyset)$, where b indicates bit factor which depends on the bit type. The term $\emptyset$ indicates rotational displacement of the bit. The total torque on bit (TOB) is related to frictional and cutting conditions, and dynamic WOB. When bit rotary speed is in the positive direction then TOB can be written as

$$\text{TOB} = \begin{cases} \text{TOB}_f + \text{TOB}_C & WOB > \text{W}_{fs} \\ \text{TOB}_f & WOB \leq \text{W}_{fs} \end{cases} \tag{20}$$

In the case of zero bit rotary speed,

$$\text{TOB} = \begin{cases} \text{TOB}_C & WOB > \text{W}_{fs} \\ 0 & WOB \leq \text{W}_{fs} \end{cases} \tag{21}$$

Finally for negative bit rotary speed,

$$\text{TOB} = \text{TOB}_f \tag{22}$$

where TOB_f and TOB_C represent frictional and cutting torque on bit and both are calculated as below,

$$\text{TOB}_f = (\text{WOB}) r_b \mu(\dot{\emptyset}) \tag{23}$$

$$\text{TOB}_C = (\text{WOB}) r_b \xi \sqrt{\frac{\delta_C}{r_b}} \tag{24}$$

The term $\dot{\emptyset}$ indicates instantaneous bit rotary speed, and the function $\mu(\dot{\emptyset})$ characterizes the friction process at the bit and it is given as [25]

$$\mu(\dot{\emptyset}) = \mu_0 \left(\tanh \dot{\emptyset} + \frac{\alpha \dot{\emptyset}}{(1+\beta \dot{\emptyset}^{2\gamma})} + \nu \dot{\emptyset} \right) \tag{25}$$

where μ_0, α, β, γ, and ν are the experimentally-determined parameters of the frictional model. Figure 4.26 shows the sketch of frictional behavior between the bit and the

formation. In equation (24) the terms r_b and δ_C indicate bit radius and depth of cut per revolution, the latter given as

$$\delta_C = \frac{2\pi \mathrm{ROP}}{\dot{\emptyset}} \tag{26}$$

The instantaneous rate of penetration (ROP) is a function of dynamic WOB, instantaneous bit speed $\dot{\emptyset}$, and rock/bit characteristics. The modified ROP equation from [25] can be written as

$$\mathrm{ROP} = C_1 \mathrm{WOB} \sqrt{\dot{\emptyset}} + C_2 \tag{27}$$

where ξ, C_1 and C_2 characterize the cutting action at the bit and depend on the type of the bit and formation.

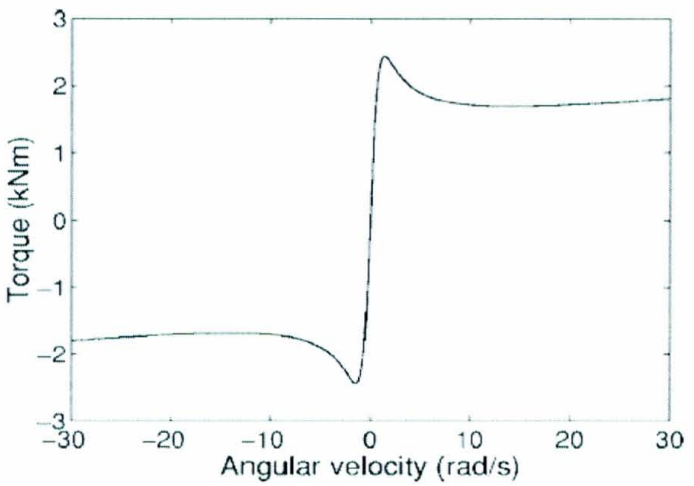

Figure 4.26: Frictional behavior between the bit and the formation (adopted from [25])

4.5.1 Rock Stiffness and Damping Coefficient

An approximate value of stiffness (k) and damping coefficient (b) estimation has been discussed in [64]. The equations of stiffness and damping coefficient can be written as [64]:

$$k = Gr\frac{f_1}{f_1^2 + f_2^2} \tag{28}$$

$$b = \frac{r^2}{a_0}\sqrt{G\rho}\,\frac{f_2}{f_1^2 + f_2^2} \tag{29}$$

where, a_0 is dimensionless frequency, f_1 and f_2 are the Reissner's displacement functions, G is the shear modulus, ρ is the density of rock, and r is the radius of effective contact area [64]. Physical parameters of rocks, which can be used in simulation, are shown in table 4.4. In this present work Berea Sandstone is taken for simulation.

Table 4.5: Physical parameters of rocks

Rock Type	*k, N.m*	*b, N.s/m*
Hackensack Siltstone	$2.23\text{x}10^{9}$	$2.3\text{x}10^{5}$
Berea Sandstone	$1.16\text{x}10^{9}$	$1.5\text{x}10^{5}$
Pierre Shale I	$6.93\text{x}10^{7}$	$3.89\text{x}10^{4}$

4.6 Derivation of Top Drive Motor Dynamics

In the present work, it is assumed that the rotary system is driven by an armature controlled dc motor through a gearbox. The sketch of this system is shown in Figure 4.27. The terms I, L, R_m, K_m, V_C and $\dot{\emptyset}_m$ indicate armature current, inductance, resistance, motor constant, input voltage to the motor and motor speed, repectively. The bond graph

model of top drive motor dynamics is shown in Figure 4.28.

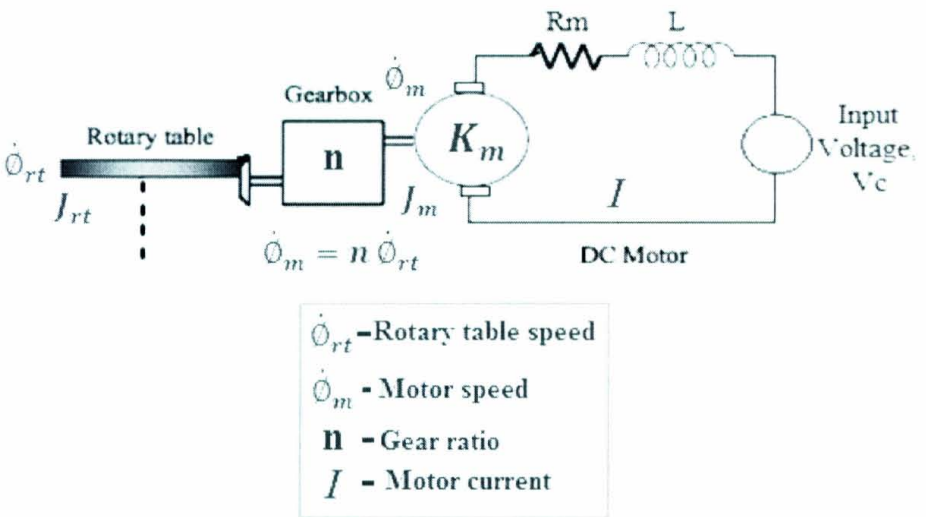

Figure 4.27: Schematic of a DC motor.

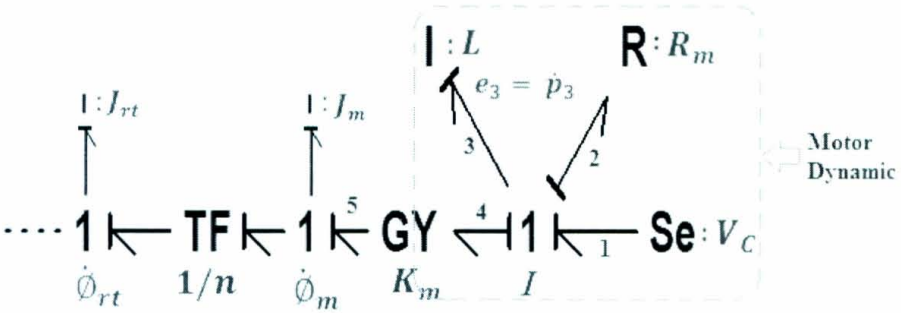

Figure 4.28: Bond graph model of a DC motor.

In Figure 4.28 the terms P_3 and $\dot{P}_3$ indicate magnetic flux and voltage drop (effort) for inductance (inertia element). At the I current 1–junction summation of effort (e) are zero but all flows (f) are equal. Hence:

$\sum e = 0$ and $f_1 = f_2 = f_3 = f_4 = I$ (Motor Current);

$$\rightarrow e_1 - e_2 - e_3 - e_4 = 0 \tag{30}$$

Now, $e_1 = \text{Se} = V_C$ (input voltage), $e_3 = \dot{P}_3 = L\dot{I}$, $e_2 = R_m f_2 = R_m I$, and $e_4 = K_m f_5 = K_m \dot{\emptyset}_m = K_m n \dot{\emptyset}_{rt}$.

Again the equation (30) can be written as,

$$\rightarrow V_C - R_m I - L\dot{I} - K_m n \dot{\emptyset}_{rt} = 0 \tag{31}$$

Finally drive motor dynamic equation can be written as,

$$\rightarrow L\dot{I} + R_m I + K_m n \dot{\emptyset}_{rt} = V_C \tag{32}$$

4.7 Bond graph model of rotary drilling system

The bond graph model of the rotary drilling system is shown in Figure 4.29. It has three main parts: axial dynamic model, torsional dynamic model and rock-bit model. The rock-bit model provides coupling between axial and torsional dynamic model. The input (flow excitation) of the axial model depends on the bit rotation of the torsional model and the input (effort excitation) of the torsional model depends on the WOB of the axial model. Appendix A summarizes all relevant data that is used in the current simulation.

This chapter has provided a brief description of a bond graph method, axial and torsional modeling of drillstring, and suitable rock-bit model. It has also provided a derivation of the motor dynamics equation. In the next chapter, the simulation results of the model will be discussed including the effect of WOB and rotary speed on stick-slip and bit-bounce vibration.

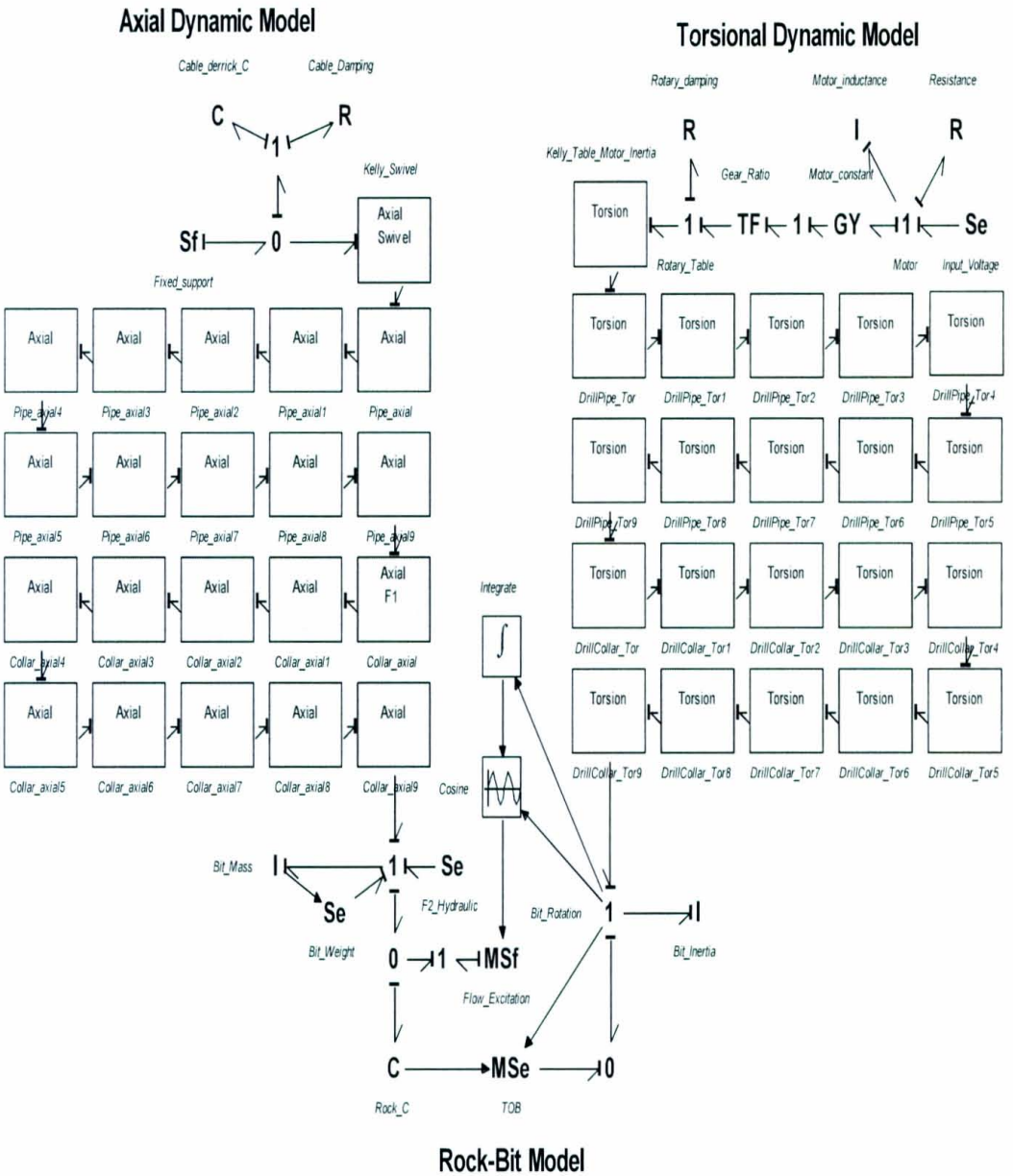

Figure 4.29: Bond graph model of rotary drilling system

CHAPTER 5

SIMULATION RESULTS

The main objective of the current simulations is to study stick-slip vibrations and the effect of this vibration on bit-bounce. During bit-bounce the drill bit alternately separates from and impacts the rock surface in the longitudinal direction during drilling. When the bit is off-bottom the first eight critical frequencies are: 2.3, 8.7, 15.7, 20.9, 25.7, 32.7, 40.0, 47.3 rad/sec for axial resonance; and found to be 1.2, 5.3, 10.1, 14.9, 19.8, 24.4 28.9, 33.3 rad/sec for torsional resonance. When the bit is in contact with rock (on-bottom condition) the first eight critical frequencies for axial resonance are found to be 7.7, 15.1, 20.5, 25.1, 31.8, 37.9, 42.1, 48.0 rad/sec; and for torsional resonance are found to be same as before because a free boundary condition was taken at the bottom of the drillstring for the torsional model. It was found that for axial vibrations the frequencies 31.8, 37.9 and 42.1 rad/sec gave the greatest increases in dynamic forces at the bit. When the bit rotary speed reached that critical frequency range then high dynamic forces at the bit or bit bounce resulted as shown in Figures 5.1-4.

Figure 5.1 shows the simulation results when the desired rotary table speed is 13 rad/sec with 100 kN applied WOB. Table speed is outside the critical frequency range mentioned above. Though the motor appears to control the rotary table speed as desired, the bit experiences large fluctuations evolving into a limit cycle and the frequency is 1.08 rad/sec which is close to the first natural frequency of the torsional modes. As mentioned

earlier, this behavior is known as stick-slip oscillation [22-33]. The stick-slip vibration of the drillstring is characterized by alternating stops (during which the bit sticks to the rock) and intervals of large angular speed of the bit. When the bit speed fluctuation approaches the critical speed range mentioned above, bit bounce occurs as demonstrated in Figure 5.1 where dynamic WOB periodically becomes zero. Reducing the applied WOB (which reduces static friction and allows less winding of the drillstring during stick) and increasing rotary table speed (which avoids the static to dynamic transition period) is a standard technique to help alleviate torsional problems [25].

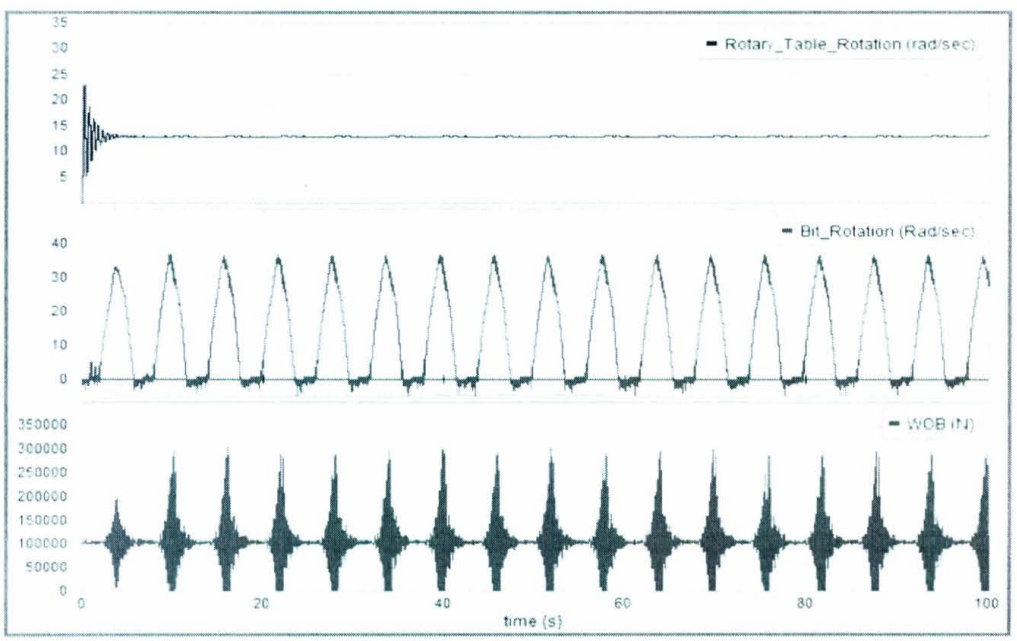

Figure 5.1: High stick-slip vibrations with bit-bounce at 13 rad/sec rotary table speed and 100 kN applied WOB

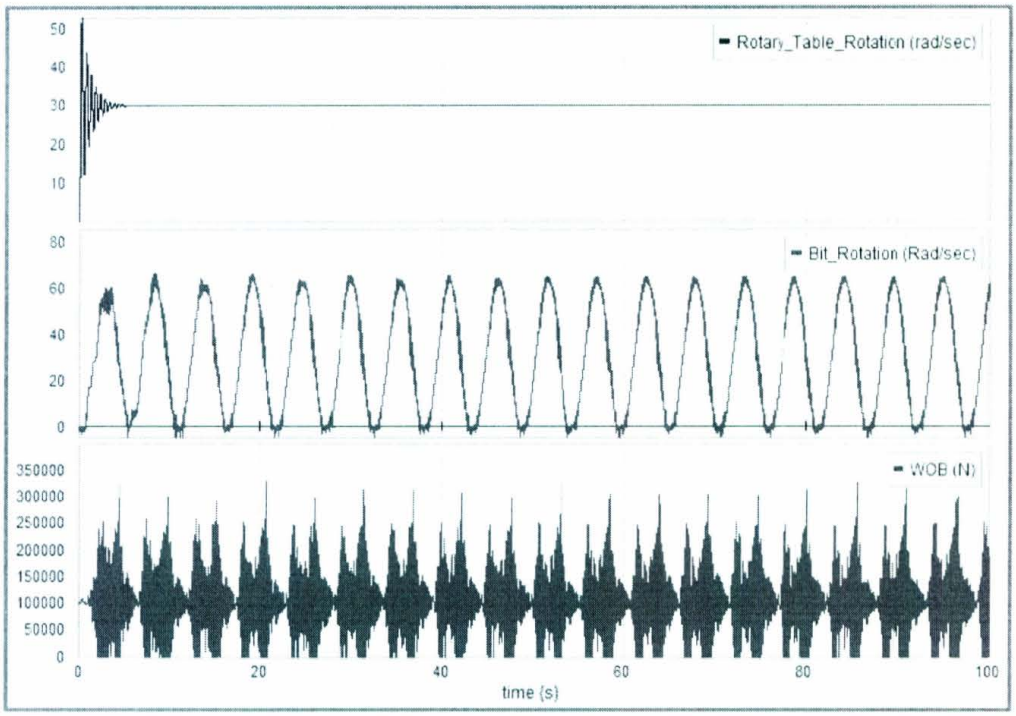

Figure 5.2: Stick-slip with high bit-bounce at 30 rad/sec rotary table speed and 100 kN applied WOB

Figure 5.2 shows the simulation results when the desired table speed is 30 rad/sec at 100 kN applied WOB. Although stick-slip vibrations appear in the figure the time interval of stick decreases and the bit speed experiences smaller fluctuation as a proportion of the mean. The peak speed of the bit is approximately two times the desired speed whereas in Figure 5.1 it was approximately three times the desired speed. Bit-bounce appears more predominant than in the previous figure due to bit speed entering the critical speed range mentioned above. Figure 5.2 shows the FFT frequency spectrum for bit rotation at 30 rad/sec rotary speed and 100 kN applied WOB. Peak amplitude is found in Figure 5.2

when the frequency is 1.196 rad/sec which is exactly the first natural frequency for the torsional model. There is no such peak for higher frequencies in Figure 5.3 which indicates enough damping at the higher natural frequencies so that input frequencies close to higher mode natural frequencies do not cause large amplitude vibrations.

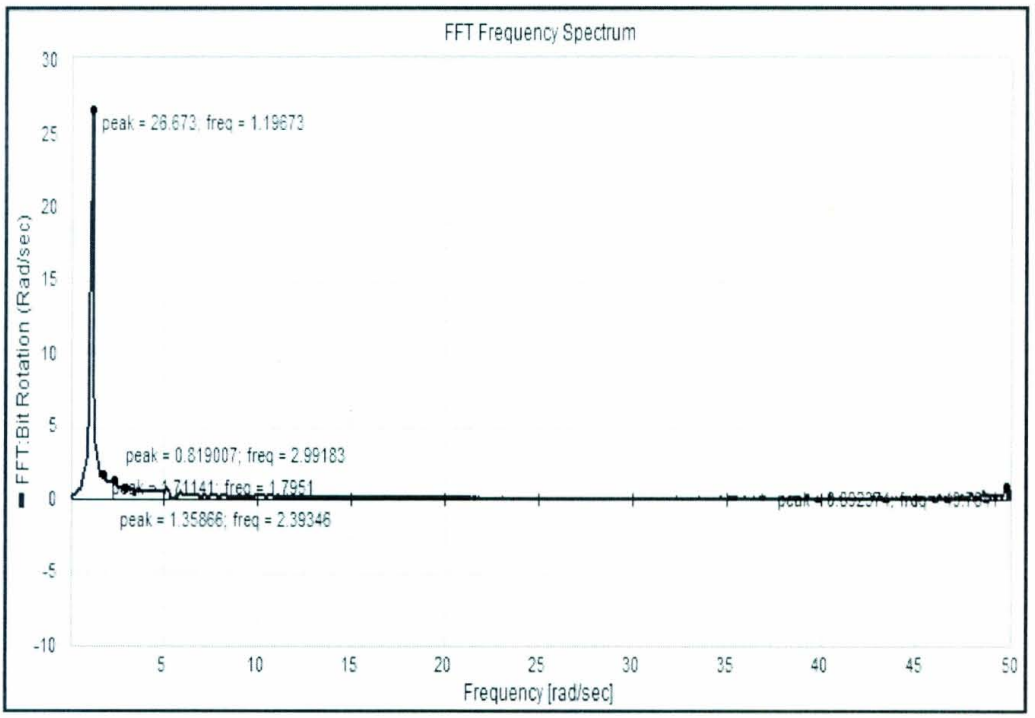

Figure 5.3: FFT frequency spectrum for bit rotation at 30 rad/sec rotary speed and 100 kN applied WOB

Figure 5.4 shows both stick-slip and bit-bounce completely eliminated by increasing rotary table speed to 75 rad/sec. A nearly constant steady-state bit rotation speed is attained. This is due to the positive slope of the friction behavior curve discussed earlier [25]. At very low speed the transition from static to kinetic friction coefficient causes a

drop in the frictional torque and the negative slope causes instability in torsional motion. At high speed the slope of frictional torque is found to be positive and suppresses torsional instability. Bit-bounce is eliminated due to bit rotary speed being out of the critical speed range mentioned above.

Figure 5.5 shows the simulation results when the applied WOB is 50 kN at 30 rad/sec rotary table speed. Stick-slip vibration reduces due to decreasing the applied WOB, but it increases the bit-bounce vibrations compared to Figure 5.2.

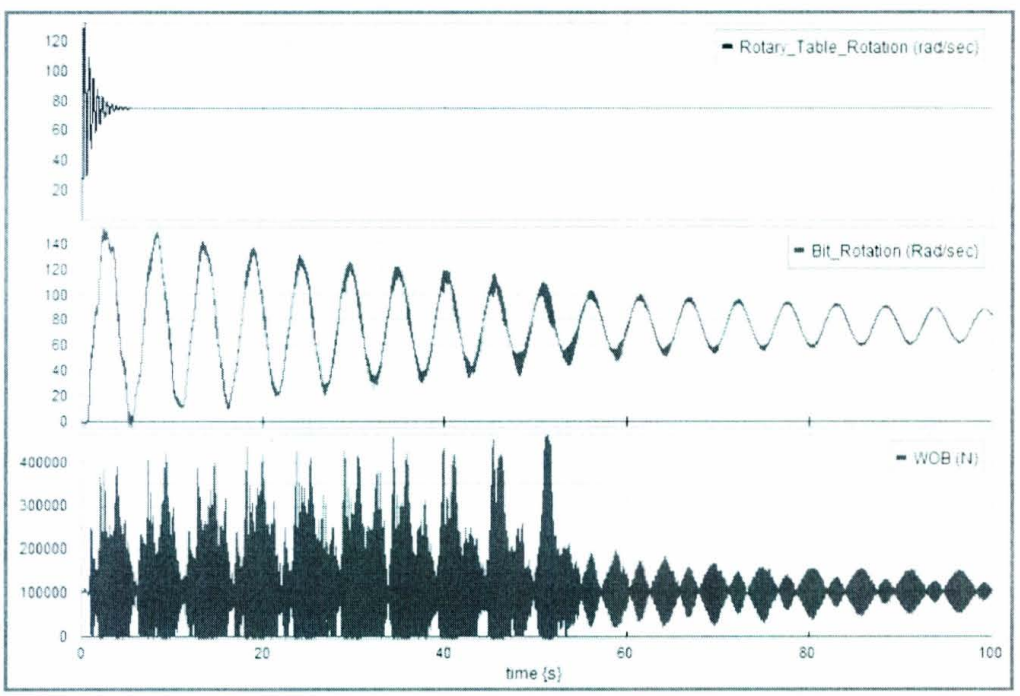

Figure 5.4: Both stick-slip and bit-bounce eliminated by increasing the rotary table speed to 75 rad/sec at 100 kN applied WOB

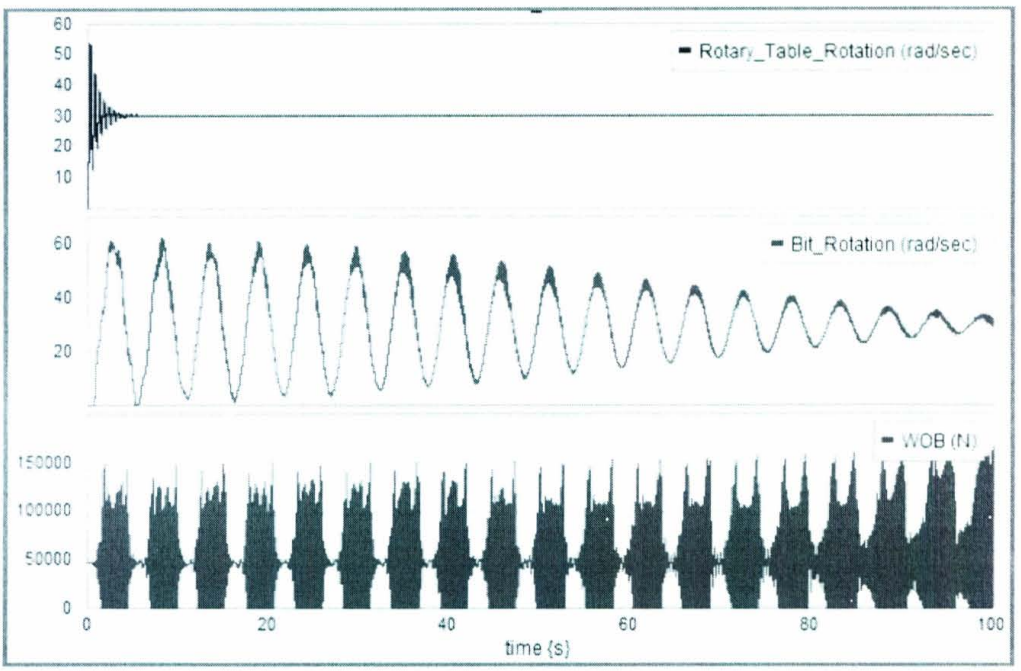

Figure 5.5: Stick-slip vibrations eliminated, but bit-bounce increased, by decreasing applied WOB to 50 kN at 30 rad/sec table speed

From simulation results it is found that by decreasing applied WOB and increasing desired table rotary speed beyond a threshold it may possible to eliminate stick-slip vibrations. The results obtained are in excellent agreement with the actual drilling optimization workflow in the field [23]. By avoiding critical speed ranges it may possible to eliminate bit-bounce. However, increasing the rotary speed may cause lateral vibration problems, such as backward and forward whirling. Decreasing applied WOB may not be a desirable solution as it will result in reduced rate of penetration (ROP). Active control will be investigated in the next chapter as a means of eliminating stick slip and bit bounce without affecting drilling performance or worsening other modes of vibration.

CHAPTER 6

CONTROLLER DESIGN

Using the Linear Quadratic Regulator (LQR) method an optimal controller can be designed in which the state feedback gain matrix [K] is selected to eliminate stick-slip vibration in the drillstring. LQR is a well-known design technique that provides optimal feedback gains. In order to determine LQR gains, a performance index is required. A performance index is the integral over time of several factors which are to be minimized. The Riccati equation is solved to calculate optimal linear gains [41-42]. In order to reduce the dimension of the state vector and to minimize the number of states that must be physically measured or estimated, a simplified lumped parameter torsional model (Figure 6.1) is used instead of taking 21 segments. The state space equation of the simplified model in Figure 6.1 is:

$$\dot{\mathbf{X}} = \mathbf{AX} + \mathbf{B}V_C \tag{33}$$

where X, A, and B are the state vector, coefficient, and input matrices, respectively and V_C is optimal control input (rotary table motor voltage).

$$\mathrm{A} = \begin{bmatrix} -\frac{R_m}{L} & 0 & -\frac{nK_m}{L} & 0 & 0 \\ 0 & 0 & 1 & 0 & 0 \\ \frac{nK_m}{J_k+J_{rt}+n^2J_m} & 0 & \frac{-C_{rt}}{J_k+J_{rt}+n^2J_m} & \frac{-K_t}{J_k+J_{rt}+n^2J_m} & 0 \\ 0 & 0 & 1 & 0 & -1 \\ 0 & 0 & 0 & \frac{K_t}{J} & \frac{-C_v}{J} \end{bmatrix} \tag{34}$$

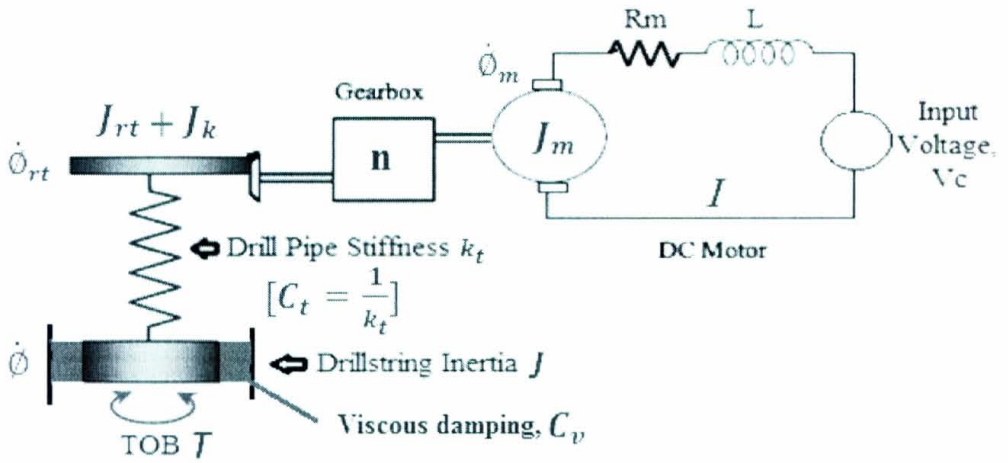

(a)

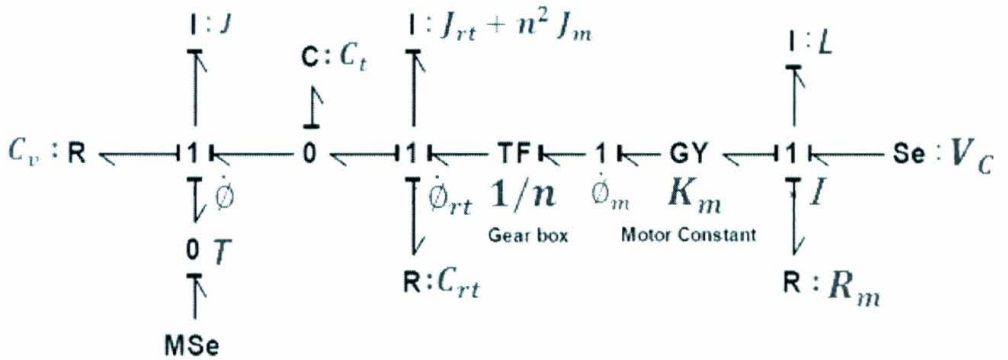

(b)

Figure 6.1: (a) Physical schematic of model used for control design. (b) Bond graph torsional model using simplified lumped parameter model

$$X^T = [\, I \;\; \emptyset_{rt} \;\; \dot{\emptyset}_{rt} \;\; (\emptyset_{rt} - \emptyset) \;\; \dot{\emptyset} \,] \tag{35}$$

$$\mathrm{B}^{\mathrm{T}} = [\, \frac{1}{L} \quad 0 \quad 0 \quad 0 \quad 0 \,] \tag{36}$$

The main goal here is not to place the new closed loop poles at an exact specified location at any cost, but to keep vibration state variables within reasonable limits using minimal control effort. The control problem is to find out the necessary gain vector $[K]$ that will minimize the following performance index [24]:

$$C = \frac{1}{2}\int_0^{\infty}(x^T Q x + r V_C^2)\, dt \tag{37}$$

where Q is a weighting matrix chosen to reflect the relative importance of each state and r is a weighting factor to adjust the control effort. If the desired state vector is x_d then the resulting optimal control input (rotary table motor voltage) can be written as:

$$V_C = V_{ref} - K(x - x_d) \tag{38}$$

The gain matrix, K can be written as:

$$K = r^{-1} B^T P \tag{39}$$

where P is the symmetric, positive-definite solution matrix of the algebraic Riccati equation given by:

$$A^T P + PA - r^{-1} PBB^T P + Q = 0 \tag{40}$$

If V_{ref} is a constant reference voltage applied to maintain the desired speed ω_d at steady state in the absence of any disturbance then the control voltage necessary to keep the torsional vibrations zero while maintaining a desired bit and rotary table speed is given by [24]:

$$V_C = V_{ref} - K_1 I - K_2(\emptyset_{rt} - \omega_d * t) - K_3(\dot{\emptyset}_{rt} - \omega_d) - K_4(\emptyset_{rt} - \emptyset) - K_5(\dot{\emptyset} - \omega_d) \quad (41)$$

The feedback gain matrix K is obtained by solving equation (40). Since an analytical solution to equation (40) is quite difficult, numerical methods are the best option. There are quite a few numerical methods in Matlab's Control toolbox [65] which can apply to obtain approximate solutions.

In the present work, an LQR controller is designed by using the function 'care' in the Matlab control toolbox [65]. The matlab codes for this function are shown in appendix C. the weighting matrix Q and factor r, that are used are:

$$r = 950 \quad (42)$$

$$Q = \begin{bmatrix} 1 & 0 & 0 & 0 & 0 \\ 0 & 20000 & 0 & 0 & 0 \\ 0 & 0 & 1 & 0 & 0 \\ 0 & 0 & 0 & 80000 & 0 \\ 0 & 0 & 0 & 0 & 950000 \end{bmatrix} \quad (43)$$

It should be noted that the values for the weighting matrix and factor are chosen arbitrarily. According to the performance requirements the values for weighting matrix and factor are adjusted. The selected weighting matrix and factor result in the following gain matrix K,

$$K = [0.0285 \quad 4.588 \quad 1.809 \quad 35.165 \quad 10.74] \quad (44)$$

6.1 Simulation Results Using LQR Controller

The gains from equation (44) are used in the high order model for simulation. The bond graph model of rotary drilling system with LQR controller is shown in Figure 6.3. Figure 6.2 shows the response of the high order combined axial-torsional model discussed earlier, when the rotary table controller is active at the simulation time of 40 seconds, for the case of 100 kN applied WOB and a desired speed of 10 rad/sec. As can be seen, stick-slip vibration is controlled and a smooth drilling condition is achieved. At the same time the controller eliminates high dynamic force at the bit compared to Figure 5.1, and there is no bit bounce.

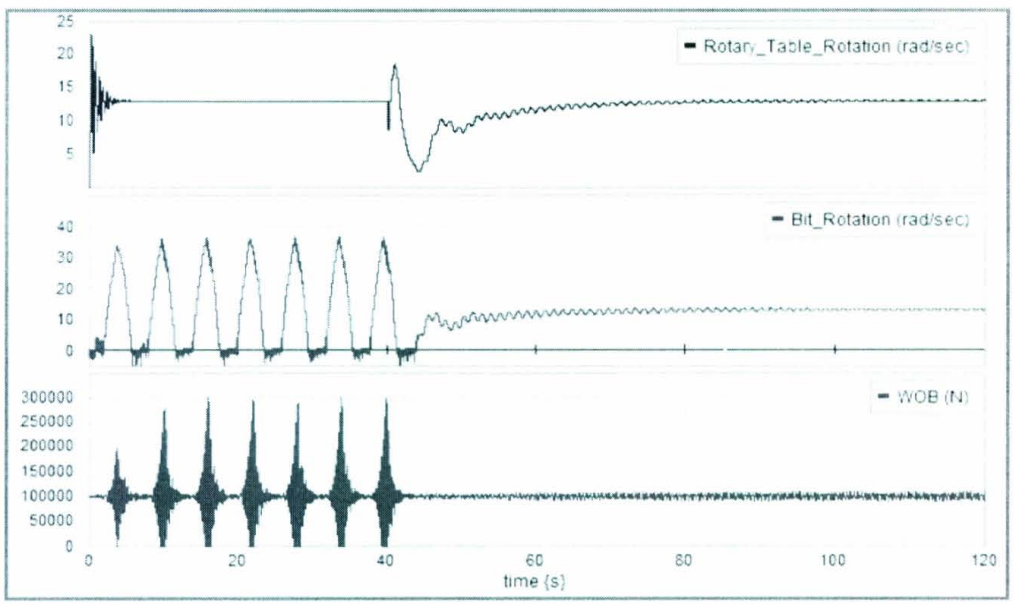

Figure 6.2: Stick-slip and bit-bounce vibrations eliminated by rotary table control at 13 rad/sec table speed and 100 kN applied WOB (2000 m drillpipe & 200 m drill collar)

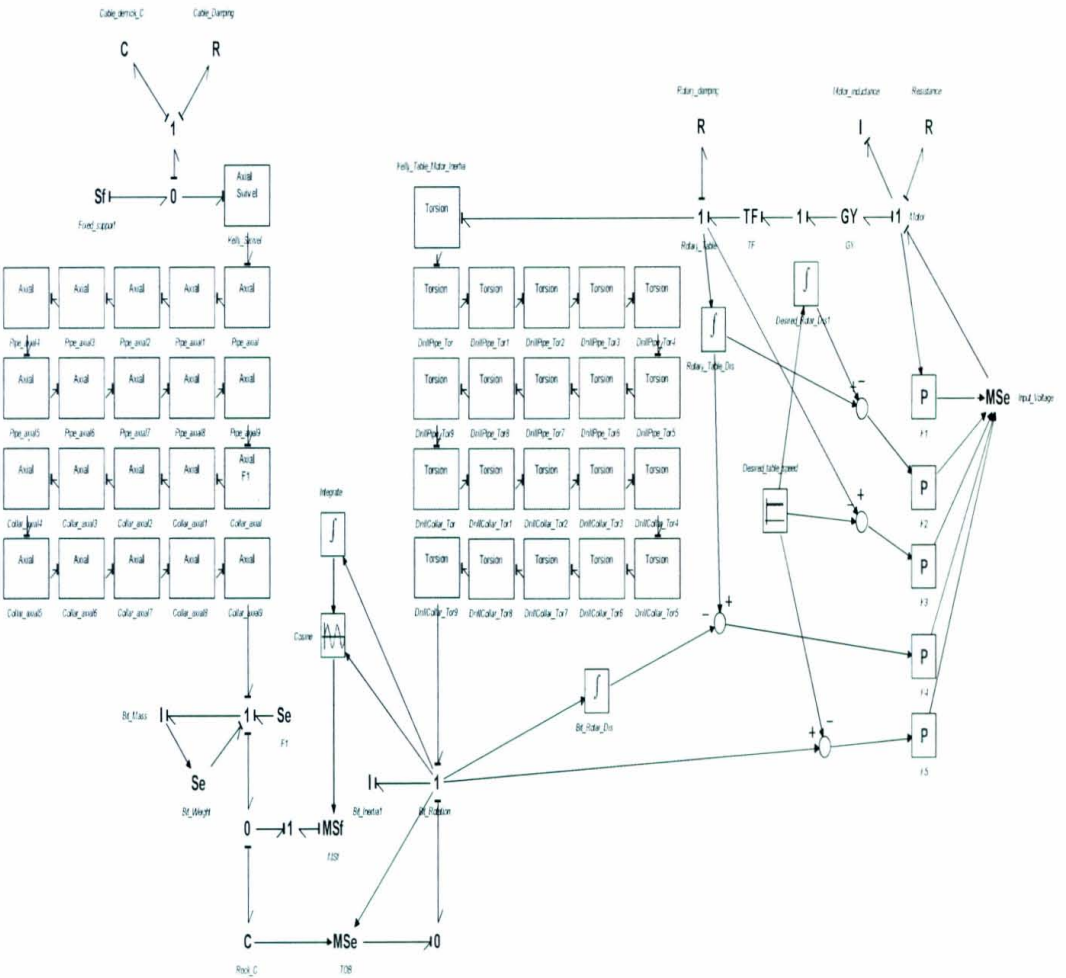

Figure 6.3: Bond graph model of rotary drilling system with LQR controller

CHAPTER 7

ADVANTAGES OF LQR CONTROL

This chapter addresses the advantages of a linear quadratic regulator (LQR) controller, compared to a spring-damper isolator, for stick-slip and bit-bounce mitigation in an oilwell drillstring.

7.1 Alternative Control Schemes

In the literature, numerous solutions have been presented to control stick-slip oscillations, such as robust μ-synthesis controller [43], H∞ controller [44], genetic algorithm optimized controller [45], D-OSKIL controller [46], torque estimator-based controller [47], and modeling error compensation based controller [48]. Many such controllers have practical limitations. However, one system that has achieved real-world acceptance is the soft torque rotary system (STRS) [22, 49-50]. STRS is a torque feedback at the top of the drillstring which makes the system behave in a "softer" way rather than as a fixed heavy flywheel, so that the torsional waves arriving at the surface are absorbed, breaking the harmful cycling motion. The STRS increases the system damping to the extent that rotational speeds will not drop to levels where there is a risk of the bottom hole assembly (BHA) sticking. Therefore, the feedback system, which acts on the rotary drive speed input, modifies the speed of the motor such that the vibrational energy is optimally extracted from the drillstring. The effect of this feedback circuit, in

practice fully implemented by electronics, is to emulate a parallel combination of a torsional spring and damper in series with an ideal motor as shown in Figure 7.1.

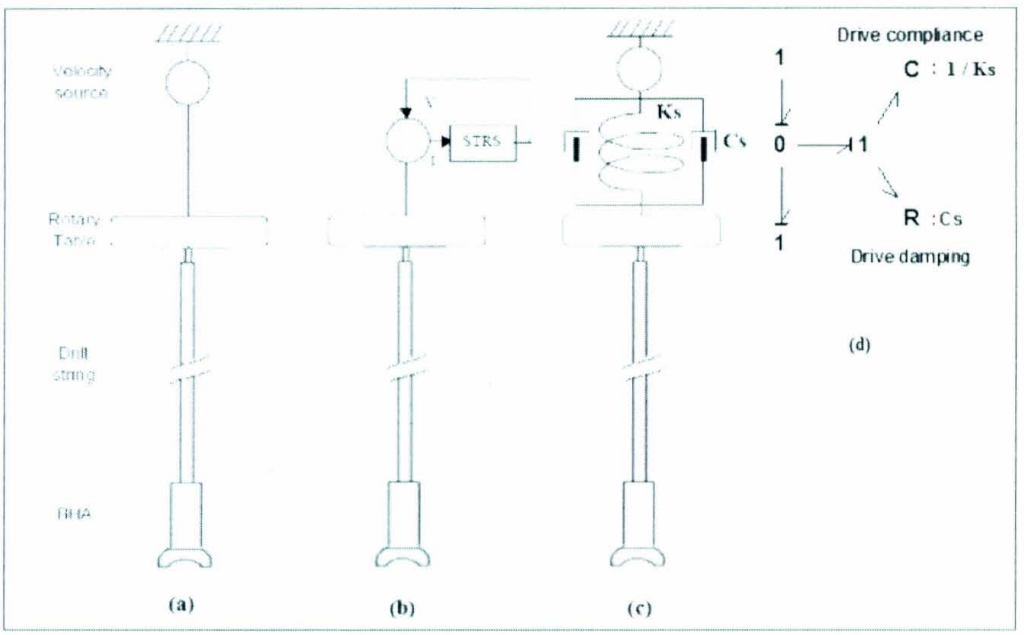

Figure 7.1: (a) Conventional or Normal (no STRS) drilling [50], (b) STRS schematic [50], (c) STRS virtual mechanical elements [50], (d) Bond graph model of the STRS virtual elements.

The STRS must be tuned by giving values of K_s (drive stiffness in Nm/rad) and C_s (drive damping in Nms/rad) [22]. The parameters must change as the drillstring length (and thus compliance and inertia) increase. For a particular C_s (700 Nms/rad) value the range of possible values of K_s for which stick slip does not occur has been determined, using the bond graph system model, for different drilling depths as shown in Figure 7.2. Setting the drive stiffness outside this range will not mitigate stick-slip.

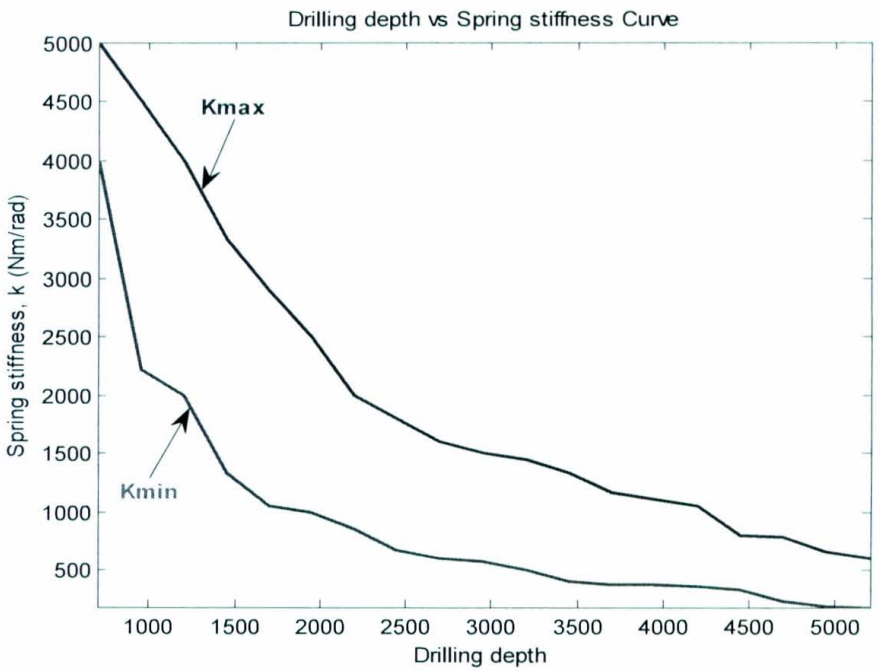

Figure 7.2: Drive spring stiffness (K_s) vs. drilling depth curve for a particular drive damping (C_s = 700 Nms/rad)

7.2 Comparison Results

The main objective of the current simulations is to study the theoretical performance of an LQR controller compared to a torsional spring-damper (or virtual spring-damper as in the STRS system) on the mitigation of stick-slip and bit-bounce vibrations in an oilwell drillstring. The simulation results for a drilling depth 4200 m, where drill pipe and collar lengths are 4000 m and 200 m, are shown below in Figures 7.3-6. The gains vs. depth curves (Figure D.1) for the LQR controller are shown in Appendix D.

Figure 7.3 shows the full model simulation results in the case of conventional drilling when the desired rotary table speed is 15 rad/sec (142 rpm) with 175 kN applied WOB. The large fluctuations in bit speed shown in Figure 7.3 indicate stick-slip vibration, which was discussed in previous chapters. Also, at the same time the torque at surface experiences large fluctuations consistent with stick-slip [22, 50]. When the input torque grows sufficiently to overcome static friction and the bit releases, bit speed approaches the axial vibration critical speed range that is discussed in an earlier chapter. Bit-bounce then occurs as demonstrated in Figure 7.3 where dynamic WOB periodically becomes zero.

Figure 7.4 shows the response of the model when LQR control is activated at the simulation time of 40 seconds, for the case of 175 kN applied WOB and a desired speed of 15 rad/sec (142 rpm). The time interval from 40 to 64 sec is the applied torque storing period. When the applied torque reaches the resisting torque at the bit then bit starts to rotate which takes sufficient times because of controller less responses, and then controller quickly manages the desired bit speed. As can be seen, when LQR controller is active the stick-slip vibration is controlled and a smooth drilling condition is achieved. That means the drill bit is rotating with constant desired speed and the torque at the surface becomes constant. At the same time the controller eliminates high dynamic force and bit-bounce, as a result of the axial-torsional coupling at the bit-rock interface.

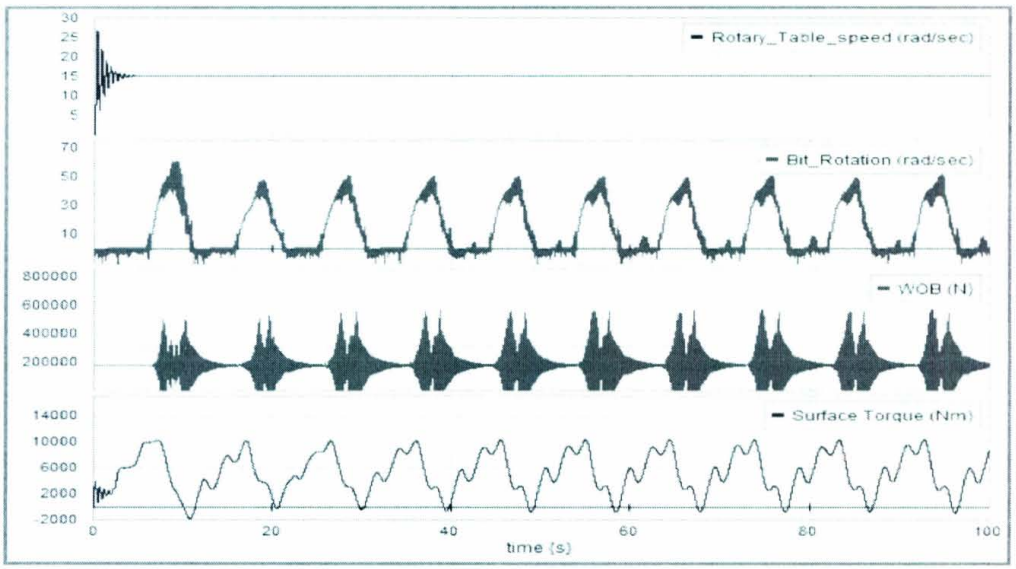

Figure 7.3: High stick-slip vibrations with bit-bounce at 15 rad/sec (142 rpm) rotary table speed and 175 kN applied WOB

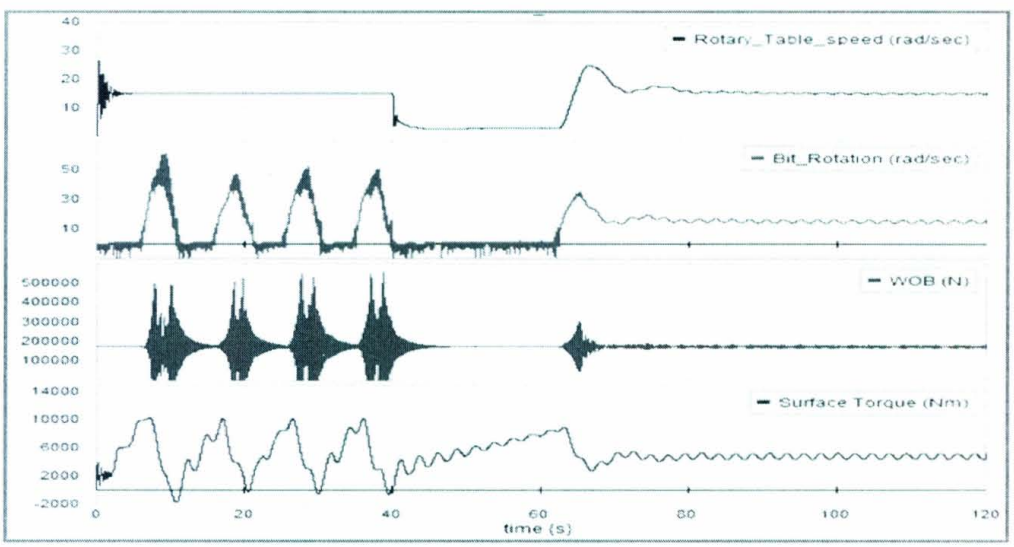

Figure 7.4: Stick-slip and bit-bounce eliminated by LQR control at 15 rad/sec (142 rpm) table speed and 175 kN applied WOB

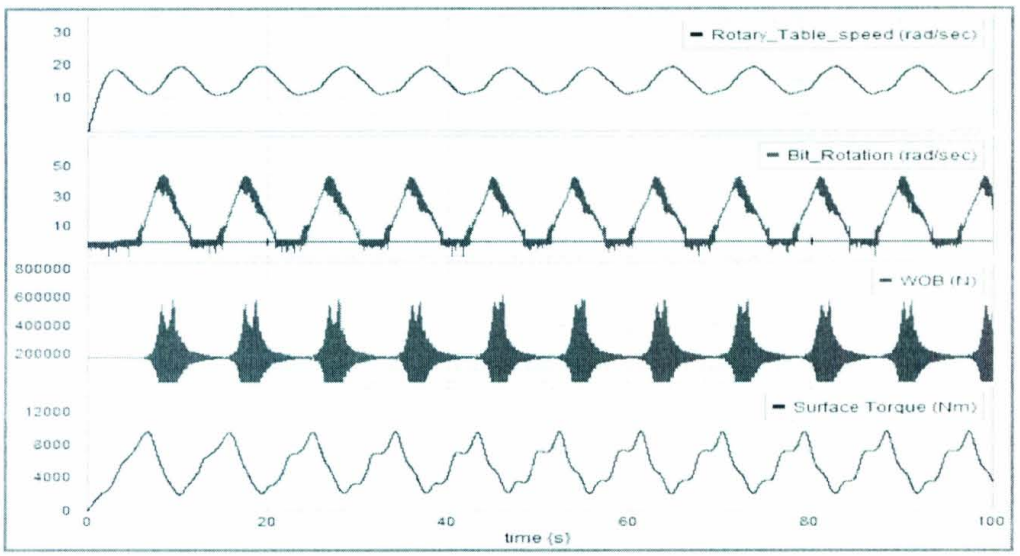

Figure 7.5: Torsional spring-damper system unable to eliminate stick-slip and bit-bounce vibrations at 15 rad/sec (142 rpm) table speed and 175 kN WOB

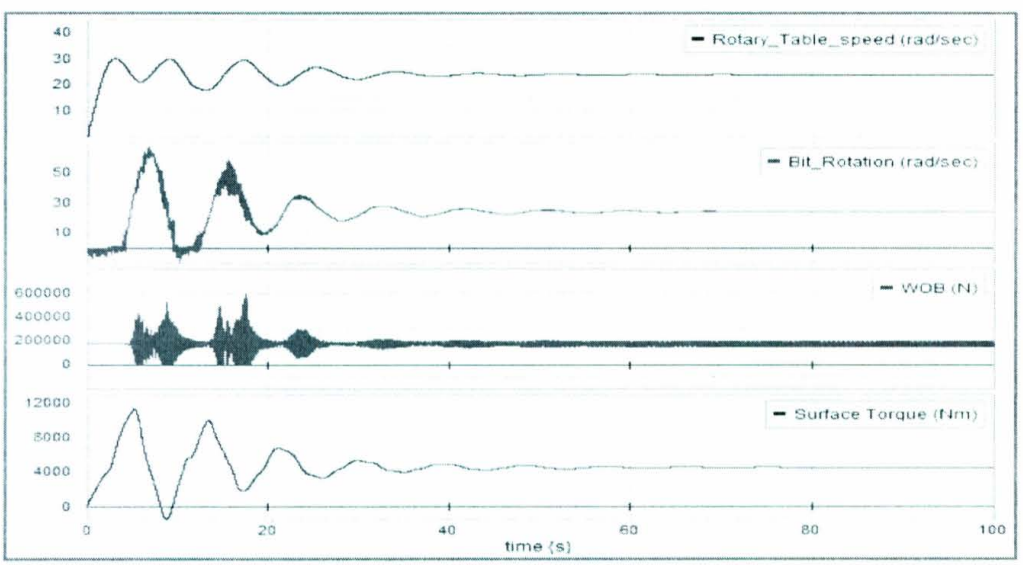

Figure 7.6: Stick-slip and bit-bounce vibrations eliminated by torsional spring-damper system at 24 rad/sec (230 rpm) table speed and 175 kN applied WOB

Figure 7.5 shows the response of the model when a torsional spring-damper system is used, for the case of 175 kN applied WOB and a desired speed of 15 rad/sec (142 rpm). The torsional spring-damper system with the assigned parameters should be unable to eliminate stick-slip vibration at the desired speed. By increasing the desired speed to 24 rad/sec (230 rpm) in Fig. 7.6, the torsional spring-damper system becomes able to eliminate stick-slip vibration.

7.3 Advantages of LQR Controller

Stick-slip occurs at a rotary speed below a certain threshold value. Figure 7.7 shows the threshold phenomena of stick-slip vibrations. The threshold value depends on system parameters such as design of the drillstring, mud, bit, BHA and weight on bit (WOB). Figures 7.8 and 7.9 show the threshold rotary speed for different applied WOB for conventional drilling, drilling with torsional spring-damper system near the rotary table, and drilling with the LQR controller. Simulation results show that for a particular applied WOB the LQR controller gives the lowest magnitude of the threshold rotary speed. At higher WOB the difference in the threshold rotary speed between the LQR controller and torsional spring-damper system increases, and it indicates that at higher WOB, and notwithstanding certain practical implementation issues to be discussed later, an LQR controller can increase the no stick-slip zone significantly compared to a torsional spring-damper system.

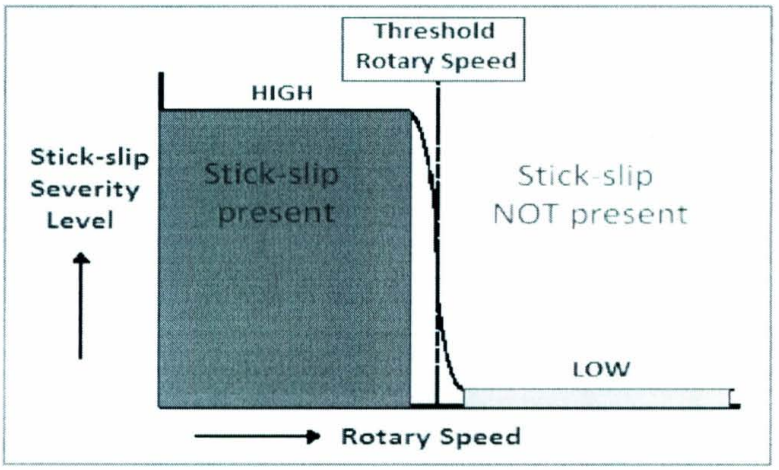

Figure 7.7: Threshold speed for stick-slip vibration

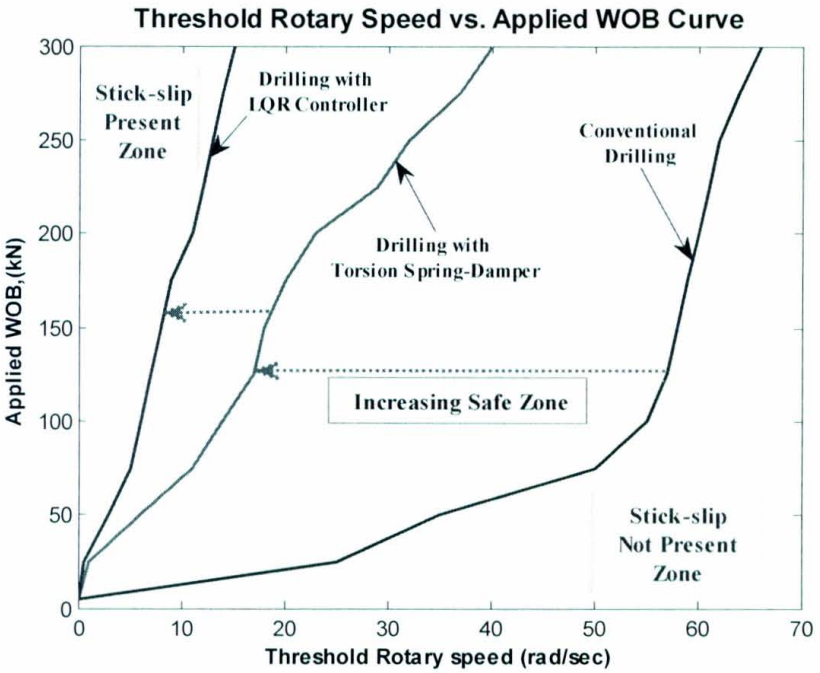

Figure 7.8: Threshold rotary speed vs. applied WOB curve for different operating conditions at 2200 m depth.

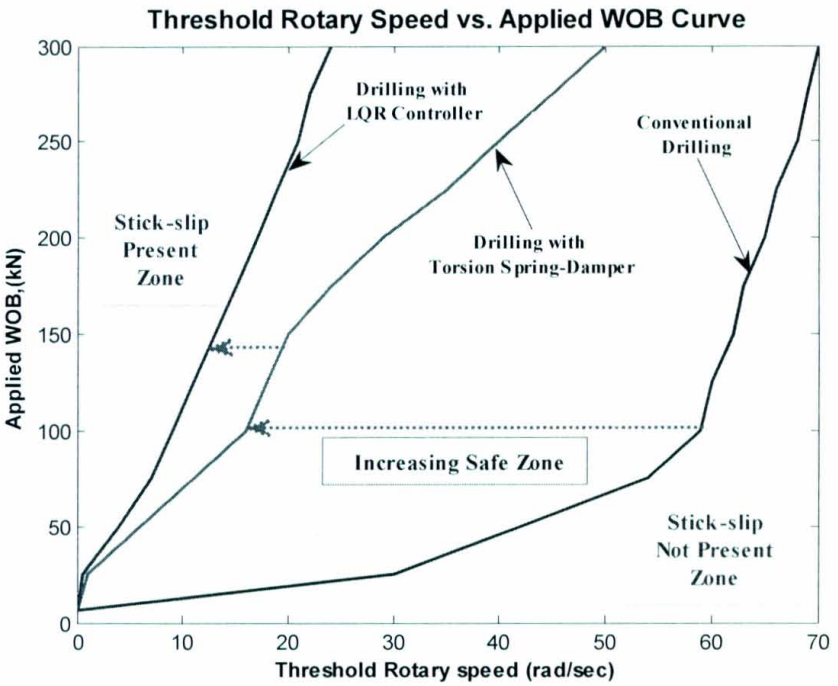

Figure 7.9: Threshold rotary speed vs. applied WOB curve for different operating conditions at 4200 m depth.

During drilling, the LQR controller requires: (i) motor current, (ii, iii) rotary table rotary speed and displacement, (iv-v) bit rotary speed and displacement. Except for the bit speed and displacement, all other quantities in the controller can be measured. The bit speed measurement (and calculation of bit rotary displacement through integration) requires downhole equipment that is expensive and at this point not typically used in well drilling, because the information is not needed if a controller is not used. Bit speed measurement is the biggest challenge preventing LQR and other sophisticated controller implementations, as discussed also in [6, 25, 48]. The virtual spring-damper of the STRS system requires

only measurement of motor current, giving it an economic and implementation advantage at present. The additional potential benefits of LQR are expected to motivate drillers to eventually use advanced downhole measurement tools, to enable such control. The additional cost of instrumentation would be justified by even smoother drilling and fewer tool failures.

CHAPTER 8

CONCLUSIONS AND RECOMMENDATIONS

8.1 Achivements

This thesis introduced a suitable approach for modeling, simulation and control of stick-slip and bit-bounce vibration in an oilwell drillstring. The stated objectives were fulfilled by accomplishing several diverse tasks, listed below:

1. A bond graph model of a drillstring using a lumped segment approach was developed. The proposed dynamic model includes the mutual dependence of axial and torsional vibrations, and coupling between axial and torsional vibration due to bit-rock interaction. While the top drive motor dynamics assume a DC motor, the bond graph formalism allows for easy substitution of an AC or hydraulic motor submodel (all three types are in common use in the drilling industry).
2. A comprehensive software package (20sim) was used in modeling and simulation. The implementation of the high-order model in 20sim commercial software that allows block diagrams to be superimposed on bond graphs greatly facilitated inclusion of the coupled axial and torsional degrees of freedom due to bit-rock interaction, along with the controller. The simulation time is very fast compared to high order finite-and discrete-element models, making the model suitable as a tool for design and sensitivity analysis. Simulation results from the model show the same

qualitative trends as field observations regarding stick-slip oscillations and their relationship to rotary speed, WOB, and bit bounce. These vibrations are self excited, and they generally disappear as the rotary speed is increased beyond a threshold value and the applied weight on bit decreases. However, increasing rotary speed may cause lateral problems and decreasing applied weight on bit decreases rate of penetration.

3. A suitable state feedback controller (LQR control) was investigated as a means of eliminating stick-slip and bit-bounce without affecting drilling performance or worsening other modes of vibration. It has been shown that the proposed control can be effective in suppressing stick-slip oscillations once they are initiated.
4. A top drive system (torsion spring-damper isolator), which is currently used in industry as a means of eliminating stick-slip, was modeled in 20sim software. From comparison results between LQR control and a spring-damper isolator, it can be summarized that self-excited stick-slip oscillations in oilwell drillstrings are better suppressed by the application of LQR control. Therefore, it is possible to drill smoothly at very low speeds which are otherwise not possible without LQR control. It has been shown that the advantages of using LQR control increase with higher applied WOB. Use of a different type of motor would require rederiving the LQR matrices and gains; however, the procedure outlined herein would still apply. The performance of LQR control for mitigation of stick-slip decreases with increasing depth. It nonetheless retains an advantage compared to a system with a spring-damper isolator. This should motivate the use of LQR controllers in future when practical

challenges in measuring required state variables for LQR control are addressed by advances in downhole measurement technology.

8.2 Primary Research Contribution

Several dynamic models related to drillstring vibration modeling have been proposed in the past, however, the majority were developed low order drillstring model and simple rock-bit model. This thesis presents a bond graph model of a drillstring that predicts axial vibration, torsional vibration, and coupling between axial and torsion vibration due to rock-bit interaction. This model accounts for the effect of higher modes, the flow inside and outside the drillpipe and collars, or complicated cutting and friction conditions at the bit/formation interface.

Although numerous control systems are offered by some researchers or drilling equipment manufacturers; a simple but effective LQR control system has been simulated by developing a model in 20sim. Simulation results show that self-excited stick-slip oscillations in oilwell drillstring are more effectively suppressed by the application of LQR control than by using a real or virtual torsional spring-damper isolator.

8.3 Industry Relevance

Rotary drilling manufacturers have shown increasing interest in the work presented in this thesis [67]. The presented active control may eventually be adopted for their stick-slip vibration control purpose.

The dynamic model of the drillstring can be used by the drilling manufacturers to construct their own model on their computing facilities. This would enable them to test or

predict stick-slip and bit-bounce vibration in drillstrings. They can change the factors (WOB, rotational speed, rock parameters, bit parameters, and LQR control gains etc.) according to their requirements and they can select the suitable values for eliminating stick-slip and bit-bounce vibration.

8.4 Recommendations for Future Research

Further research and development in the following areas would be of interest:

1. Comprehensive studies on the mechanical behavior of rock-bit interaction under different types of PDC bits are required. Different shape and size bits are available in drilling. Different bits should have different coefficients related to cutting action and frictional behavior. With such experimentally determined parameters, different models can be made for different types of PDC bits.
2. The developed model is currently limited to axial vibration, torsional vibration, and coupling between axial and torsional vibration due to bit-rock interaction. This model should be extended to the study of coupled axial, lateral and torsional vibrations for more accurate results. A fully coupled model for axial, lateral, and torsional vibrations of a drillstring was presented in [26]. This model includes the mutual dependence of these vibrations, which arises due to bit/formation and drillstring/borehole wall interactions as well as other geometric and dynamic non-linearities. This model could be the starting point for developing the fully coupled model in 20sim commercial software.
3. The currently developed model should be parameterized to match a field drillstring for studying field vibration data, and to validate the current model. In field data, the

values of WOB, ROP, TOB and bit speed are available. The main difficulty is to determine the coefficients related to cutting action and frictional behavior. This thesis provides the suitable ROP equation (27), frictional torque equation (23), and cutting torque equation (24). However, these three equations require empirical coefficients.

4. The feedback controller (LQR) that is discussed successfully suppresses stick-slip and bit-bounce vibration. Comprehensive studies on the effect of LQR controller in lateral vibration are required. Also this thesis provides a simple LQR control method and it was working well, but more complicated LQR control methods are available that can be applied to a drillstring.
5. Finally, the study is limited to vertical drilling systems. Currently, most of the oilwells are directional wells (non-vertical wells). Studies on the modeling of directional drilling systems are required.

Bibliography

1. Lopez, E. M. N. (2010). Bit-sticking Phenomena in a Multidegree of freedom Controlled Drillstring. *Drilling & Well Technology*, UK.
2. Chunjie, H., & Tie, Y. (2009). The Study on Vibration of Drill-String in the Deeper Wells by ANSYS. In *Proceedings of the 2009 International Conference on Computational Intelligence and Natural Computing - Volume 01* (CINC '09), Vol. 1. IEEE Computer Society, Washington, DC, USA, 433-436. DOI=10.1109 / CINC. 2009.86.
3. Eronini, I. E. (1978). A Dynamic Model for Optimization and Control of Rock Drilling. *Ph.D. thesis*, University of California, Berkeley.
4. *Oilwell.* Wikipedia. http://en.wikipedia.org/wiki/Oil_well.
5. *Offshore Drilling*. Wikipedia. http://en.wikipedia.org/wiki/Offshore_drilling.
6. Leine, R. I., Van Campen, D. H., & keultjes, W. J. G. (2002). Stick-slip Whirl Interaction in Drillstring Dynamics. *Journal of Vibration and Acoustics, 124*(2), 209 - 220.
7. Dupriest, F. E., & Koederitz, W. L. (2005). Maximizing Drill Rates with Real-Time Surveillance of Mechanical Specific Energy. SPE/*IADC Drilling Conference*. Amsterdam, Netherlands: SPE/IADC Drilling Conference.
8. Ledgerwood, L. W., Hoffmann, O. J., Jain, J. R., Hakam, C. E., Herbig, C., & Spencer, R. (2010). Downhole Vibration Measurement, Monitoring and Modeling Reveal Stick-Slip as a Primary Cause of PDC Bit Damage in Today's Applications.

SPE Annual Technical Conference and Exhibition. Florence, Italy: Society of Petroleum Engineers.

9. Plácido, J. C. R., Santos, H. M. R., & Galeano, Y. D. (2002). Drillstring Vibration and Wellbore Instability. Journal of Energy *Resources* Technology, Transactions of the ASME, 124(4), 217–222.
10. Fear, M. J., Abbassian, F., Parfitt, S. H. L., & McClean, A. (1997). The Destruction of PDC Bits by Severe Slip-Stick Vibration. *SPE/IADC Drilling Conference*. Amsterdam, Netherlands: Society of Petroleum Engineers.
11. Leseultre, A., & Lamine, E. (1998). An Instrumented Bit: A Necessary Step to the Intelligent BHA. *IADC/SPE Drilling Conference*. Dallas, Texas: IADC/SPE Drilling Conference.
12. Kyllingstad, A., & Halsey, G.W. (1988). A Study of Slip/Stick Motion of the Bit. *SPE Drilling Engineering, 3(4).*
13. Jain, J. R., Ledgerwood, L. W., Hoffmann, O. J., Schwefe, T., & Fuselier, D. M. (2011). Mitigation of Torsional Stick-Slip Vibrations in Oil Well Drilling through PDC Bit Design: Putting Theories to the Test. *SPE Annual Technical Conference and Exhibition.* Denver, Colorado, USA: Society of Petroleum Engineers.
14. Sotomayor, G. P. G., Placido, J. C., & Cunha, J. C. (1997). Drill String Vibration: How to Identify and Suppress. *In Latin American and Caribbean Petroleum Engineering Conference.* Rio de Janeiro, Brazil.
15. A, D., V., Fereldoun, A., & Arnis, J. (1993). Dynamic Stability of Drillstrings Under Fluctuating Weight on Bit. *SPE Drilling & Completion, 8(2).*

16. Sotomayor, G. P. G., Placido, J. C., & Cunha, J. C. (1997). Drill String Vibration: How to Identify and Suppress. *In Latin American and Caribbean Petroleum Engineering Conference.* Rio de Janeiro, Brazil.

17. Bailey, J. J., & Finnie, I. (1960). Analytical Study of Drill-string Vibration. *American Society of Mechanical Engineers -- Transactions --* Journal *of Engineering for Industry Series B, 82*(2), 122–128.

18. Finni, I., & Bailey, J. J. (1960). Experimental Study of Drill-string Vibration. American Society of Mechanical Engineers – Transactions – Journal of Engineering for Industry Series B, 82(2), 129-135.

19. Jardine, S., Malone, D., & Sheppard, M. (1994). Putting a Damper on Drilling's Bad Vibration, *Oilfield Review*, January 1994. http://www.slb.com/resources/publications/industry_articles/oilfield_review/1994/or19940102_drillings_bad_vibrations.aspx

20. DrillstringVibrations and Vibration Modeling. http://www.slb.com/~/media/Files/drilling/brochures/drilling_opt/drillstring_vib_br.ashx

21. Hawker, D., Vogt, K., & Robinson, A. (2001). Wellsite Procedures and Operations. *Datalog wellsite Operation Manuals.* Version 3.0.

22. Soft Torque. http://www.softtorque.com

23. http://www.slb.com/~/media/Files/drilling/brochures/mwd/drilling_dynamics_sensors_opt_br.ashx

24. Yigit, A. S., & Christoforou, A. P. (2000). Coupled Torsional and Bending Vibrations of Actively Controlled Drillstrings. *Journal of Sound and Vibration, 234*(1), 67–83.

25. Yigit, A. S., & Christoforou, A. P. (2006). Stick-slip and Bit-bounce Interaction in Oil-well Drillstrings. *Journal of Energy Resources Technology, 128*(4), 268–274.

26. Christoforou, A. P., & Yigit, A. S. (2003). Fully Coupled Vibrations of Actively Controlled Drillstrings. *J Sound Vib, 267*(5), 1029–1045.

27. Yigit, A. S., & Christoforou, A. P. (1998). Coupled Torsional and Bending Vibrations of Drillstrings Subject to Impact with Friction. Journal of Sound and Vibration, 215(1), 167–181.

28. Richard, T., Germay, C., & Detournay, E. (2004). Self-excited Stick-slip Oscillations of Drill Bits. *Comptes Rendus – Mecanique, 332*(8), 619–626.

29. Richard, T., Germay, C., & Detournay, E. (2007). A Simplified Model to Explore the Root Cause of Stick-slip Vibrations in Drilling Systems with Drag Bits. *Journal of Sound and Vibration, 305*(3), 432–456.

30. Richard, T., Detournay, E., Fear, M., Miller, B., Clayton, R., & Matthews, O. (2002). Influence of Bit-rock Interaction on Stick-slip Vibrations of PDC Bits. *SPE Annual Technical Conference and Exhibition.* San Antonio, Texas: Copyright 2002, Society of Petroleum Engineers Inc.

31. Khulief, Y. A., & Al-Naser, H. (2005). Finite Element Dynamic Analysis of Drillstrings. *Finite Elements in Analysis and Design*, 41(13), 1270–1288.

32. Khulief, Y. A., Al-Sulaiman, F. A., & Bashmal, S. (2007). Vibration Analysis of Drillstrings with Self-excited Stick-slip Oscillations. *Journal of Sound and Vibration*, 299(3), 540–558.

33. Khulief, Y. A., & Al-Sulaiman, F. A. (2009). Laboratory Investigation of Drillstring Vibrations. Proceedings of the Institution of Mechanical Engineers, *Part C: Journal of Mechanical Engineering Science*, 223(10), 2249–2262.

34. Challamel, N., Sellami, H., Chenevez, E., & Gossuin, L. (2000). A Stick-slip Analysis Based on Rock/Bit Interaction: Theoretical and Experimental Contribution. *IADC/SPE Drilling Conference*. New Orleans, Louisiana: Copyright 2000, IADC/SPE Drilling Conference.

35. Viggo, A., Thor, & Age, K.,. (1988). An Experimental and Theoretical Study of a Coupling Mechanism Between Longitudinal and Torsional Drillstring Vibrations at the Bit. *SPE Drilling Engineering*, 3(1).

36. Tucker, R. W., & Wang, C. (1999). An Integrated Model for Drill-string Dynamics. *Journal of Sound and Vibration*, 224(1), 123–165.

37. Dareing, D. W., & Livesay, B. J. (1968). Longitudinal and Angular Drill-string Vibrations with Damping. In ASME Meeting Pet-31, Sep 22-25 1968 (9). *American Society of Mechanical Engineers -- Papers*. New York, NY, United States: American Society of Mechanical Engineers (ASME).

38. http://www.20sim.com/

39. Karnoop, D. C., Margolis, D. L., & Rosenberg, R. C., (1999). *System Dynamics: Modeling and Simulation of mechatronics Systems*, 3rd ed., John Wiley & Sons, Inc., New York.

40. Rao, S.S. (1995). *Mechanical Vibrations*, 3rd ed., Addison-Wesley Publishing Company, New York.

41. Ogata, K. (1992). System Dynamics, 2rd ed., Prentice Hall, Englewood Cliffs, New Jersey.

42. Büchi, R. (2010). State Space Control, LQR and Observer step by step introduction, with Matlab examples, Books on Demand, Norderstedt.

43. Karkoub, M., Zribi, M., Elchaar, L., & Lamont, L. (2010). Robust μ-Synthesis Controllers for Suppressing Stick-slip Induced Vibrations in Oil Well Drill Strings. *Multibody System Dynamics*, *23*(2), 191–207.

44. Serrarens, A. F. A., van de Molengraft, M. J. G., Kok, J. J., & van den Steen, L. (1998). H_∞ Control for Suppressing Stick-slip in Oil Well Drillstrings. *Control Systems, IEEE*, *18*(2), 19–30.

45. Karkoub, M., Abdel-Magid, Y. L., & Balachandran, B. (2009). Drill-string Torsional Vibration Suppression Using GA Optimized Controllers. *Journal of Canadian Petroleum Technology*, *48*(12), 32–38.

46. Canudas-de-Wit, C., Rubio, F. R., & Corchero, M. A. (2008). D-OSKIL: A New Mechanism for Controlling Stick-slip Oscillations in Oil Well Drillstrings. *IEEE Transactions on Control Systems Technology*, *16*(6), 1177–1191.

47. Pavkovic, D., Deur, J., & Lisac, A. (2011). A Torque Estimator-based Control Strategy for Oil-well Drill-string Torsional Vibrations Active Damping Including an Auto-tuning Algorithm. *Control Engineering Practice*, *19*(8), 836–850.

48. Puebla, H., & Alvarez-Ramirez, J. (2008). Suppression of Stick-slip in Drillstrings: A Control Approach Based on Modeling Error Compensation. *Journal of Sound and Vibration*, *310*(4-5), 881–901.

49. Womer, K. A., Torkay, D. R., Villanueva, G. P., Geehan, T., Brakel, J., Pirovolou, D., et al. (2011). Results of July 15, 2010 IADC Stick-Slip Mitigation Workshop. *SPE/IADC Drilling Conference and Exhibition. Amsterdam, The Netherlands: Society of Petroleum Engineers.*

50. Kriesels, P. C., Keultjes, W. J. G., Dumont, P., Huneidi, I., Owoeye, O. O., & Hartmann, R. A. (1999). Cost Savings through an Integrated Approach to Drillstring Vibration Control. *SPE/IADC Middle East Drilling Technology Conference. Abu Dhabi, United Arab Emirates: Society of Petroleum Engineers.*

51. '*Rotary Table*'. http://www.glossary.oilfield.slb.com

52. http://www.akersolutions.com/en/Global-menu/Products-and-Services/technology-segment/Drilling-technologies/Drilling-equipment/Handling-tools/

53. http://www.offshore-technology.com/projects/kravtsovskoye/kravtsovskoye6.html

54. '*Top Drive*'. http://www.glossary.oilfield.slb.com/Display.cfm?Term=topdrive

55. '*Top Drive Solution*'. (2011). *Top Drive Catalog.* http://www.nov.com

56. '*Mud Motor*'. http://en.wikipedia.org/wiki/Mud_motor

57. https://sites.google.com/site/directionaldrillingclub/downhole-mud-motors

58. '*Shock sub*'. http://www.slb.com/services/drilling/tools_services/jars_accelerators/shock_sub.aspx

59. '*ST5 Shock Tool*'. http://www.cougards.com/tool/st5-shock-tool/

60. '*Directional Drilling Technology*'. http://directionaldrilling.blogspot.ca/2011/07/rotary-assemblies-building-assembly.html

61. '*Shocks and Vibration*'. http://www.spe-uk.org/Downloads/Past%20Presentations%20Aberdeen/martin%20hayes%20schlumberger.pdf

62. Breedveld, P. (2003). Bond Graphs. http://www-lar.deis.unibo.it/euron-geoplex-sumsch/files/lectures_1/Breedveld/Breedveld_03_BGConcepts.pdf

63. '*About Bond Graphs – The System Modeling World*'. http://groups.csail.mit.edu/drl/journal_club/papers/Samantaray__2001__www.bondgraphs.com_about.pdf

64. Sazidy, M. S., Rideout, D. G., Butt, S. and Arvani, F. (2010). Modeling Percussive Drilling Performance using Simulated Visco-Elasto-Plastic Rock Medium, 44th US Rock Mechanics Symposium, Salt Lake City, USA June 27–30, 2010.

65. *LQR control*. http://www.mathworks.com/help/toolbox/control/getstart/f2-1049484.html#f2-1053272

66. Drill Bit (Bakerhuges) .http://www.bakerhughes.com/products-and-services/drilling/drill-bit-systems

67. Personal communication with Ryan Directional Services, Calgary, AB, 2012.

68. http://www.slb.com/~/media/Files/drilling/posters/shock_vibration_posters.ashx

69. Spanos, P., A. Sengupta, R. Cunningham, and P. Palsay. (1995). Modeling of Roller Cone Bit Lift-Off Dynamics in Rotary Drilling. *Journal of Energy Resources Technology* 117, no. 2, 115-124.

70. http://www.diamonddrillingindustries.com/downloads/PDC%20Bit%20Running%20Procedures%20DDI.pdf

71. L. van den Steen. (1997). Suppressing Stick-slip Induced Drillstring Oscillations: A Hyper Stability Approach, *Ph.D Thesis*, University of Twente.

72. D.K. Ashley, X.M. McNary, and J.C. Tomlinson. (2001). Extending BHA Life with Multi-Axis Vibration Measurements. *SPE/IADC Drilling Conference*.

Appendix A

SIMULATION DATA

Table A.1: Drillstring data

Drillstring data	
Cable and derrick spring constant	9.3e+06 N/m
Swivel and derrick mass	7031 kg
Kelly length	15 m
Kelly outer diameter	0.379 m
Kelly inner diameter	0.0825 m
Drill pipe length	2000 m
Drill pipe outer diameter	0.101 m (4 in)
Drill pipe inner diameter	0.0848 m (3.34 in)
Drill collar length	200 m
Drill collar outer diameter	0.171 m (6.75 in)
Drill collar inner diameter	0.0571 m (2.25 in)
Drill string material	Steel
Wellbore diameter	0.2 m

Table A.2: Drill bit-rock data

Drill bit-rock data	
Bit type	PDC (Single cutter)
Drill bit diameter	0.2 m (7.875 in)
Drill bit mass	65 kg
Rock stiffness	1.16e+09 N/m
Rock damping	1.5e+05 N.sec/m
Surface elevation amplitude s_0	0.001
Bit factor, b	1
Cutting coefficient ξ, C_1, C_2	1, 1.35e-08, -1.9e-4
Frictional coefficient $\mu_0, \alpha, \beta, \gamma$ & ν	0.06, 2, 1, 1 & 0.01
Threshold force, W_{fs}	10000 N
Equivalent fluid viscosity for fluid resistance to rotation μ_e	30e-03 Pa.sec
Weisbach friction factor outside drill pipe or collar, α_a	0.045
Weisbach friction factor inside drill pipe or collar, α_p	0.035

Table A.3: Drilling hydraulic data

Hydraulic data	
Mud fluid density	1198 kg/m^3
Mud flow rate, Q	$Q_m + Q_a \sin(qt)$
Mean mud flow rate, Q_m	0.022 m^3/sec
Mud flow pulsation amplitude, Q_a	0.002 m^3/sec
Freq. of variation in mud flowrate, q	25.13 rad/sec

Table A.4: Motor data

Motor data	
L, K_m, n, R_m and J_m	0.005 H, 6 V/s, 7.2, 0.01 Ω and 23 kg-m^2

Appendix B

Formulas For LQR Controller Design

1. Inertia of the kelly, J_k

$$J_k = \frac{\pi}{2} \rho L_k (r_{ok}^4 - r_{ik}^4) \tag{45}$$

2. Effective inertia of the drillstring, J

$$J = \frac{1}{3} J_p + J_c \tag{46}$$

$$J = \frac{1}{3} \frac{\pi}{2} \rho L_p \left(r_{op}^4 - r_{ip}^4\right) + \frac{\pi}{2} \rho L_c (r_{oc}^4 - r_{ic}^4) \tag{47}$$

3. Effective torsional stiffness of the drillstring, K_t

$$K_t = \frac{G \pi (r_{op}^4 - r_{ip}^4)}{L_p} \tag{48}$$

4. Effective viscous damping of the drillstring, C_v

$$C_v = \frac{\pi \mu_e d_{op}^3 L_p}{2 (d_h - d_{op})} \tag{49}$$

5. Rotary table inertia, J_{rt}

$$J_{rt} = 930 \text{ Kg-m}^2 \tag{50}$$

Appendix C

MATLAB PROGRAMMING CODES

%Gains Calculation Codes%

```
global R  A B  C D

%Parameters
n = 7.2;
Jm = 23;
Rm = 0.01;
L = 0.005;
Crt = 0;
Jrt = 930;
Jk = 239.54;
Km = 6;
J = 159.84;
Kt = 214.99;
Cv = 1.00;  %10

A = [-Rm/L  0  -n*Km/L  0  0;
   0  0  1  0  0;
   n*Km/(Jk+Jrt+n^2*Jm)  0  -Crt/(Jk+Jrt+n^2*Jm)  -Kt/(Jk+Jrt+n^2*Jm)  0;
   0  0  1  0  -1;
   0  0  0  Kt/J  -Cv/J];

B=[1/L;
   0;
   0;
   0;
   0];

C=[1  0  0  0  0;
   0  1  0  0  0;
   0  0  1  0  0;
   0  0  0  1  0;
```

```
   0  0  0  0  1];

D=[0;
   0;
   0;
   0;
   1];


Q1 = [1 0 0 0 0; 0 20000 0 0 0; 0 0 1 0 0; 0 0 0 80000 0; 0 0 0 0 950000];

N = [0;
   0;
   0;
   0;
   0];

R = 950;

S = N;

%P = manipulated variables
%E = closed loop eigenvalues
%G = gain matrix

[P,E,G]=care(A,B,Q1,R,S)
```

Appendix D

LQR Controller Gains Curve

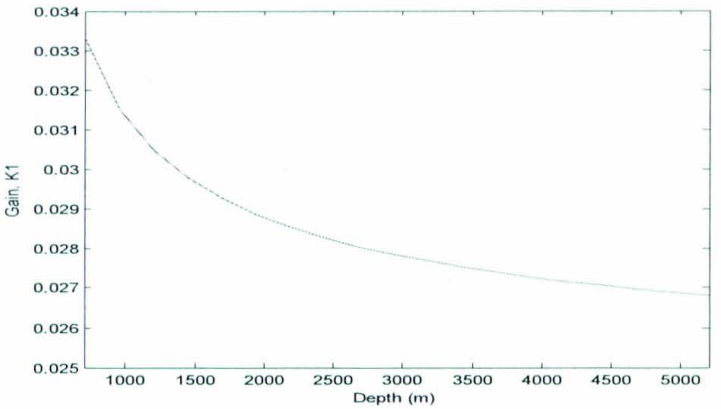

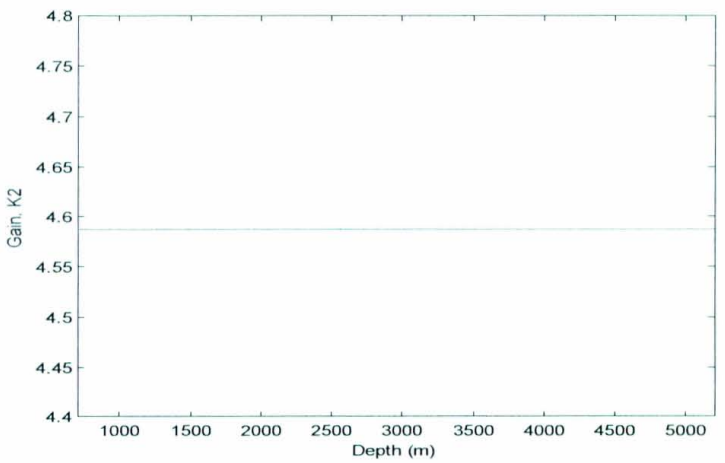

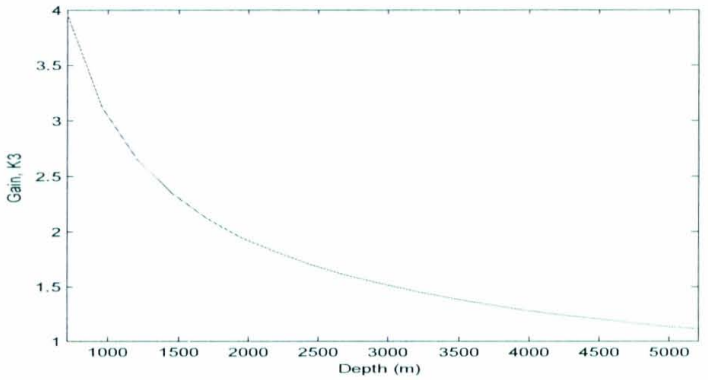

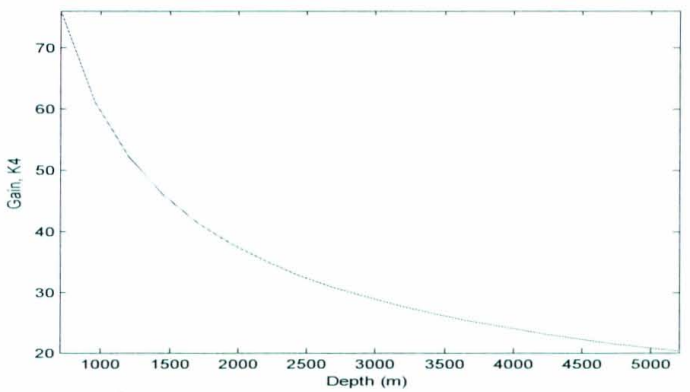

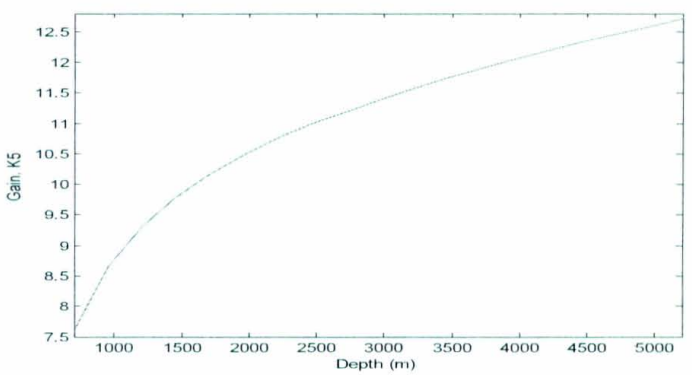

Figure D.1: Gains vs. depth curves for LQR controller

Appendix E

20SIM PROGRAMMING CODES

// Mud Flow Rate 20sim Codes//

```
parameters
        real Qm = 0.022;          // mean mud flow rate,
        real Qa = 0.002;      // mud flow pulsation amplitude,
        real q = 25.13 {rad/s};   // frequency of variations in mud flowrate, 25.13 1/s

variables
        boolean hidden change;
        real hidden half;
        real global Q;    // Volume rate of flow of drilling mud'

equations
        "calculate at least 2 points per cycle to get a triangle"
        half = pi / q;
        change = frequencyevent (half, half / 2);

        "calculate the sine wave"
        Q = Qm + Qa * sin ( q * time);
```

// Mud Fluid Properties 20sim Codes//

```
parameters
        real mud_rho = 1200;  // mud density kg/m3
        real Friction_factor_outer = 0.045;   // weisbach friction factor outside drii pipe
or collar
        real Friction_factotor_inner = 0.035;          // weisbach friction factor inside drii
pipe or collar

variables
        real global mud_density;
        real global friction_factor_outer;
        real global friction_factor_inner;
```

equations

mud_density = mud_rho;
friction_factor_outer = Friction_factor_outer;
friction_factor_inner = Friction_factotor_inner;

// Load Calculation 20sim Codes//

parameters

real static_applied_WOB = 100000; // N
real Swivel_mass = 7031; // mass of swivel kg

variables

real global swivel_mass;
real global kelly_n;
real global kelly_mass;
real global pipe_length;
real global pipe_n;
real global pipe_mass;
real global pipe_area;
real global collar_length;
real global collar_n;
real global collar_mass;
real global collar_area;
real global hook_load;
real global bouyancy_factor;
real global steel_density;
real global mud_density;
real global avg_WOB;
real global hydraulic_force_top;
real global hydraulic_force_bottom;

real global Pipe_Collar_weight;
real global kelly_swivel_weight;
real global total_mat_weight;

equations

swivel_mass = Swivel_mass;
avg_WOB = static_applied_WOB;
*hydraulic_force_top = mud_density * 9.81 * pipe_length * (collar_area - pipe_area);*
*hydraulic_force_bottom = mud_density * 9.81 * (pipe_length + collar_length) * collar_area;*
bouyancy_factor = 1 - (mud_density/steel_density);

```
kelly_swivel_weight = (swivel_mass + collar_n * collar_mass)* 9.81;
Pipe_Collar_weight = (pipe_n * pipe_mass + collar_n * collar_mass) * 9.81;
total_mat_weight = kelly_swivel_weight + Pipe_Collar_weight;
hook_load = total_mat_weight - static_applied_WOB + hydraulic_force_top -
hydraulic_force_bottom;
```

// Axial and Torsional Model Constant Calculation 20sim Codes//

parameters

```
real E = 211000000000;  // modulus of elasticity, N/m2
real G = 80e9;                                  // shear modulus, Pa
real rho = 7860 ;                               // steel density, kg/m3

real kelly_L = 15;                      // length of kelly, m
real Kelly_n = 1;                       // number of segments for kelly
real kelly_OD = 0.3795;
real kelly_ID       = 0.08255;
real kelly_Mat_damp = 15000;    // material damping, Axial
real kelly_Mat_tor_damp = 150;  // material damping, torsional

real pipe_L = 2000;                     // length of drillpipe, m
real Pipe_n = 10;                       // number of segments for drillpipe
real pipe_OD = 0.1016;
real pipe_ID = 0.08484;
real pipe_Mat_damp = 15;    // material damping
real pipe_Mat_tor_damp = 0.06;  // material damping, torsional
real Pipe_viscouse_damp_factor = 0;   // from dareing paper, 38.29 N.s/m

real collar_L = 200;                    // length of drillcollar, m
real Collar_n = 10;                     // number of segments for drillcollar
real collar_OD = 0.17145;
real collar_ID      = 0.05715;
real collar_Mat_damp = 2500;      // material damping
real collar_Mat_tor_damp = 15;  // material damping, torsional
real Collar_viscouse_damp_factor = 0;   // from dareing paper,239.40 N.s/m

real torsion_viscosity_resis = 30e-03;   // equivalent viscosity for fluid resistance
to rotation, pa.sec (mud vicosity)
```

variables

```
real global steel_density;

real global kelly_n;
```

```
real global kelly_delx;
real global kelly_mass_inertia;
real global kelly_area_inertia;
real global kelly_torsion_comp;
real global kelly_area;
real global kelly_mass;
real global kelly_axial_comp;
real global kelly_mat_damp;
real global kelly_mat_tor_damp;

real global pipe_length;
real global pipe_n;
real global Pipe_OD;
real global Pipe_ID;
real global pipe_delx;
real global pipe_mass_inertia;
real global pipe_area_inertia;
real global pipe_torsion_comp;
real global pipe_torsion_fluid_resis;
real global pipe_area;
real global pipe_mass;
real global pipe_axial_comp;
real global pipe_mat_damp;
real global pipe_mat_tor_damp;
real global pipe_axial_viscous_damp;

real global collar_length;
real global collar_n;
real global Collar_OD;
real global Collar_ID;
real global collar_delx;
real global collar_mass_inertia;
real global collar_area_inertia;
real global collar_torsion_comp;
real global collar_torsion_fluid_resis;
real global collar_area;
real global collar_mass;
real global collar_axial_comp;
real global collar_mat_damp;
real global collar_mat_tor_damp;
real global collar_axial_viscous_damp;

real global wellbore_radius;
```

```
equations
        steel_density = rho;

        kelly_n = Kelly_n;
        kelly_delx = kelly_L / kelly_n;
        kelly_area = 3.1416*((kelly_OD/2)^2 - (kelly_ID/2)^2);
        kelly_mass_inertia = 0.5 * rho * kelly_area * kelly_delx * ((kelly_OD/2)^2 +
(kelly_ID/2)^2);
        kelly_area_inertia = 0.5 * 3.1416* ((kelly_OD/2)^4 - (kelly_ID/2)^4);
        kelly_torsion_comp = kelly_delx/(G*kelly_area_inertia);
        kelly_mass = rho * kelly_area * kelly_delx;
        kelly_axial_comp = kelly_delx/(E * kelly_area);
        kelly_mat_damp = kelly_Mat_damp*kelly_delx;
        kelly_mat_tor_damp = kelly_Mat_tor_damp*kelly_delx;

        pipe_length = pipe_L;
        pipe_n = Pipe_n;
        Pipe_OD = pipe_OD;
        Pipe_ID = pipe_ID;
        pipe_delx = pipe_L / pipe_n;
        pipe_area = 3.1416*((pipe_OD/2)^2 - (pipe_ID/2)^2);
        pipe_mass_inertia = 0.5 * rho * pipe_area * pipe_delx * ((pipe_OD/2)^2 +
(pipe_ID/2)^2);
        pipe_area_inertia = 0.5 * 3.1416* ((pipe_OD/2)^4 - (pipe_ID/2)^4);
        pipe_torsion_comp = pipe_delx/(G*pipe_area_inertia);
        pipe_torsion_fluid_resis = (2*3.1416* torsion_viscosity_resis * (pipe_OD/2)^3
/(wellbore_radius - (pipe_OD/2)))* pipe_delx;
        pipe_mass = rho * pipe_area * pipe_delx;
        pipe_axial_comp = pipe_delx/(E * pipe_area);          // axial model
        pipe_mat_damp = pipe_Mat_damp*pipe_delx;          // axial model
        pipe_mat_tor_damp = pipe_Mat_tor_damp*pipe_delx;
        pipe_axial_viscous_damp = Pipe_viscouse_damp_factor * pipe_delx;

        collar_length = collar_L;
        collar_n = Collar_n;
        Collar_OD = collar_OD;
        Collar_ID = collar_ID;
        collar_delx = collar_L / collar_n;
        collar_area = 3.1416*((collar_OD/2)^2 - (collar_ID/2)^2);
        collar_mass_inertia = 0.5 * rho * collar_area * collar_delx * ((collar_OD/2)^2 +
(collar_ID/2)^2);
        collar_area_inertia = 0.5 * 3.1416* ((collar_OD/2)^4 - (collar_ID/2)^4);
        collar_torsion_comp = collar_delx/(G*collar_area_inertia);
```

```
collar_torsion_fluid_resis = (2*3.1416* torsion_viscosity_resis *
(collar_OD/2)^3 /(wellbore_radius - (collar_OD/2)))* collar_delx;
collar_mass = rho * collar_area * collar_delx;
collar_axial_comp = collar_delx/(E * collar_area);  // axial model
collar_mat_damp = collar_Mat_damp*collar_delx;  // axial model
collar_mat_tor_damp = collar_Mat_tor_damp*collar_delx;
collar_axial_viscous_damp = Collar_viscouse_damp_factor * collar_delx;
```

// Motor Constant 20sim Codes//

```
parameters
    real Jrt = 930;  //mass moment of inertia for ratary table
    real Crt = 0;   // damping in torsional motion
    real Jm = 23;   //mass moment of inertia for motor
    real n = 7.2;   // gear ratio
    real L = 0.005;  // Inductance
    real Rm = 0.01;  // Armature resistance
    real Km = 6;   // motor constant
    real Wd = 30;  // Rotary table desired speed

variables
    real global Table_Inertia;
    real global Torsional_damping;
    real global Motor_Inertia;
    real global gear_ratio;
    real global Inductance;
  real global Resistance;
    real global motor_constant;
    real global Desired_table_speed;

equations
    Table_Inertia = Jrt;
    Torsional_damping = Crt;
    Motor_Inertia = Jm;
    gear_ratio = n;
    Inductance = L;
    Resistance = Rm;
    motor_constant = Km;
    Desired_table_speed = Wd;
```

// Rock-bit Constant 20sim Codes//

```
parameters
        real r = 0.1;                   // bit radius
        real zeta = 1;          //parameters
        real c1 = 1.35e-08;     //parameters
        real c2 = -1.9e-04;     //parameters
        real alpha = 2;         //parameters
        real beta = 1;          //parameters
        real gama = 1;          //parameters
        real munot = 0.06;      //parameters
        real nu = 0.01;         //parameters

        real Kc = 1.16e09;              // Berea Sandstone rock stiffness N.m
        real R = 1.5e05;
        real bit_mass = 65;
        real bit_flow_area = 2.3865e-04;

variables
        real global bit_radius;
        real global Zeta;
        real global C1;
        real global C2;
        real global Alpha;
        real global Beta;
        real global Gama;
        real global Munot;
  real global Nu;
        real global rock_compliance;
        real global rock_damping;
        real global Bit_Mass;
        real global Bit_Inertia;
        real global bit_nozzle_radius;

equations
        bit_radius = r;
        Zeta = zeta;
        C1 = c1;
        C2 = c2;
        Alpha= alpha;
        Beta = beta;
        Gama = gama;
        Munot = munot;
```

```
Nu = nu;
rock_compliance = 1/Kc;
rock_damping = R;
Bit_Mass = bit_mass;
Bit_Inertia = 0.5 * Bit_Mass * bit_radius^2;
bit_nozzle_radius = (bit_flow_area/3.14159)^0.5;
```

// Wellbore Constant 20sim Codes//

```
parameters
        real r_w = 0.1;                 // wellbore radius, m

variables
        real global wellbore_radius;

equations
        wellbore_radius = r_w;
```

// Torque on Bit (TOB) 20sim Codes//

```
variables
        real flow;
        real phidot_function;
        real ROP;
        real depth_of_cut;
        real global bit_radius;
        real global Zeta;
        real global C1;
        real global C2;
        real global Alpha;
        real global Beta;
        real global Gama;
        real global Munot;
  real global Nu;
        real global avg_WOB;
        real global Desired_table_speed;

equations
        phidot_function
=
Munot*(tanh(phidot)+Alpha*phidot/(1+Beta*(phidot)^(2*Gama))+Nu*phidot);

        if WOB <= 10000 then
```

```
        ROP = 0;
        depth_of_cut = 0;
        if phidot == 0.0 then
          p.e = 0;
        else
          p.e = WOB*bit_radius*phidot_function;
        end;
      else
        if phidot == 0.0 then
          ROP = 0;
          p.e = WOB*bit_radius*phidot_function + 5000;
        else
          if phidot < 0 then
            ROP = 0;
            p.e = WOB*bit_radius*phidot_function;
          else
            ROP = C1*(WOB)*phidot^0.5;
            depth_of_cut = (2*3.1415926*ROP)/phidot;
            p.e = WOB*bit_radius*phidot_function +
(WOB)*bit_radius*Zeta*(depth_of_cut/bit_radius)^0.5;
          end;
        end;
      end;

flow = p.f;
```

// Rock Compliance 20sim Codes//

```
variables
        real global rock_compliance;
        real global rock_damping;

equations
        X = int(p.f);
        if X >=0 then
                p.e = (1/rock_compliance) * X + rock_damping*p.f;
        else
                p.e = 0;
        end;
WOB = p.e;
```

PUBLICATIONS

1. Sarker, M., Rideout, D.G., & Butt, S.D. (2012). "Dynamic Model of an Oilwell Drillstring with Stick-Slip and Bit-Bounce Interaction". *10th International Conference on Bond Graph Modeling and Simulation. Genoa, Italy, July 8-11, 2012. The Society for Modeling and Simulation International, San diego, CA, USA.*
2. Sarker, M., Rideout, D.G., & Butt, S.D. (2012). "Advantages of an LQR Controller for Stick-slip and Bit-bounce Mitigation in an Oilwell Drillstring". Submitted to *International Mechanical Engineering Congress & Exposition. Houston, Texas, November 9-15, 2012. American Society of Mechanical Engineers.*